UNIVERSITY OF CAPE TOWN
IYUNIVESITHI YASEKAPA • UNIVERSITEIT VAN KAAPSTAD

25cc HCCI Engine Fueled with Diethyl Ether

Author:
Ian Lemberger

Supervisor:
Mr. Gareth Floweday

Co.Supervisor:
Prof. Andrew Yates

A dissertation submitted to the Department of Mechanical Engineering, University of Cape Town, in partial fulfilment of the requirements for the degree of Master of Science in Engineering.

April 30, 2009

Chapter 1

Preface

1.1 Acknowledgements

This study was funded and supported by the SASOL Technology Fuels Research team which is headed by Dr. Johnto Dixon. The author would like to extend his gratitude and thanks to the following people for their contributions in the completion of this project:

Mr. Gareth Floweday - Project Supervisor

Prof. Andrew Yates - Co. Supervisor

Mr. Mark Wattrus - SASOL Technology

Mr. Paul Schaberg - SASOL Technology

Mr. Kyle Collair - SASOL Advanced Fuels Laboratory

Mr Gavin Tomlinson - SASOL Advanced Fuels Laboratory

Workshop Staff - University of Cape Town

To my family and friends, for their constant support, guidance and motivation throughout the duration of this project

1.2 Plagiarism Declaration

1. I know that plagiarism is wrong. Plagiarism is to use another's work and to pretend that it is ones own.
2. I have used the convention for citation and referencing. Each significant contribution to, and quotation in, report for the work, or works, of other people has been attributed, and has cited and referenced.
3. This report is my own work
4. I have not allowed, and will not allow, anyone to copy my work with the intention of passing it off as his or her own work.

Author:
Ian Lemberger:

April 30, 2009

1.3 Executive Summary

Background to Investigation

This research forms part of an ongoing HCCI study at the SASOL Advanced Fuels Laboratory to investigate and understand engine configuration and fuel chemistry effects on combustion in HCCI engines. This project continues from a previous project where a small Progress Aero Works (PAW) 6.5cc high speed model "diesel" aeroplane engine was found to operate in HCCI mode with surprising ease and flexibility. A 25cc, four-stroke, single cylinder Honda GX25 engine, possessing 2-valves with an overhead cam and separate oil sump lubrication system was used. This research aimed to provide insight with respect to which engine characteristics such as size, heat transfer, speed and fuel blending effects, play the primary role in operational differences between the Honda GX25, conventional HCCI engines and the remarkable operational flexibility of the PAW engine.

Procedure Used

The engine was mounted on a test bench with a reduction drive, regenerative DC dynamometer and Electronic Control System (ECS). Various HCCI combustion control systems were added to to ascertain their effects on small HCCI engine combustion stability, heat release phasing and exhaust emissions. Diethyl Ether (DEE) was used as the primary testing fuel due to its volatility and high ignition quality.

An engine model, using thermodynamic and auto-ignition modeling techniques, was used to explore the engine's operational behavior. Particular attention was given to the modeling of the engine's slightly unusual combustion heat transfer characteristics.

Results of Investigation

Stable HCCI operation was possible between 1000 - 4000 rpm, similar to that in conventional HCCI engines. Lower operational speed limits were a result of combustion quality, resulting in engine misfire and upper speed limits were a result of excessive pressure rise rates.

Maximum operational ϕ was greater than in conventional HCCI engines. The GX25's maximum operational ϕ was 0.75 when operating without EGR. This was due to thermal gradients induced by the high surface area to volume ratio of the small engine size resulting in excessive combustion chamber heat transfer, allowing for increased fueling during operation. Evidence of engine heat transfer was illustrated when operating without additional engine cooling, resulting in fuel NTC behaviour.

Testing of the various control strategies seem to indicate points of optimal operation and so called "sweet spot" operation. These "sweet spots" are expected to be completely engine dependent and thus engine characteristics including heat-loss and breathing characteristics dominate in determining where inside the operational envelope they exist.

The major operational differences between the GX25 and P.A.W occur due to:

- DEE's cetane number being higher than that of the D1000 utilised in the PAW engine testing.
- PAW's compression ratio is much higher than that of the GX25. The ability to vary compression ratio was used extensively in the PAW engine testing to vary engine operating conditions and extend the engine's performance.
- The PAW operates using a high REG % as a result of the engine's two-stroke operation. This results in the PAW engine possessing a higher operational ϕ as compared to the GX25. However, the use of EGR and REG in the GX25 does allow for a similar operational ϕ as the PAW engine.
- The PAW's high engine speed, high compression ratio and temperature controlled water-cooling system reduce the effects of engine heat transfer when compared to the GX25 engine.

A modified heat transfer correlation was able to accurately predict engine operation, when coupled with a single-zone combustion model. The major discrepancy between the different heat loss model correlations and the modified correlation as provided in this research, suggests that heat loss experienced in small engines during operation is primarily related to engine geometric characteristics and the method of engine cooling and not the mode of combustion.

1.4 List of Symbols

AFR: Air/Fuel Ratio
cc: cubic centimetres
CAD: Crank Angle Degrees
C.I: Compression Ignition
CO: Carbon Monoxide
CO_2: Carbon Dioxide
DEE: Diethyl Ether
DI: Direct Injection
G: Gibbs Free Energy
HC: HydroCarbon
HRR: Heat Release Rate (J/CAD)
h: Enthalpy (kJ/kg)
EVO: Exhaust Valve Opening
EVC: Exhaust Valve Closure
IQT: Ignition Quality Tester
IVO: Inlet Valve Opening
IVC: Inlet Valve Closure
NOx: Nitrogen Oxides
p: Cylinder Pressure (bar or kPa)
PM: Particulate Matter
PRR: Pressure Rise Rate (bar/CAD)
Q: Heat Loss (J)
R: Universal Gas Constant (J/mol.K)
S.I: Spark Ignition
SOI: Start of Injection
s: Entropy (kJ/kg)
U: Internal Energy (kJ)
v: Volume (m^3)
VCR: Variable Compression Ratio
w: local gas velocity (m/s)
W: Work J)
A_h: pre-exponential constant of proportionality
B_h: exponential temperature coefficient
c_p: Specific Heat Constant Pressure
h_c: Heat Transfer Coefficient
L_v: Valve Lift (m)
n_h: autoignition pressure exponent
p_m: Motored Cylinder Pressure (kPa)

S_p: Piston Sliding Speed (m/s)
τ: Ignition Delay (ms)
β: exponent relating to air/fuel equivalence ratio effect on ignition delay
η: Efficiency
ΔT: Temperature change
ϕ: fuel/air ratio
ω: proportionality constant for the cool-flame temperature rise
λ: air/fuel ratio

1.5 Glossary of Terms

Air/Fuel Ratio (AFR): See Fuel/Air Equivalence Ratio

Auto-ignition: Spontaneous combustion without any form of external initiation (such a spark or glow-plug) which is characterised by the simultaneous bulk combustion of the cylinder reactants.

Burn Duration: Time from Start if Ignition until Heat Release Rate is zero which can be specified either in CAD or a time measurement.

Cetane: Concept used to describe to auto-ignition performance of (usually diesel-like) fuels. A higher cetane number implies a propensity for auto-ignition.

Cumulative Heat Release: Total heat released during combustion (J).

Data Acquisition (DAQ) Card: Data Acquisition typically involves acquisition of signals and waveforms and processing of the signals to obtain desired information. The components of data acquisition systems include appropriate sensors that convert any measurement parameter to an electrical signal, which is acquired by data acquisition hardware. The DAQ card may be able to process a combination of analogue and digital signals.

Engine Knock: High pressure oscillations caused by simultaneous, uncontrolled auto-ignition of un-reacted combustion gasses. The high pressure oscillations are caused by resulting shock waves reflecting off the inside of the combustion chamber. Often knock may be heard as a pinging or hammering sound accompanied by rough running. Knock is usually detrimental to engine performance and longevity.

Field-Programmable Gate Array (FPGA): FPGA's are programmed using a logic circuit diagram or a source code in a hardware description language (HDL) to specify how the chip will work. They can be used to implement any logical function that an application-specific integrated circuit (ASIC) could perform.

Fuel/Air Equivalence Ratio, ϕ: The ratio of the fuel mass flow $\dot{m}_f$ and the air mass flow $\dot{m}_a$ are normally measured. A ϕ of 1 indicates a stoichiometric fuel/air ratio. $\phi < 1$ indicates excess air and $\phi > 1$ indicates excess fuel such that:

$$\phi = \frac{F/A_{acutal}}{F/A_{stoichiometric}}$$

This then follows that the reciprocal of ϕ is known as the air/fuel ratio (AFR) (λ) such that:

$$\lambda = \frac{A/F_{acutal}}{A/F_{stoichiometric}}$$

Heat Release Rate (HRR): Is defined as the heat release rate per crank angle degree during combustion specified in J/CAD.

Homogeneous Charge: Infers a well mixed mixture of charge, being fuel and air.

Ignition Delay: Time measured in CAD from time of injection to the point of ignition.

Indicated Mean Effective Pressure (IMEP): A theoretical pressure that if applied constantly to the piston during the expansion stroke, will produce the same work per cycle as the engine produces.

Ignition Quality Tester (IQT$^{\text{TM}}$): The Ignition Quality Tester is a type of combustion bomb commonly used for industrial fuel ignition-quality testing. It is used to test the ignition delay of a fuel by comparing the ignition delay of the test fuel to the known ignition delay of n-heptane. A derived cetane number can then be obtained according to the ASTM method D6890.

n-Heptane: Paraffinic hydrocarbon with seven carbon atoms and saturated with hydrogen. Primary reference fuel with zero octane rating often used to calibrate the performance of other fuels.

Otto Cycle: The thermodynamic analysis of the actual four-stroke or two-stroke cycles can be simplified using air-standard assumptions. The resulting cycle, which closely resembles the actual operating conidtions is the ideal **Otto Cycle** and consists of four internally reversible processes.

Primary Reference Fuels (PRF's): N-heptane and iso-octane are Primary Reference Fuels and are used for octane rating of Spark Ignition Engine fuel in the CFR engine according to the ASTM method D2699.

Contents

List of Figures

List of Tables

Chapter 2

Introduction

Fuel efficiency requirements and ever more stringent emissions legislation require Internal Combustion Engines to improve fuel economy and concurrently reduce exhaust emissions. One possible solution is the advancing of combustion technology in the form of a Homogeneous Charge Compression Ignition (HCCI) Engine engine which could operate either as a single or dual combustion mode engine [1, 2].

HCCI combustion is the process in which a homogeneous air and fuel mixture is spontaneously auto-ignited through compression of the piston. Combustion characteristics allow HCCI to combine the best features of Spark Ignition (SI) and Compression Ignition (CI) engines. HCCI engines offer significantly reduced engine out nitrogen oxide (NOx) emissions and fuel economy improvements up to 20% [2], as compared to S.I Engines, while reducing particulate matter emissions (PM) when compared to C.I Engines. However, due to the nature of ignition being via the compression of the piston, combustion stability and combustion timing (phasing) over a wide engine load range is a major technical challenge in the development of HCCI combustion. Various combustion control methods are presently being researched and implemented in order to produce stable and reliable combustion, while also expanding the HCCI load range. HCCI Electronic Control System (ECS) research is ongoing with respect to closed-loop control of HCCI engine dynamics [3].

HCCI has been demonstrated to work under laboratory conditions achieving low emissions and good efficiency under steady state operation, however technical challenges arise when attempting to extend this performance to

transient operating conditions.

Primary technical challenges with HCCI development are: [2]

- Combustion phasing control
- Rapid heat release rates and noise level with possible engine damage especially at higher loads
- Transient operation difficulties
- Excess carbon monoxide (CO) and hydrocarbon (HC) emissions, particularly at light loads
- Increased NOx at high loads
- Cold start difficulty
- A narrow operation range (as result of the above)

This research forms part of an ongoing HCCI study at the SASOL Advanced Fuels Laboratory to investigate and understand engine configuration and fuel chemistry effects on combustion in HCCI engines. This project continues from a previous project where a small Progress Aero Works (PAW) 6.5cc high speed model "diesel" aeroplane engine was found to operate in HCCI mode with surprising ease and flexibility [4]. The engine was shown to run from idle through a fixed speed-load curve (propeller) to the maximum speed and load point of the engine at 11000rpm and stoichiometric air-fuel ratio, while maintaining nominally constant combustion phasing without any form of combustion control system. This study continued the investigation by removing lubricant from the fuel and switching to 4-stroke operation while retaining a very small engine size. A 25cc, four-stroke, single cylinder Honda GX25 engine, possessing 2-valves with an overhead cam and an oil sump lubrication system was used in the study.

This project aimed to provide insight with respect to which engine characteristics such as size, heat transfer, speed and fuel blending effects, play the primary role in operational differences between the Honda GX25, conventional HCCI engines and the remarkable operational flexibility of the engine used in [4].

As a result of the above mentioned, the research objectives were defined as:

1. Design and build a "small engine" HCCI test rig and model and compare its operation to the PAW model "diesel" aeroplane engine.
2. Investigate engine operation with respect to the engines:
   (a) Operational speed range
   (b) Operational load (ϕ) range. Where ϕ is the ratio of the fuel mass flow and air mass flow, such that $\phi = (F/A)_{actual} / (F/A)_{stoichiometric}$
   (c) Potential "natural compensation" ability to maintain combustion phasing without the use of control strategies, similar to that observed during PAW engine testing.
3. Investigate engine operation in HCCI mode by installing various combustion control strategies and investigating their relative effects on small HCCI engine operation.
4. Provide insights and recommendations for future research

Chapter 3

HCCI Technology

3.1 Introduction to HCCI

Homogeneous Charge Compression Ignition (HCCI) is the auto-ignition of a homogeneous mixture of air and fuel through compression of a piston. The mixture is auto-ignited purely by piston compression with no external ignition control mechanism as utilised in a Spark Ignition (S.I) or Direct Injection Compression Ignition (DICI) Engine. A Spark Ignition Engine while compressing a homogeneous mixture relies on a spark as an ignition source and a Compression Ignition engine compresses air and injects fuel which auto-ignites [5]. These operational differences are illustrated in the comparative Figure 3.1 below.

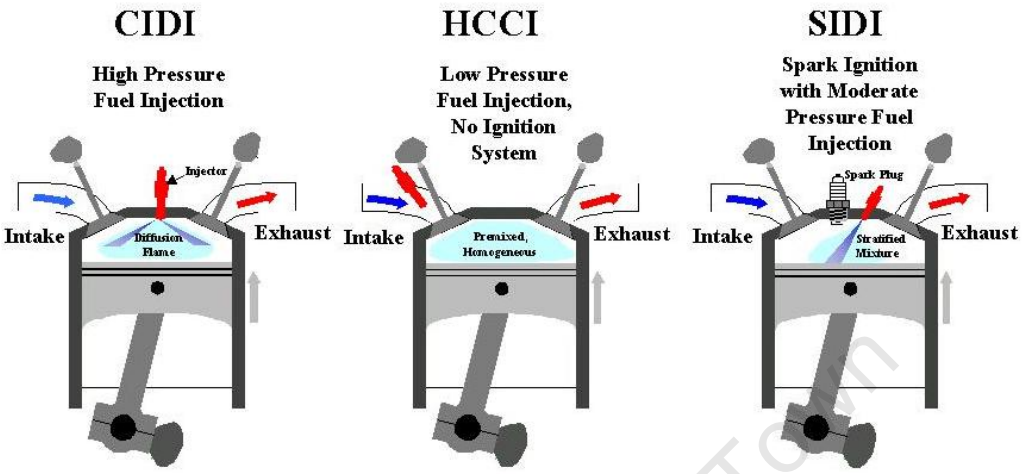

Figure 3.1: Comparison of HCCI Combustion to Direct Injection Compression Ignition (DICI) and Direct Injection Spark Ignition (DISI) Combustion [1]

HCCI's mixture charge is typically well mixed and combustion is described as a bulk controlled auto-ignition, with combustion occurring simultaneously throughout the combustion chamber (see Figure 3.1 above). Combustion is governed by chemical kinetics rather than turbulent flame propagation as in Spark Ignition (S.I) Engines or a stratified diffusion flame as in Compression Ignition (C.I) Engines [2]. Bulk combustion causes rapid heat release rates, with almost all heat release occurring in approximately 5 - 15 crank angle degrees (CAD) [6, 7], with acceptable pressure rise rates of 10 bar/CAD used to distinguish between engine knock and normal engine operation [8, 9, 10].

HCCI engines have the potential ability to combine into one system, the two respective benefits of conventional gasoline and diesel engines; namely low emissions and high efficiency [2]. The homogeneous bulk combustion of the lean mixture results in relatively low temperature combustion which can potentially lower NOx formation [11]. Additionally, a reduction in particulate matter (PM) emissions occurs as a result of the well mixed mixture charge and the absence of throttling losses leads to high efficiency [1].

HCCI Engines have the ability to use higher compression ratios (when compared to S.I Engines) in addition to utilizing higher levels of residual

exhaust gas (REG) and Exhaust Gas Recirculation (EGR) to increase fuel economy and reduce combustion temperatures. HCCI engines approach indicated thermal efficiencies attained by C.I Engines [1]. Operating advantages and disadvantages of HCCI operation are summarised in Table 3.1 below [12]:

Table 3.1: Advantages and Disadvantages of HCCI Combustion

Advantages	Disadvantages
Thermal Efficiency ($\eta_{thermal}$*) comparable to Diesel Engine	High HC and CO emissions
NO_x emissions $\leq$ SI Engines with 3-way catalyst	High Heat Release rates
PM emission $\ll$ Diesel Engine	Difficulty in controlling combustion phasing across entire load range

Where:

$$
\begin{aligned}
*\eta_{thermal} &= \frac{Net\ \ Work\ \ output}{Total\ \ heat\ \ input} \\
&= \frac{W_{net,OUT}}{Q_{IN}}\ \ and \\
W_{net,OUT} &= W_{out} - W_{in} \\
Q_{IN} &= Heat\ \ Energy\ \ supplied\ \ from\ \ fuel\ \ (combustion)
\end{aligned}
$$

Current HCCI technology can be seen in the Mercedes Benz F700 prototype, which utilises the DiesOtto Engine (see Fig 3.2). This engine is a dual mode SI-HCCI engine utilising various control strategies [13, 14]:

1. Turbocharging for increased power
2. Direct gasoline injection for fuel economy gains
3. Variable valve control for engine breathing control as well as REG control
4. Variable compression ratio leading to increased fuel economy and the ability to adapt to engine speed/load requirements when switching between S.I and HCCI combustion modes

5. Exhaust Gas Recirculation (internal REG control and temperature controlled external)

Figure 3.2: Mercedes Benz DiesOtto Engine [13]

The DiesOtto Engine (Figure 3.2) operates as a dual mode engine such that when starting and under full load, the engine runs in spark mode as a conventional spark-ignition engine. Controlled auto ignition, to which the DiesOtto automatically reverts within its working cycle, occurs under partial load conditions. The result is the very low NO_x emissions of homogeneous combustion at reduced reaction temperatures. All further emissions control in the DiesOtto engine is by means of a standard three-way catalytic converter and a highly efficient engine management and control system to combine the individual sub-system advantages [13]. Expected DiesOtto specifications are shown in Table 3.2 below.

Table 3.2: Diesotto Prototype Engine Specifications [15]

Engine Displacement	1.8l
Combustion Mode	Dual mode SI-HCCI
Number of Cylinders	4
Aspiration Method	Twin turbocharged
Power	175 kW
Torque	400 N.m
Compression Ratio	7 - 14:1
Fuel Consumption	5.3l / 100km (Petrol)
Emissions Regulations	EU6
$C0_2$ **emissions**	127 g/km
NOx emissions	Negligible

3.2 History Behind HCCI Technology

Homogeneous Charge Compression Ignition combustion was discovered as a combustion phenomenon by Onishi [2, 16] as an alternative combustion mode for two-stroke IC engines. The first practical application of HCCI was in 1979 when Onishi [2, 16] discovered that HCCI combustion could be used to improve two-stroke engine operation that possessed the following shortcomings:

- The high levels of residuals at light load
- Engines tendency to have run-on combustion when engine operation has ceased

These operational problems were overturned by introducing a combustion mode that relied on high residuals and high initial temperatures. Research found that one could achieve significant reductions in emissions and an improvement in fuel economy by creating conditions that led to a spontaneous ignition of the in-cylinder charge, of which was termed "Active Thermo-Atmospheric Combustion" or ATAC [2].

Onishi [2, 16] was unable to achieve HCCI combustion at low or high loads. Combustion could be achieved however at a mid-load range with gasoline at a Compression Ratio (CR) of 7.5:1 over the engines speed range. Through research Onishi [2, 16] recognized the critical parameters for obtaining HCCI combustion as follows:

- High levels of exhaust dilution to obtain high enough temperatures for autoignition
- Uniform mixing between residual gases and the fresh charge
- Repeatable cycle-to-cycle scavenging

Najt and Foster (1983) followed on from the two-stroke work of Onishi [2, 16] and extended the work to four-stroke engines by trying to understand the physics of HCCI combustion. Their research utilised blends of paraffinic and aromatic fuels combined with heated inlet air, due to the lack of retained residuals, to obtain HCCI combustion. Najt and Foster (1983) concluded that HCCI was not a mixing-controlled combustion process but that the engine behaves like a compression-ignited chemical reactor. Furthermore they noted that HCCI suffered from a lack of combustion control and limited operating range similar to that concluded by Onishi [2, 16].

Thring [2, 17] furthered the research conducted by Najt and Foster using four-stroke engines by examining engine operation using fully-blended gasoline. A single cylinder engine was mapped as a function of air/fuel ratio and external EGR rates. Thring [2, 17] noted that operation was also restricted to part-load and the combustion phasing was problematic. Thring [2, 17] then suggested that HCCI combustion be used at part-loads and a transition into S.I flame propagation at higher loads - a so called dual mode engine as known today.

3.3 Methods of Control for HCCI Combustion

There are generally two accepted methods of achieving HCCI operation:

1. control of cylinder gas temperatures or
2. control of the chemical reactivity of the fuel/air mixture.

Homogeneous Charge Compression Ignition combustion therefore suffers from only possessing an indirect means of controlling the thermal conditions in the cylinder to initiate combustion with optimal phasing. Various HCCI technologies are being explored to try and address the challenges of having to improve S.I efficiencies and reduce emissions from C.I Engines. Various tools that are being used by engine developers to meet these challenges can be categorised as: [18]

- Combustion chamber design changes
- Air management improvements including variable valve systems
- Fuel injection developments to improve the air-fuel mixture formation
- Exhaust Gas Recirculation (EGR) to control combustion phasing
- Engine management and combustion control systems, including closed loop combustion control using in-cylinder pressure measurements

3.3.1 Fuel Injection System

Obtaining a homogeneous mixture requires good fuel atomisation and sufficient time for mixing of fresh air, fuel and REG. It would seem that early injection using a conventional PFI system would be the best to obtain good mixture homogeneity for HCCI combustion. Successful HCCI operation has been achieved by many researchers using a PFI fuel injection [2, 19, 20], but there are drawbacks to this operating mode. A PFI injection offers no potential for additional combustion phasing control and limits the maximum usable compression ratio. This places significant limits on the fuel injection strategies available when using a PFI injection system for HCCI engines.

Utilisation of a Direct Injection (D.I) system allows for increased compression ratio's and therefore an expansion of HCCI light load limits. Direct Injection timing strategies allow for combustion phasing control, especially when coupled with Negative Valve Overlap. This was shown by Urishihara [21] who employed a direct injection system coupled with a negative valve overlap system. The fuel was injected directly into the residual in-cylinder gas during the negative valve overlap interval. This approach expanded the HCCI operating region without any increase in NOx emissions which were seen in the case of compression stroke injection.

The use of direct injection has shown that combustion phasing could be controlled by changes in injection timing. By altering the injection timing from early in the intake stroke to late in the compression stroke it is possible to obtain optimum combustion phasing over a range of intake air temperatures, engine loads and speeds [2, 21].

If the engine operates using a dual mode SI-HCCI combustion, the engine must use SI mode for cold starting and at the highest operating loads. The use of direct injection allows for stratified-charge mode that preserves the high fuel economy benefits at the lightest loads, although increased NOx is possible, a lean NOx aftertreatment system can be used to meet emissions regulations [2]. With HCCI engines, 10% of the fuel can exit in the unburned regions [22, 23] and this amount of the fuel does not contribute to the cylinder pressure rise. Results show that the use of varying the inhomogeneity in fuel distribution in the pre-mixture is effective as a method for controlling the combustion duration in HCCI engines [22]. Research [22, 23, 24, 25, 26] has shown that it is possible to influence and control HCCI combustion by charge stratification. Mixture stratification modifies local AFR's and has been suggested as a potential mechanism for controlling HCCI combustion.

However, fuel stratification may produce excessive NOx emissions and this requires that charge stratification combustion needs to meet the control and high power output requirements of modern engines while reducing NOx emissions [22].

A further injection parameter to consider is the spray injection angle. IFP proposed a Narrow Angle Direct Injection (NADI^{TM}) concept for early injection HCCIs' [18, 27, 28, 29, 30]. This concept works by optimising the fuel injectors and combustion chamber to produce a homogeneous combustion. A narrow cone angle of the fuel injection spray, directs the fuel toward the rising piston, which avoids the problem of wall wetting at lower loads, but at high loads may increase the chance of fuel impingement on the piston.

3.3.2 Fully Variable Valve Timing

Fully Variable Valve Timing (FVVT) allows for control of valve lift, duration, timing or a combination thereof. This control plays an important role in control of HCCI combustion and combustion phasing as it allows for full control of the gas exchange process.

FVVT allows for the control of residual exhaust gas (REG) in the cylinder which controls the end of compression cylinder temperature by having a higher specific heat when compared to the air/fuel mixture. This can be used to control HCCI combustion phasing [19].

The geometric compression ratio of an engine is usually fixed. VVT can be used to alter the effective compression ratio by controlling the volume of REG trapped in the cylinder as well as the mass of charge inducted into the cylinder. The ability to vary in-cylinder mass controls post-compression pressures and temperatures and thus controls combustion phasing. If a high geometric compression ratio is chosen, the effective compression ratio can be reduced by reducing the intake mass charge, usually by very early or very late closing of the intake valve [18].

Additionally, the valves can be used to introduce more swirl into the cylinder and allow for better mixing. This is possible when using an engine, with 2 or more inlet valves, such that each the valve is supplied by separate inlet port intended to allow for swirl variability based on the valve timing strategy used [18].

Allen and Law [19] utilised VVT to obtain HCCI combustion in a single cylinder research engine with CR 10.5:1. Load Control was achieved by varying the quantity of exhaust gas trapped in the cylinder with a maximum BMEP attained of 4.5 bar [19].

3.3.3 Exhaust Gas Recirculation

External Exhaust Gas Recirculation (EGR) is a widely used method to suppress NOx emissions in Diesel Engines, and offers the possibility to lower combustion temperatures [31]. Additionally EGR is now being used as a basic control method of ignition timing and burn rates in HCCI engines. EGR has numerous effects on HCCI combustion and emissions [32].

1. When using hot EGR the inlet charge temperature is increased. This creates a **pre-heating effect** which raises compression cycle temperatures
2. **Dilution effect** - which reduces oxygen concentrations and therefore lowers required fueling for a given ϕ
3. **heat capacity effect** due to the higher heat capacity of carbon dioxide and water vapour. This leads to a reduction in compression temperatures
4. **Chemical effect** due to the combustion products in the EGR taking part in the chemical reactions during combustion Unburned Hydrocarbons, CO, CO_2, NO, H_2O etc, take part in the combustion reaction, which affects the overall reaction rate

Increased EGR % retards the ignition delay (see Figure 3.3 below)[18]. Tests on a single cylinder engine with CR of 18.7 showed that ignition delay increased by a factor of about 2.5 as EGR increased from zero up to 65% [18, 33]. However if the levels of EGR are too high, combustion quality can deteriorate and efficiency may suffer, which results in practical EGR rate limits.

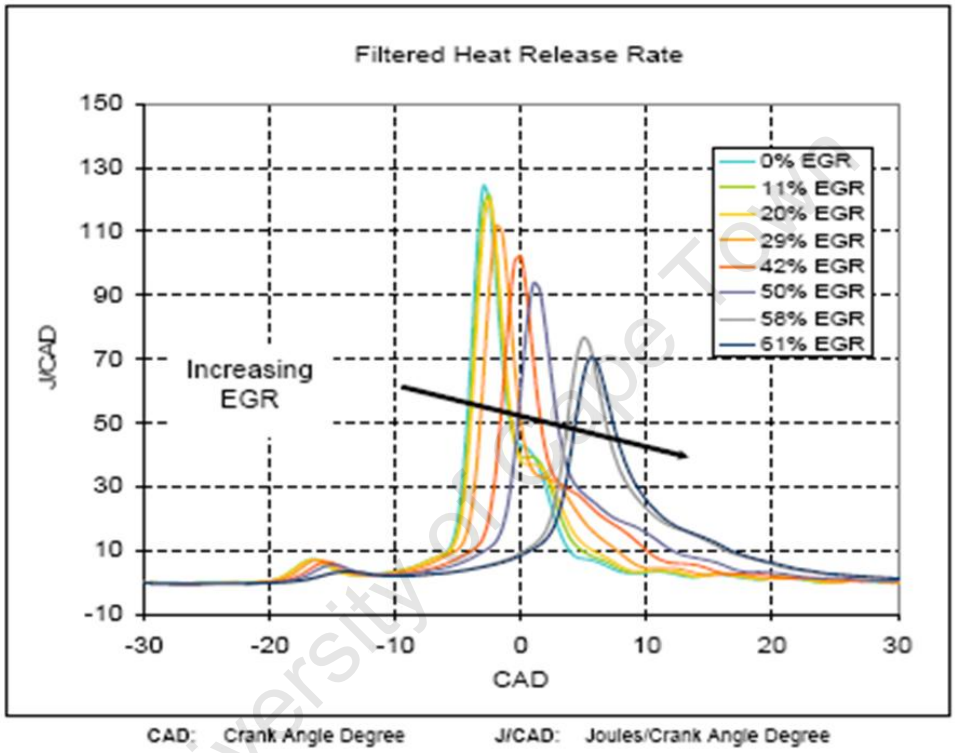

Figure 3.3: Effects of EGR on Ignition Delay [34]

Tests on a gasoline engine of CR 7.9 [18, 35], intake air was required to be heated to at least 400K to enable auto-ignition without the use of EGR. However, use of negative valve overlap allowed up to 60% internal REG, and HCCI combustion was achieved without heating the intake air.

3.3.4 Inlet Manifold Temperature Control

HCCI combustion is dominated by chemical reactions and hence the intake charge temperature plays an important role in affecting combustion phasing. Inlet manifold charge temperature control results in control of mixture temperatures pre-compression and is thus a powerful control for combustion phasing [36, 8]. Lu, Chen and Huang [32] showed that increased inlet manifold temperatures increased combustion cycle temperatures and hence advanced ignition timing. The case in which fuels exhibit this behavior is dependent on fuel type and whether operation is within the fuel's Negative Temperature Coefficient (NTC) region.

Aleiferis [18, 35] performed tests on a gasoline engine of CR 7.9 and required an intake air temperature of at least 400K to enable auto-ignition. Persson and Johansson [36] utilised a combination of intake temperature control (288K - 323K) and negative valve overlap to attain HCCI combustion in a 6-cylinder Volvo engine. The Engine was operated under a spark assisted mode at higher loads with a maximum attainable IMEP when operating in HCCI mode of 2.8 bar. Operation in Spark-assisted mode, when using standard gasoline, showed that an increase in inlet temperature resulted in increased NO_x emissions, reduced specific CO and HC emissions and reduced ISFC.

Aroonispoon and Foster [8] also researched the impact of intake temperature control (300K - 400K) on HCCI combustion, using a CFR single cylinder research engine, while also investigating the affects of engine speed and fuel composition. When using PRF 91.8, maximum IMEP achieved was approximately 3.8 bar - however this was achieved at a higher intake temperature when compared to Persson and Johansson's research.

3.3.5 Variable Compression Ratio

Variable Compression Ratio (VCR) is a control system that is one of the key aspects of HCCI combustion control. The ability to alter the compression ratio on-the-fly provides a high degree of control over the combustion phasing, however such systems are difficult to perfect especially for transient operating cycles.

Lowering the compression ratio can be used to delay ignition timing, slow heat release rates and reduce pressure rise rates [37] to an acceptable level which is approximately 10 bar/CAD [8, 9, 10].

Spark ignition engines are limited to compression ratios lower than the optimum to avoid knocking, while diesel engines require compression ratios higher than the theoretical optimum to assure good cold start performance [18].

Higher compression ratio's are required to obtain auto-ignition temperatures of high-octane fuel without excessive inlet air heating and excessive exhaust residuals, which is an important fact when designing production engines. Figure 3.4 illustrates the effect of altering compression ratio on the ignition delay of PRF40 and n-Heptane as investigated by Machrafia and Cavadiasab [38].

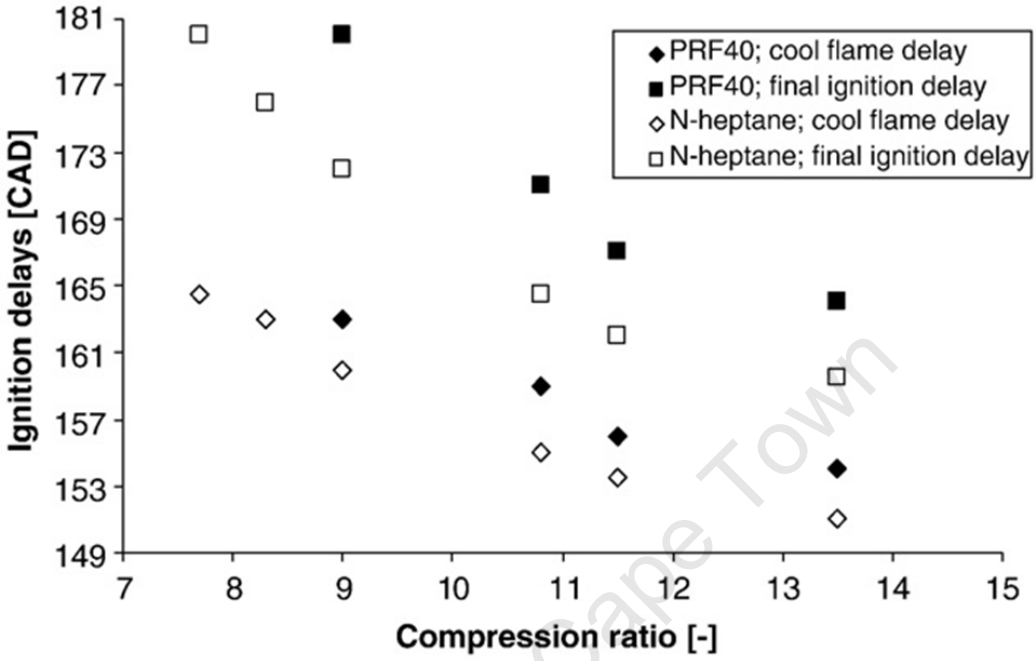

Figure 3.4: Effect of Compression Ratio on Ignition Delay [38]

Engines such as the SAAB Variable Compression Ratio engine have the ability to alter the CR from 8:1 to 14:1 [39]. Increasing Compression Ratio improves engine thermodynamic efficiency up to a certain point after which further gains attributed to increasing compression ratio's are negated by increased pumping losses and mechanical friction. An increase in the compression ratio results in an increase in the thermal efficiency. This relationship is shown by the thermal efficiency for an isentropic Otto cycle [40]:

$$w_{net} = q_{in} - q_{out} \tag{3.1}$$

$$\frac{T_1}{T_2} = \frac{T_4}{T_3} \; using \; isentropic \; relationships \tag{3.2}$$

$$\begin{aligned} \eta_{th,Otto} &= \frac{work_{net}}{q_{in}} \\ &= 1 - \frac{q_{out}}{q_{in}} \; Substituting \; Equation \; 3.1 \\ &= 1 - \frac{T_4 - T_1}{T_3 - T_2} \; Substituting \; Equation \; 3.2 \\ &= 1 - \frac{1}{r^{k-1}} \end{aligned} \tag{3.3}$$

Where:

1. $T_{1,2,3,4}$ = Gas temperatures at start of compression, start of combustion, end of combustion, end of expansion respectively
2. r = Compression Ratio = V_{BDC}/V_{TDC}
3. k = Gamma, which is the ratio of specific heats Cp/Cv

A single cylinder engine test program by Ogawa [18, 41], evaluated performance in a diesel engine where the compression ratio was changed by fitting pistons with different bowl volumes. They found that the range of smokeless operation with very high EGR (62%) was improved at compression ratios lower than the standard 18:1, although at the cost of slightly lower thermal efficiency (Figure 3.5). The benefits of lower compression ratio were attributed to better mixing, because of the longer ignition delay, and lower in-cylinder temperatures. A similar effect has been seen in HCCI engines based on an early fuel injection strategy. Colliou [18, 42] found that reducing compression ratio led to an increase in the area of HCCI combustion, but noted an increase in fuel consumption and some impacts on cold start performance.

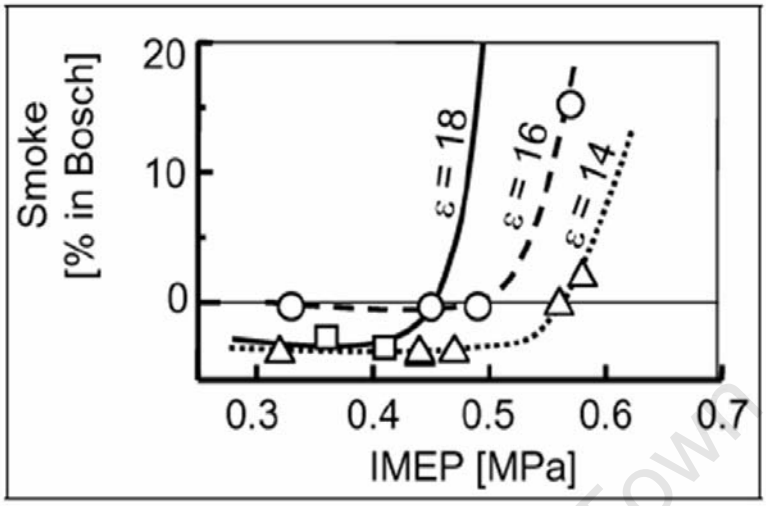

Figure 3.5: Lower Compression Ratio Allows High Load Operation [41]

Chen and Mitsuru [37] utilised a single cylinder engine and gauged the effects of compression ratio (12 - 28:1) on HCCI combustion. Testing was conducted using a blend of methane and Dimethyl Ether (DME) and a supercharger was added to the engine to increase power output. Conclusions from the study suggested that the possible operating range in terms of ϕ is dependent on compression ratio. It was also concluded that the ignition timing of HCCI combustion can be effectively controlled by altering the compression ratio. [37]

Hyvonen, Haraldsson and Johansson [39] combined inlet air heating with a VCR system to achieve and control HCCI combustion. A Naturally Aspirated (N.A) four-stroke Saab Variable Compression engine with CR 9 - 21:1 and Port Fuel Injection (PFI)system was used. Testing was conducted using both primary reference fuels (PRF) and gasoline, with inlet temperatures being maintained above 450 K at all engine speeds. Engine operation in HCCI combustion mode was achievable over a load range of 0 to 3.6 bar BMEP and an operational speed range of 1000 to 5000 rpm [39].

3.3.6 Inlet Manifold Boosting by Either Turbo/Supercharging

Inlet boosting by either Turbo/Supercharging increases in-cylinder charge density. The increased density allows for increased allowable fueling - when the charge is kept at the same ϕ. Inlet boosting can provide HCCI with a significant power boost. Boosting with high EGR rates increases IMEP, which is a result of increased fueling and compression pressure. Boosting has been shown to increase the HCCI load range but is then limited by engine knock [37].

The ability to vary manifold pressures, allows for the control over cylinder post-compression pressures. Boosting can be used to ensure that engine operation is within minimum required pressures for fuel auto-ignition, allowing for the use of a variety of fuels and preventing engine misfire. Practically, boosting could be used to increase power output and when coupled with a VCR system can be used to control the ignition timing. The advantage of boosted HCCI operation is lean-combustion with low BSFC as well as possibility of engine "'downsizing"' and engine load map extension [43].

Chen and Mitsuru [37] utilised Supercharging in the range of 0 - 200 kPa on a Diesel Engine with compression ratio capability of 12.2 - 27.8. Boosting resulted in increased IMEP in the range of 25% and was limited to engine knock with a general equivalence ratio for best HCCI combustion being 0.4, when using a fuel blend of methane and DME (Dimethyl Ether).

Sjoberg and Dec [44] investigated the possibilities of utilising EGR and intake boost for the management of HCCI heat-release. One cylinder of a Cummins B-series diesel engine was used, with a volume of 0.98l and a CR of 14:1. The study found that intake boost-control can be used very effectively to control the amount of LTHR as the engine speed is changed. This allows for engine operation with a constant inlet temperature, T_{in}, across a wide engine-speed range (600 - 2400rpm). This is advantageous because the amount of LTHR increases with intake pressure and can eliminate the need for rapid T_{in} control [44]. It was also noted that IMEP increased at higher engine speeds, a consequence of increased inlet pressure while maintaining constant ϕ.

3.3.7 HCCI Control by Fuel Design

"An HCCI engine can be operated on a wide range of fuels, but the fuels have different properties which have significant effects on the operation range. Fuel properties should be such that the engine can run in HCCI mode both at low and high load. Since the benefits with HCCI decrease at high load, the fuel could be used for SI operation. Octane numbers, Research Octane Number (RON) and Motor Octane Number (MON), are used to characterize fuel for SI engines and cetane number to characterize fuel for CI engines. Whereas RON, MON and cetane may have limited relevance to characterize HCCI combustion, it remains important to find effective characterisation methods of HCCI fuel properties. HCCI engines have fuel requirements that differ from other engines. A fuel specification of HCCI combustion should be developed and it should be noted that fuels with similar octane numbers may result in different HCCI combustion". [2]

One of the advantages of HCCI combustion is its intrinsic fuel flexibility. HCCI combustion has little sensitivity to fuel characteristics such as lubricity and laminar flame speed. Fuels with any octane or cetane number can be burned, although the operating conditions must be adjusted to accommodate different fuels, which can impact efficiency. An HCCI engine with VCR or VVT could, in principle, operate on any hydrocarbon or alcohol liquid fuel, as long as the fuel is a homogeneous mixture, that being vaporized and well mixed.

HCCI combustion is dominated by local chemical-kinetic reaction rates, with no requirement for flame propagation. Chemical kinetics modeling of HCCI combustion has concluded that HCCI ignition is controlled by hydrogen peroxide (H_2O_2) decomposition. Hydrogen peroxide decomposes into two OH- radicals, which are very efficient at releasing the fuels energy. Hydrogen peroxide decomposition occurs at a temperature range between 1050K and 1100K. This fundamental chemistry of HCCI autoignition and combustion is identical to the chemistry of knock in spark-ignition engines. With high-octane fuels, little heat is released prior to this main ignition event at 1050-1100 K; however, with low-octane fuels (e.g. diesel fuel) significant heat-producing reactions begin at temperatures of about 800 K. However, the amount of energy liberated is too small to be considered ignition. These low-temperature reactions quickly drive the mixture up to the autoignition temperatures for the peroxide heat release [1].

CHEMKIN^{TM}studies shown below present the fuel chemistry for two fuels: n-heptane 3.6(a) and iso-octane 3.6(b), which are the chemical surrogates of diesel and gasoline fuel respectively. The figures show the differences between the two fuels. For n-heptane a cool flame reaction is clear and shows two stage auto-ignition. In contrast, iso-octane allows for compression to higher temperatures while exhibiting single stage combustion [1].

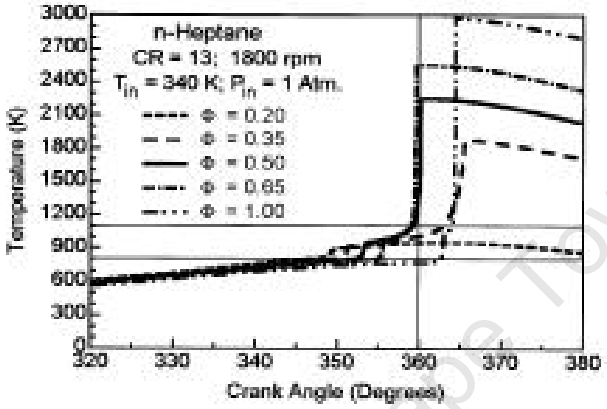

(a)CHEMKIN calculations showing the effect of changes in fuel load on HCCI combustion using n-heptane

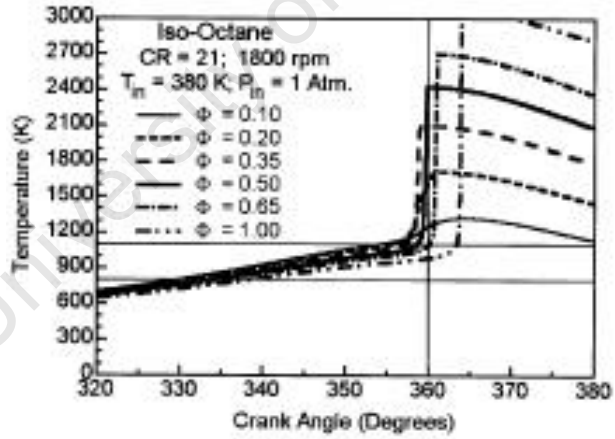

(b)CHEMKIN calculations showing the effect of changes in fuel load on HCCI combustion using iso-octane

Figure 3.6: CHEMKIN calculations showing the effect of changes in fuel load on HCCI combustion using PRF Fuels (a), (b) [1]

The compression to higher temperatures allows for higher compression ratios when using gasoline type fuels. An increase in the compression ratio results in increased thermal efficiency as was discussed in Section 3.3.5.

Lu, Chen, Hiu and Huang [45] performed HCCI combustion testing using various PRF blends of n-heptane and iso-octane. A four-stroke high speed direct injection (DI) diesel engine was used with a compression ratio of 18.5:1. Several of the results obtained are shown in Graph 3.7 below, illustrating changes in ignition delay, peak pressure, heat release and combustion duration with varying RON and observed trends noted in Table 3.3.

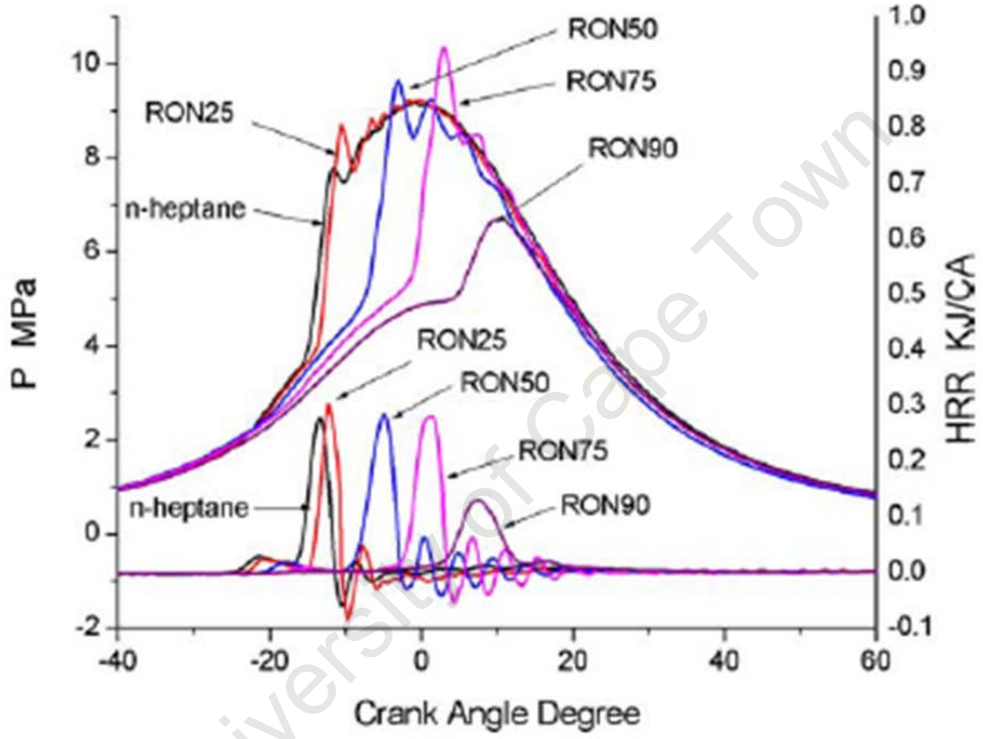

Figure 3.7: Effects of RON on HCCI Combustion [45]

Table 3.3: Observed Effects of Increased RON on Combustion [45]

Ignition Delay	Retarded
Peak Pressure	Various changes depending on PRF blend used
Maximum Heat Release Rate	General decrease in maximum heat release rate
Combustion Duration	Shortens
Cool Flame Heat Release	Reduced

3.3.8 Summary of HCCI Control Strategies

A summarised Table 3.4 of HCCI Control Strategies with respect to their advantages and application difficulties can be seen below:

Table 3.4: Evaluation of HCCI Control Strategies [46]

Strategy	Advantage	Disadvantage
VCR	Wide Operating Range	Difficulty Implementing
Hot Residuals	low CR	small range, low gamma
EGR	Low Cost	small range, low gamma
Intake heating	wide range	thermal inertia
Inlet Boosting	higher load	high peak pressures
Stratified Charge	low CO at idle	high load NOx
DI timing	fast control	small range, NOx and PM emissions

3.4 HCCI Engine Out Emissions

3.4.1 NOx Emissions

Currently, NOx engine out emissions are high for both S.I and C.I engines. Aftertreatment systems such as three-way catalysts have been used successfully to reduce S.I engine emissions, provided the engine operates at a stoichiometric AFR.

NOx formation is governed by the Zeldovich mechanism where nitrogen and oxygen from the air combine to form NO at high temperatures (see Equations 3.4, 3.5 and 3.6 below). The forward rate constant for Equation 3.4, and reverse rate constants for Equation 3.5 and Equation 3.6 have large activation energies. The large activation energies mean that the reaction is extremely temperature sensitive. This causes the present NO to freeze, such that the reaction rates slow down to a rate which produces negligible change in a given timescale, as combustion gases cool and eventually become NO_2.

$$O + N_2 = NO + N \tag{3.4}$$

$$N + O_2 = NO + O \tag{3.5}$$

$$N + OH = NO + H \tag{3.6}$$

HCCI combustion can produce very low levels of NO. The reduced NO formation makes NO formation pathways important. It has been estimated that half of NO at these conditions come from alternative formation pathways other than that expressed by the Zeldovich mechanism. It is therefore important to reduce combustion temperatures to avoid thermal NO formation and lower NOx emissions [18].

Lu, Chen, Hou and Huang [45] obtained NOx emissions up to 60ppm when performing tests on various PRF fuel blends when using a four-stroke high speed DI diesel engine with CR 18.5:1. Sjoberg and Dec [44] attained NOx emissions below 1ppm when testing the effects of EGR and inlet manifold boosting on HCCI combustion using a Cummin B-series diesel engine with CR 14:1.

EGR is an effective means of controlling NOx emissions. The exhaust gas acts as an inert diluent, which will reduce combustion temperatures and

hence directly control NOx formation. EGR effects on NOx formation can be seen in Figure 3.8 below which was obtained from tests performed on 1.0-lire single cylinder DI engine with CR 16:1 [18].

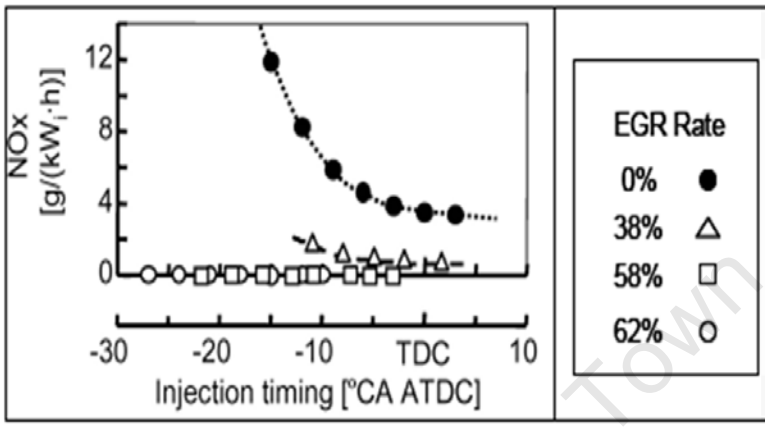

Figure 3.8: Effects of EGR on NOx Emissions [18]

3.4.2 Particulate and Soot Emissions

Formation of soot primarily a function of mixture preparation. Thus, gasoline PFI engines have low soot emissions due to the air and fuel mixture being almost homogeneous. Diesel Engines, although operating at a lean AFR possess rich fuel pockets due to the nature of the combustion and hence produce high amounts of soot in the early combustion stages, with most being oxidized as combustion progresses.

In HCCI combustion, the fuel is injected very early in the cycle resulting in a homogeneous mixture. This allows for significant mixing before ignition occurs, avoiding the very rich conditions where soot can form [18].

3.4.3 HC and CO Emissions

In HCCI combustion, "where excess oxygen is reduced and temperatures lowered to reduce PM and NOx emissions, conditions for complete oxidation of the fuel are much less favourable and virtually all studies of HCCI combustion have reported significant HC and CO emissions. It therefore seems inevitable that HCCI engines will require an oxidation catalyst to reduce emissions. In some cases, however incomplete combustion can be sufficient to have an impact on the engine's overall efficiency." [18]

The HC emissions are the result of incomplete combustion of the mixture caused by the low combustion temperatures. The low temperature makes HCCI combustion sensitive to flame quenching at the combustion chamber walls and cylinder crevice volumes [47].

The source of CO is fuel that oxidizes late enough for the mixture to "freeze" before CO is further oxidized to CO2. The formation of CO is temperature dependent and a higher temperature will allow for full oxidation of CO to form CO_2. CO emissions formation decrease when the combustion phasing is advanced due to higher combustion temperatures and longer time for oxidation [47].

Sjoberg and Dec [44] recorded maximum CO emissions at 2% when investigating the effects of EGR and inlet manifold pressure on HCCI combustion. Tests were performed on a Cummins B-series diesel engine, where testing was performed using one cylinder with a CR of 14:1 and displacement of 0.9L.

Lu, Chen, Hou and Huang [45] obtained CO emissions of between 0.05% to 1% when performing emissions measurements on various PRF blends. Testing was conducted using one cylinder of a four-cylinder, four-stroke high-speed direct injection diesel engine. The cylinder possesses a displacement of 0.78L and a CR of 18.5:1.

3.5 Typical HCCI Operational Limits

3.5.1 Conventional HCCI Operation

A classical HCCI engine aspirates and compresses a homogeneous air-fuel mixture (like a carburettor or port injected gasoline engine). The mixture is auto-ignited purely by compression of the piston with no external ignition control mechanism. The bulk combustion of the mixture results in low temperature combustion which can potentially lower NOx formation [11]. The homogeneity of the combustion also decreases particulate formation as there are no locally rich zones to initiate particulate formation [11]. HCCI combustion allows for leaner, more thermally efficient combustion and is not limited to near stoichiometric AFR [1]. The entire mixture in an HCCI engine has a nominally identical air-fuel ratio and thus burns more uniformly, unlike a diesel which may have a lean bulk air-fuel ratio with locally rich areas. HCCI engines also have the ability to operate without a throttle (like a diesel) which eliminates pumping losses at part-load and increases efficiency.

HCCI has been demonstrated to work under laboratory conditions achieving low emissions and good efficiency under steady state operation, however technical challenges arise when attempting to extend this performance to transient operating conditions.

Primary technical challenges with HCCI development are: [2]

- Combustion phasing control
- Rapid heat release rates and noise level with possible engine damage especially at higher loads
- Transient operation difficulties
- Excess CO and HC emissions, particularly at light loads
- Increased NOx at high loads
- Cold Start difficulty
- A narrow operation range (as result of the above)

The operating range limits are defined by the following factors:

- **Low Load**: lean operation results in low combustion temperatures as compared to near stoichiometric AFR's and can result in engine misfiring. This leads to excess CO and HC emissions.
- **High Load**: increased burn rates results in high pressure rise rates and engine knock
- **Low-speed**: the time-effect on auto-ignition delay can advance combustion phasing causing high pressure rise rates and may result in engine knock
- **High-speed**: the time effect on auto-ignition delay can retard combustion phasing and may result in engine misfire

Transient HCCI operation is difficult due to the availability of combustion control strategies for engine speed and load control. Varying the speed or load can often simultaneously affect any number of critical factors such as air-fuel ratio, inlet pressure or the residence time of reactants. Each of these factors (and others) effect the combustion chemistry kinematics and auto-ignition reactions. The result is that it is often difficult to utilise available control strategies to obtain optimum operating conditions for one point and match the optimum operating conditions at another point [4, 2, 48].

Aroonispoon, Foster, Morikawa and Iida [8] investigated the affects of engine speed on HCCI operation using PRF 70. Engine tests were performed on a single-cylinder Cooperative Fuels Research (CFR) engine with variable compression ratio of 4 - 18:1. The effects of engine speed on HCCI operation can be seen in Figure 3.9 below.

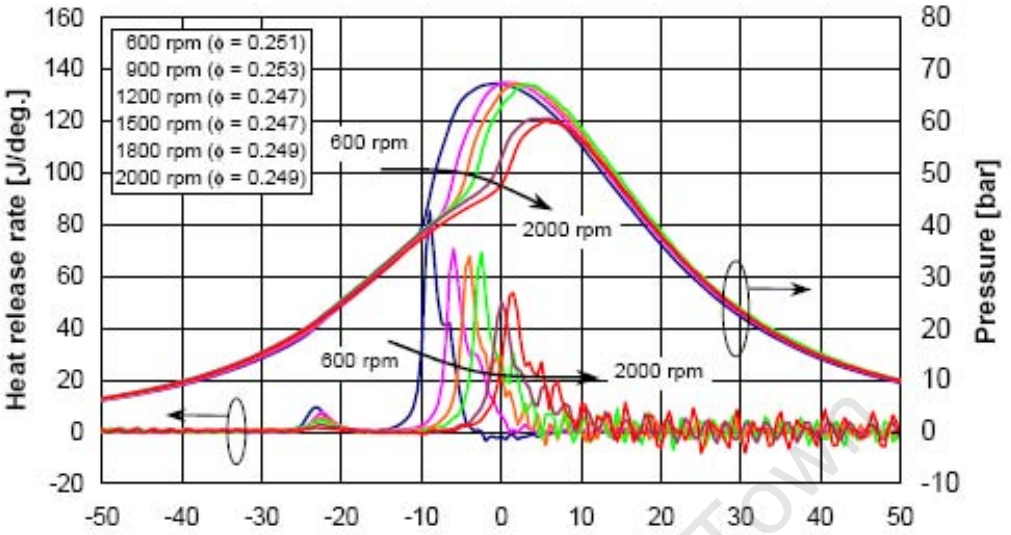

Figure 3.9: Pressure and Heat Release vs Engine Speed. CR 16.55, Phi = 0.25, Tin = 320K

As engine speed increase the combustion phasing of the main energy heat release retards. Additionally, an increase in engine speed reduces the cool flame heat release. Since HCCI autoignition process is largely kinetically controlled, the combustion process is largely time dependent. Thus, as the engine speed increases, the number of crank angles per second increases.

3.5.2 HCCI "sweet spot" Operation

The HCCI operational speed range is typically limited due to combustion phasing requirements [2, 49, 50, 51, 52, 53]. Combustion phasing is generally retarded to the point of instability at high speed operation limits and advanced to the point of excessive pressure rise rates and excessive pumping work at low speed operation limits unless phasing is corrected by changes to other parameters [54, 55]. However, it is also known that at low engine speeds, heat losses to the combustion chamber walls result in decreased peak pressures and temperatures [44, 56]. In the extreme isothermal compression case, autoignition would never take place due to insufficient temperature required to initiate combustion even within the time scales of the isothermal process. Since high engine speed results in retarded phasing, low speed in advanced phasing and ultra low speed in ultra retarded phasing, it stands

to reason that there must exist a speed range where phasing is relatively independent of engine speed changes. This speed convergence behaviour has been noticed in experimental work conducted by Sjberg and Dec [49, 56].

This phenomenon has been researched at the SASOL Advanced Fuels Laboratory where a single zone explicit discrete engine model was formulated [49]. The purpose of the model was to be capable of accurately simulating combustion chamber trapped gas thermodynamic histories as well as the effects of engine configuration and operational changes on these histories without the need for numerical solving techniques. This enabled easy assessment of trends in effects and rapid identification of optimal configurations of the many variables and was merely aimed at identifying operational trends in HCCI combustion.

Limited experimental validation was completed using a single cylinder Ricardo E6 engine with 507 cm^3 displacement. The engine possesses variable compression ratio of 6 - 20:1. The naturally aspirated engine had been modified to incorporate a port fuel injection system with inlet air heating (313 K) used to aid fuel evaporation. The engine was run using n-heptane at 600, 1200 and 1800 rpm and lambda values of 2.0, 2.5, 3.0, and 3.5. The higher engine speeds caused knocking and instability at the lower lambda values.

Conclusions from the study suggested that operational zones exist where fuel equivalence ratio can be varied independently of combustion phasing without phasing correction adjustment of other variables. Additionally the formulation of HCCI modelling can also be used to find fixed constant combustion phasing lines that run through the speed-load map from low speed and low load to high speed and high load, much like a propeller speed-load line (similar to that in [4]). This methodology can be used to determine an engines optimum operating range prior to experimental work and allow for better control over HCCI combustion phasing as well as required combustion control strategies. The study noted that engine configuration, such as cylinder size, plays an important role in determining the fuel ignition quality of an HCCI engine. Thus, the engines configuruation will strongly influence the speed range where speed can be varied without affecting combustion phasing [49].

3.5.3 Previous Small HCCI Engine Research

At the SASOL Advanced Fuels Laboratory, a standard issue two-stroke 6.5cc model-aero diesel engine (Figure 3.10) was found to operate using HCCI combustion [4]. This type of engine is of particular interest largely because it operated as a self-regulating HCCI engine over a wide range without any undesirable effects such as engine knock or misfire. This engine, unlike the more common glow-plug versions, operates without any form of combustion initiator. Fuel and air are premixed using a simple carburettor and ignited by piston compression only, thus the engine operates in HCCI mode even though it is referred to as a model diesel engine.

The engine was operated using a standard model aeroplane fuel blend (D1000), which includes Castor Oil in the fuel to act as a lubricant. The fuel possesses a cetane number of approximately 93 [4]. The fuels components are shown in Table 3.5 below.

Table 3.5: Model Aeroplane Fuel Components - D1000

Component	**% Volume**
Kerosene	35%
Diethyl Ether	35%
Castol Oil	28%
Isopropyl Nitrate	2%

Figure 3.10: P.A.W Model Aero-"Diesel" Engine

The engine possessed the ability to alter the compression ratio "on the fly", however this ability was not utilised and the CR was preset when performing engine testing. The CR was altered using an installed compression ratio (CR) screw, shown in Figure 3.11. This adjusted the cylinder head's relative position within the cylinder, thus altering the cylinder's clearance volume. CR alterations were used extensively during testing to optimise engine operation and extend the engine's operational envelope.

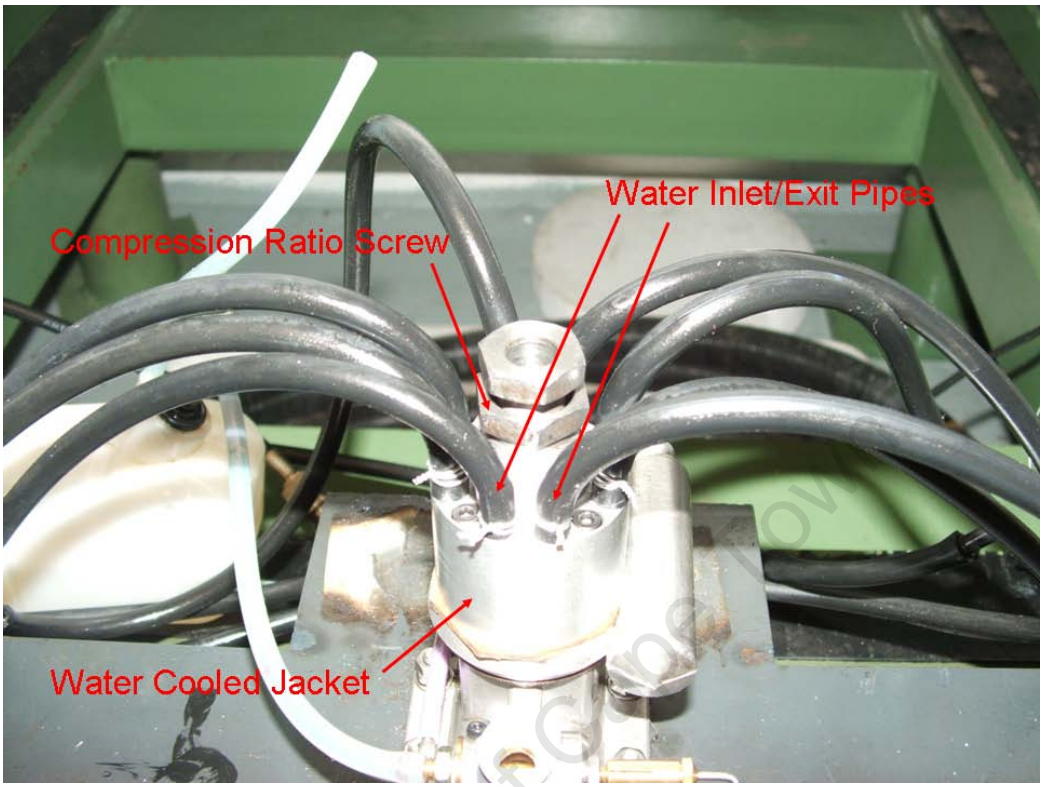

Figure 3.11: PAW Engines Compression Ratio Screw and Water Jacket

The engine was shown to run from idle through a fixed speed-load curve, using propellers, to the maximum speed and load point of the engine at 11000rpm and stoichiometric air-fuel ratio. Nominally constant combustion phasing was achieved without any form of combustion control system.

As a result of testing, the engines operational envelope is shown in Figure 3.12. The figure illustrates the engine's ability to operate along a fixed speed-load curve as was provided using various characterised propellers.

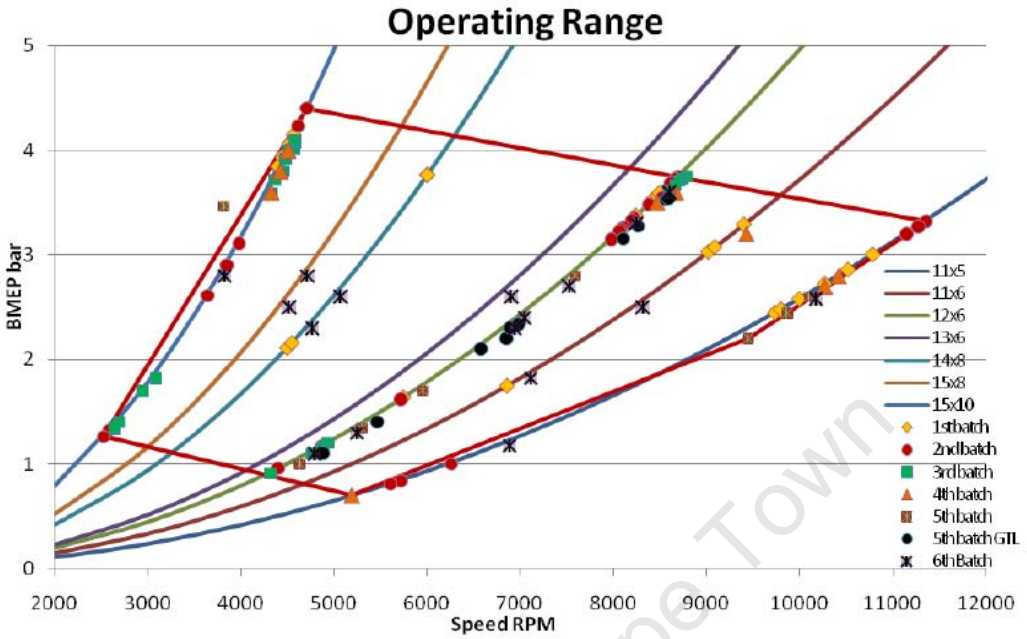

Figure 3.12: PAW Model Aeroplane Engine Operational Envelope [4]

Operation was possible at high load points across the speed range with extremely conservative pressure rise rates. Furthermore, engine knock (high pressure oscillations) was not experienced during normal engine operation. This posed questions with respect to the possibility of similar full scale HCCI engine operation and the role of engine size and fuel requirements in obtaining HCCI operation over a wide load range. Table 3.6 summaries the operational capabilities found during research [4].

Table 3.6: PAW Model Aeroplane Engine Operational Characteristics

Operational ϕ Range	0.71 - 1.05
Operational Speed Range (rpm)	2500 - 11300
Engine Compression Ratio	8 - 20.5:1
Max Operational Pressure Rise Rate (bar/CAD)	18

During engine testing it was noted that the engine displayed approximately constant phasing as the throttle was closed from maximum speed for a given propeller. Closing of the throttle lowers the speed (advances timing), decreases fueling (and hence, load which retards timing) and increases exhaust residuals (which retards timing). It was suspected that the engine possessed some natural compensation to control what would otherwise be changing combustion phasing which allowed it to operate comfortably at

various loads at speeds using a fixed engine configuration, which is a characteristic not usually associated with classic HCCI engines. With the engine optimised for maximum power using a given propeller it was possible to lower the speed (and hence load) of the engine by closing the throttle. The engine's "natural compensation" ability was affirmed as shown in Figure 3.13.

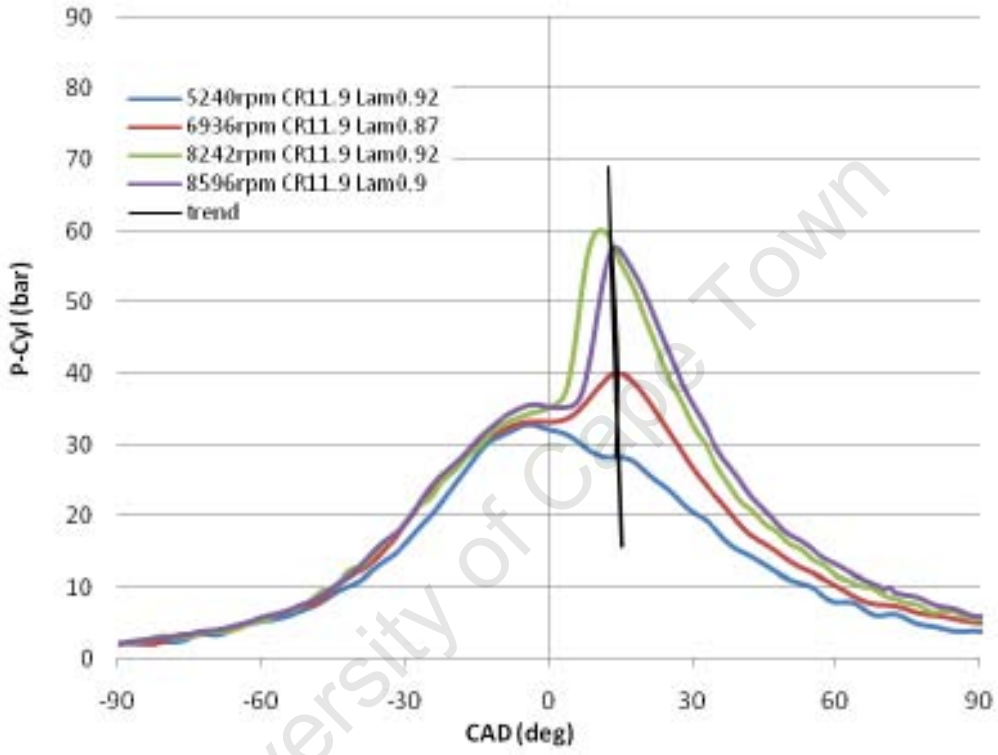

Figure 3.13: PAW Engines Pressure Traces Showing Natural Combustion Phasing Compensation [4]

Chapter 4

Modeling HCCI Operation

4.1 Singe-Zone Engine Model

Analysis tools for HCCI, such as a detailed chemical kinetic modeling mainly utilise single-zone models. Single-zone models assume that the combustion chamber is a well stirred reactor with uniform temperature, pressure and composition. This analysis method is applicable to HCCI engines where mixing is not a control factor. A single-zone model can be used to evaluate a variety of fuels and conditions when operating in HCCI mode due to the accuracy in predicting start of combustion if the cylinder conditions at the beginning of the compression stroke are well known. However single zone modeling limitations are [57]:

1. Over prediction of peak cylinder pressures as result of model inaccuracies such as combustion chamber heat transfer characteristics as well as fluid dynamic effects on HCCI combustion. Additionally, the utilisation of a single Wiebe function is not able to match the slower combustion in the cooler boundary layer adjacent to the walls and the faster combustion in the hot core [7].

2. Over prediction of NOx emissions as result of over predicted cylinder pressures and temperatures.

3. Inability to predict HC and CO emissions due to the exclusion of the formation mechanisms when using a single zone-model.

4.2 Heat Transfer Modeling

As has been stated previously, HCCI combustion occurs throughout the cylinder and is described as a bulk combustion, with the combustion process being governed by chemical kinetics. Hence, turbulence and mixing rates have a smaller effect on HCCI combustion while the in-cylinder thermal conditions have a critical impact on ignition timing and burn rates when compared to CI and SI engines. The need arises for an accurate heat transfer model for HCCI engines, due to the in-cylinder thermal conditions being closely tied to heat transfer to the cylinder walls. Forced convection from the gas to the cylinder walls is the dominant heat transfer mechanism in HCCI engines. Thus, heat transfer plays an important role in modeling with respect to prediction of ignition timing, peak cylinder pressures as well as pressure rise rates and cylinder gas temperatures in HCCI engines [5].

The global heat transfer coefficient can be written as [5] (u, b indicated unburned and burned zones respectively):

$$h_{global}(t) = \alpha_{scaling}.L(t)^{m-1}.\frac{k}{\mu^m}.p(t)^m.T(t)^{-m}.v(t)^m \quad such \ \ that \tag{4.1}$$

$$\dot{Q}_{loss} = A_{u/b,w} h_{c,u/b}(T_u/b - T_w) \tag{4.2}$$

- $A_{u,b}$ is the area unburned/burned
- $h_{c,u/b}$ is the heat transfer coefficient for the unburned/burned zone
- $T_{u/b}$ is the temperature in the unburned/burned zone

The global heat transfer coefficient (h_{global}(t)) depends on engine characteristics such as length, transport properties, pressure, temperature and characteristic velocity. $\alpha_{scaling}$ is used to match specific engine geometry and the exponent m has been proposed by several different authors, m = 0.5 for Elser and Oguri, 0.7 for Annand and Sitkei, 0.75 for Taylor and Toong and 0.8 for Woschni and Hohenberg [5].

The Woschni Heat Transfer Correlation is a commonly used model for predicting engine heat loss in HCCI engines, although this model was proposed originally for CI engines. Woschni argued that the average gas velocity

during the intake, compression and exhaust strokes should be proportional to the mean piston speed. Woschni also attempted to account directly for the gas velocities induced by the change in density that results from combustion, which are comparable to the mean piston speed. This resulted in a term being proportional to the pressure rise due to combustion being added. [11]

The Woschni Heat Transfer Correlation is shown by Equations 4.3, 4.4 below.

$$v = [C_1 S_p + C_2 \frac{V_d T_r}{p_r V_r}(p - p_m)] \tag{4.3}$$

$$h_c(W/m^2.K) = 3.26 B(m)^{-0.2} p(kPa)^{0.8} T(K)^{-0.55} v(m/s)^{0.8} \tag{4.4}$$

Where:

- B = Characteristic length usually cylinder bore
- v = Local average gas velocity
- p = Cylinder pressure
- S_p = Piston sliding speed
- p_m = Motored cylinder pressure
- V_d = Displaced volume
- p_r, V_r, T_r = Working fluids pressure, volume and temperature
- C_1, C_2 are constants depending on what part of the cylinders cycle is being considered

Combustion differences between HCCI, S.I and Diesel engines result in radically different heat loss characteristics. The dominant heat transfer mechanism in HCCI engines is forced convection from the bulk gas to the combustion chamber walls. In S.I combustion, the flame front separates the chamber into a burned zone and a cooler unburned zone and in C.I engines, combustion is so heterogeneous that heat flux probes will only accurately measure heat

flux in close proximity to the probe, making accurate heat transfer modeling difficult [5].

Chang, Guralp, Filipi, Assanis, Kuo, Najr and Rask [5] investigated the effects of heat transfer on HCCI engines, with the aim to improve the Woschni model to better predict heat transfer from HCCI engines. Model validity was confirmed by retrofitting a Ricardo Hydra engine with heat flux probes placed in various positions throughout the combustion chamber and piston.

Heat release analysis was conducted and the heat loss compared to calculated net heat release in an energy balance. An updated model was then compared to other global heat transfer models such as the original Woschni model as well as Hohenberg [58], Annand and Ma [59] relationships.

Research managed to improve the Woschni correlation (see equations 4.5 and 4.6) based on two findings:

1. The new Woschni Correlation, without any term for the gas velocity induced by combustion better captured the heat profile existing in an HCCI Engine
2. Heat transfer models do not have adequate terms accounting for sensitivity in load changes

For the above two reasons an additional term was required to relate the pressure increase during combustion as result of the high pressure rise rates during HCCI combustion. "The new model proposed a new term to capture the effect of combustion-induced gradients on heat flux" [5]. The proposed improved Woschni heat transfer correlation was thus proposed as:

$$h_{new}(t) = \alpha.L(t)^{-0.2}p(kPa)^{0.8}T(K)^{-0.73}v_{tuned}(m/s)^{0.8} \tag{4.5}$$

$$v_{tuned}(t) = C_1 S_p + \frac{C_2 V_d T_r}{6 p_r V_r}(p - p_{mot}) \tag{4.6}$$

Comparison of the two correlations clearly illustrates where modifications were made:

1. The exponent on the temperature term has been changed to 0.73

2. C_2 has been reduced to 1/6 of the original

3. The characteristic bore value (B) has been altered to use an instantaneous combustion chamber height (L), which was found to better predict the heat transfer

4.3 Ignition Delay

Ignition delay is the most significant modeling term that is required to obtain an effective and accurate tool for prediction HCCI operation. Ignition delay affects peak pressures and temperatures as well as the relative CAD position of both these terms. Detailed chemical kinetic modeling is required to accurately model and predict various fuels and fuel blend ignition delays especially in the Negative Temperature Coefficient region (NTC) which in HCCI operation is a fundamental region in accurate modeling of HCCI combustion. Additionally, cool flame modeling is important as many fuels employed in HCCI research exhibit a cool-flame reaction.

The model used for this research has been extensively studied at the SASOL Advanced Fuels Laboratory [60]. The model assumes that the highly exothermic reaction sequence that signifies normal combustion could be represented by an Arrhenius reaction, shown by Equation 4.7, which represents the gross, rate-limiting step.

$$\tau_h = A_h p^{n_h} e^{\frac{B_h}{T}} \tag{4.7}$$

Where:

1. τ_h represents the overall (hot) ignition delay for a stoichiometric constant-volume mixture initially at pressure p and temperature T
2. A_h, n_h and B_h are constants

If the fuel's temperature profile exhibits a distinct cool-flame section, characterised by points (b) and (c) in Figure 4.1, the calculation of the overall ignition delay needs to be taken in two stages which by applying the conservation-of-delay principle by [61] shown by Equation 4.8:

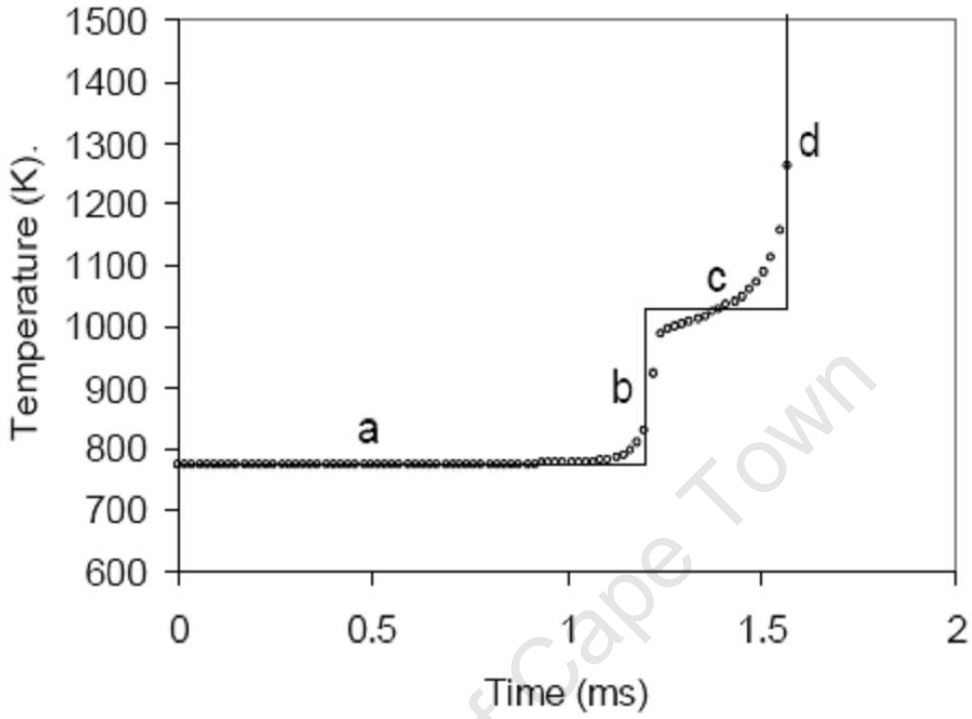

Figure 4.1: Ignition Delay Curve with Cool Flame Ignition Delay

$$\int_{t_0}^{t_1} \frac{dt}{\tau_{h,i}} + \int_{t_1}^{t_2} \frac{dt}{\tau_{h,CF}} = 1 \tag{4.8}$$

Where t_1 is defined by the appearance of the cool flame and t_2 represents the overall ignition delay time i.e of the peroxide reaction. $\tau_{h,i}$ and $\tau_{h,CF}$ represent the characteristic exothermic reaction delay calculated pre and post cool flame respectively. The overall ignition delay t_2 can then be defined as:

$$t_2 = t_1 + \tau_{h,CF}.(1 - \frac{t_1}{\tau_{h,i}})$$

This model also incorporates the affects of changing air/fuel ratio and fuel blending affects, which for this research is critical due to the testing of multiple fuels . Observations in the research performed by [60] indicated that the affects of AFR required two 'β' terms, one for each of the Arrhenius aspects of the model. Therefore Equation 4.9 is the cool flame reaction,

Equation 4.10 and 4.11 are expressions for the main exothermic reactions that represent the reaction before and after the cool flame.

$$t_1 = \phi^{\beta_1} A_1 p^{n_1} e^{\frac{B_1}{T}} \tag{4.9}$$

$$\tau_{h,i} = \phi^{\beta_h} A_h p_i^{n_h} e^{\frac{B_h}{T_i}} \tag{4.10}$$

$$\tau_{h,CF} = \phi^{\beta_h} A_h p_{CF}^{n_h} e^{\frac{B_h}{T_i + X\Delta T_{CF}}} \tag{4.11}$$

In addition, a modified empirical relation that formulates the Cool Flame temperature rise was proposed, defined by Equation 4.12.

$$\Delta T_{CF} = \omega \left(T_i - T_{EQ}.p^{\kappa}.\phi^{\mu} \left(\frac{100}{99 + \phi} \right)^{\phi} \right) \tag{4.12}$$

Where μ and σ would be likely to behave as relatively fixed constants that could be applied for a wide range of PRF fuels. The empirical coefficients used for fuels used in this research can be seen in Table A.3 in Appendix A. These coefficients are incorporated into the thermodynamic engine model and are used to calculate ignition delay - which can then be modified based on air/fuel ratio and varying fuel PRF blends.

Negative Temperature Coefficient (NTC) auto-ignition behaviour is shown by Figure 4.2 below. The expected effects are such that as the initial temperature/pressure increases, the pre-coolflame delay reduces and the associated cool-flame temperature rise also decreases. This results in an overall ignition delay reduction, lengthening and then shortening again as the temperature is progressively increased.

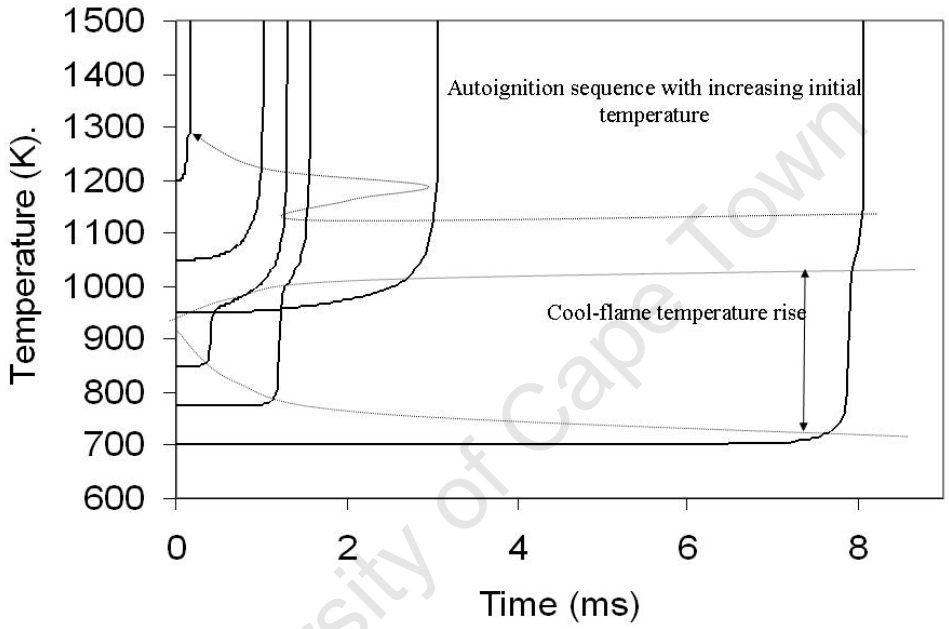

Figure 4.2: Profiles Showing the Effect of Initial Temperature on Ignition Delay of a 2-Stage Ignition in a Constant Volume Combustion Chamber

Chapter 5

Experimental Apparatus and Test Method

5.1 Experimental Apparatus

5.1.1 Research Engine: Honda GX25

A 25cc, single cylinder 4-stroke engine was chosen due to it being the smallest commercially available 4-stroke engine operating with no fuel/lubrication mixing. The manufacturer's engine specifications are shown in Table 5.1 below.

Table 5.1: Manufacturer's Engine Specifications

Engine Designation	**Honda GX25**
Engine Type	4-stroke single cylinder
Bore X Stroke	35 x 26 mm
Displacement	25cc
Compression Ratio	8:1
Fueling	Diaphragm Carburettor
Net Power Output	0.72 kW at 7000 rpm
Net Torque	1.0 N.m at 5000 rpm
Oil Capacity	80cc
Maximum No-load Speed	11 000 rpm
Operational Speed	4000 - 9000 rpm
Inlet Valve Diameter	12.5 mm
Exhaust Valve Diameter	12.0 mm
Valve Lift	2.75 mm
CAD/Tooth on Timing Belt	24 deg

The GX25 possesses two valves, inlet and exhaust, with a single overhead cam and timing belt. The single overhead cam results in a fixed valve lift, fixed relative valve timings - durations between inlet and exhaust valves. However the camshaft timing belt can be offset on the cam thus allowing for flexibility in altering of the valve timing. The measured standard valve lift profiles as well as a retarded valve lift profiles are given in Figure 5.1 below. The valves tappet clearances resulted in slight variances in recording of the valve lift profiles at a desired Crank Angle Degree (CAD). This resulted in a degree of uncertainty in obtaining the exact valve lift profiles.

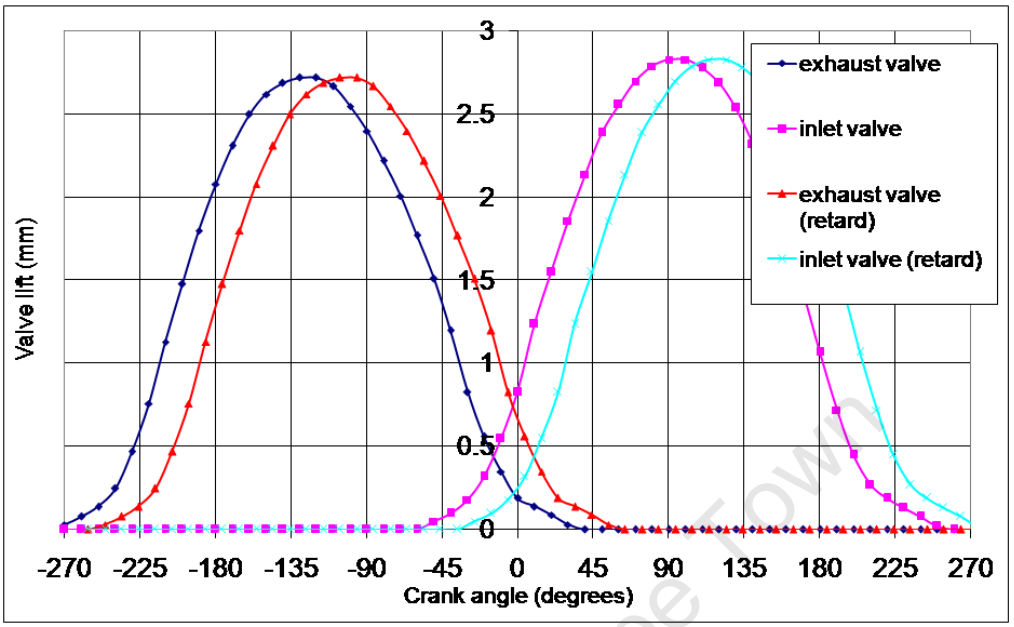

Figure 5.1: Standard and Retarded Inlet and Exhaust Valve Lift Profiles

Figure 5.2 is a cutout of a Honda GX25 engine as was used in this research. The figure shows crankshaft assembly, which consists of two separate shafts press-fitted together with counterweights on either side with support being provided by two bearings. A finned flywheel is located onto a tapered crankshaft. The flywheel is finned to provide air cooling to the engine.

The GX25 utilises a standard diaphragm type carburettor with idle mixture screw to meter the fuel mass flow rate. An oil sump separates the lubricant from the air/fuel mixture, thus allowing better comparison with conventional HCCI engines than the model "diesel" engine, which utilised Castor oil as a lubricant in its fuel.

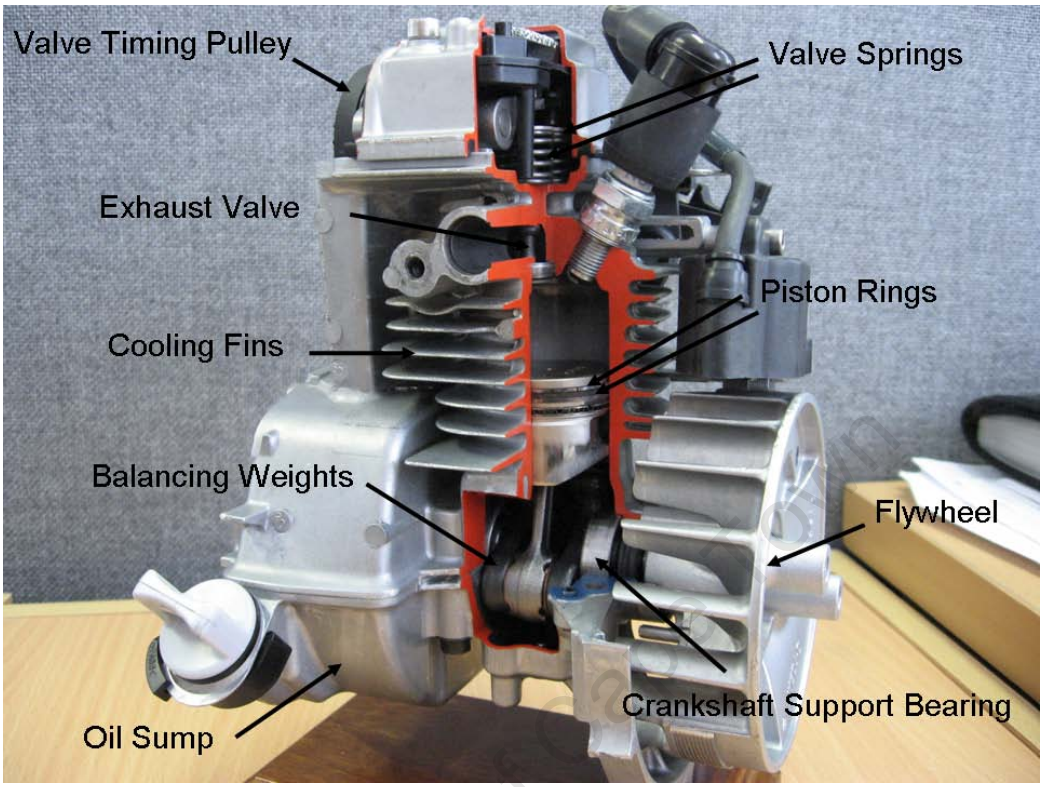

Figure 5.2: Engine Cutout Showing - Valves, Oil Sump, Piston Rings and Crankshaft Assembly

Figure 5.3 shows the mixing blade used for lubrication as well as the positioning of the valve timing belt and the connection of the crankcase to the inlet manifold. Valve lubrication is achieved by a mixing blade in the sump, "splashing" oil into the valve housing utilising a lubrication channel. Crankcase pressure driven by piston motion draws oil through a hollowed crankshaft allowing for piston, bearing and cylinder wall lubrication, with piston rings preventing oil from entering the combustion chamber as well as sealing combustion pressures. Crankcase breathing is achieved by connecting the crankcase to the overhead valve volume and then to the carburettor inlet using a flexible hose; however during operation this port was filtered and then exhausted.

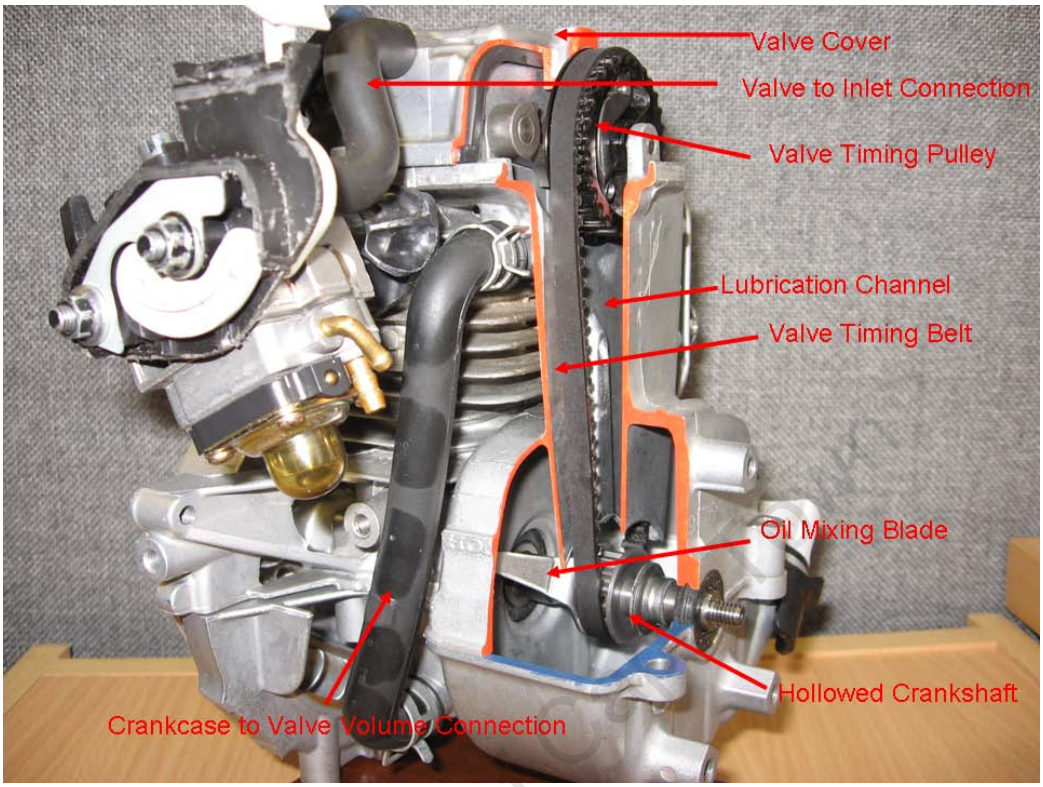

Figure 5.3: Engine Cutout Showing Oil Mixing Mechanism and Valve Timing Mechanism and Lubrication Channel

5.1.2 Test Fuels

The Honda GX25's low compression ratio of 8:1, small displacement and associated high combustion chamber heat loss, necessitated the need for a volatile, high ignition quality HCCI fuel. Primary engine testing was conducted using Diethyl Ether (DEE) as it's volatility and high cetane number (>125 [62]) allowed for operation without excessive inlet heating requirements. Properties of this test fuel are given in Table 5.2 below.

Table 5.2: Diethyl Ether Properties [62], [63]

Property	**Value**
Molar Mass (g/mol)	74.12
Density	0.7134 g/cm^3
Boiling Point (K)	307.75
Autoignition Temperature	160^0 C
Cetane Number	> 125
Stoichiometric Air/Fuel Ratio	11.1
Lower Heating Value (kJ/kg)	33892.15

DEE is a two-stage fuel [64, 65] and was thus expected to exhibit a cool-flame and peroxide autoignition reactions with corresponding Negative Temperature Coefficient (NTC) region.

Further engine testing using n-Heptane was completed in order to model observed engine operational characteristics, such as combustion phasing, heat release rates and combustion chamber heat transfer characteristics. n-Heptane was used due to the availability of thermodynamic and auto-ignition data, which was not available for DEE.

Table 5.3: n-Heptane Properties [66]

Properties	**Value**
Molar Mass (g/mol)	100.203
Density (g/cm^3)	0.682
Boiling Point (K)	371.3
Octane Rating (by definition)	0
ASTM D613 Cetane Number	52.2 ± 4.3
Cetane Number (IQT^{TM})	53.9
Lower Heating Value (kJ/kg)	44566

5.1.3 Engine Mounting

The engine is mounted on a stand with adjustable feet. Engine support consists of two slotted stainless steel plates, connected to the rear and front sides of the engine using pre-existing mounting holes. Additional mounting slots on the plates are used to fix the plates to the stand while also allowing for mounting flexibility and shaft alignment between the engine and dynamometer (see Figure 5.4 below).

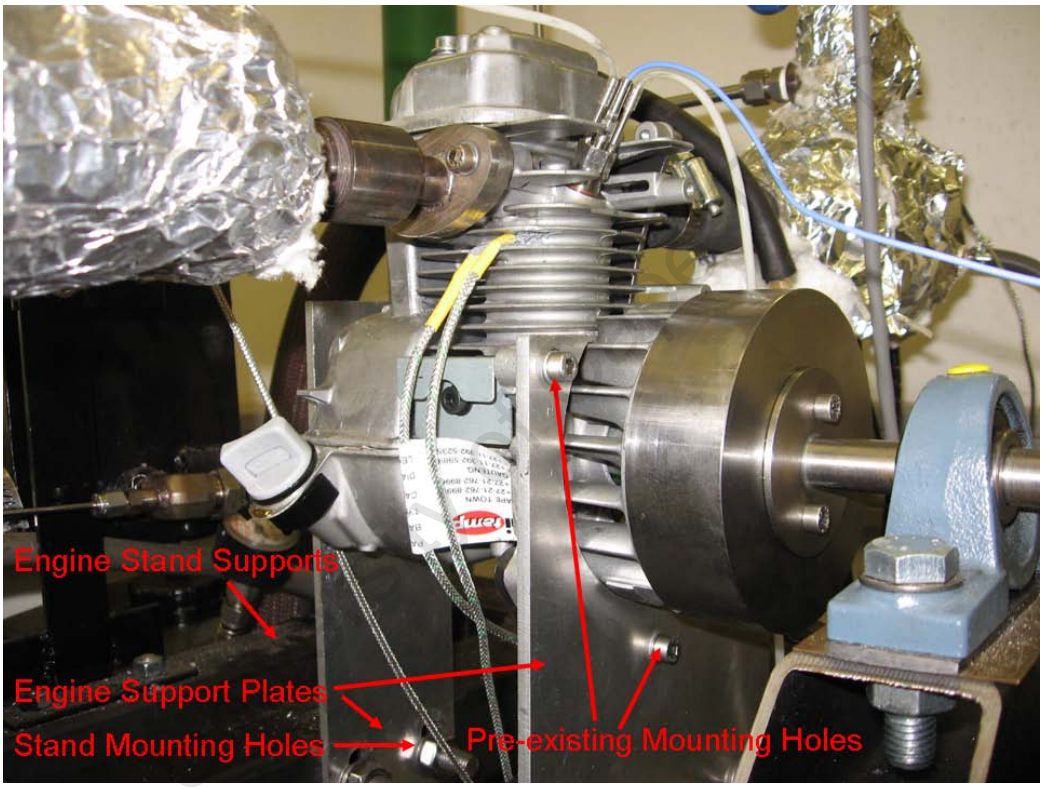

Figure 5.4: Engine Mounting Supports

5.1.4 Power Transmission

A secondary flywheel is mounted onto the existing finned flywheel, via two pre-existing holes on the original finned flywheel, using two machined locating surfaces to ensure correct alignment and installation. The additional mass of the secondary flywheel, provides additional rotational mass to increase rotational inertia; creating a smoother torque output. The crankshaft assembly consists of two separate shafts that are press-fitted with counterweights on either side and supported by bearings, creating an inherent misalignment along the crankshaft. This inherent misalignment manifests itself in an unbalanced force being transmitted through the flywheel, resulting in visible oscillations. Secondary flywheel support is provided by a self aligning bearing to minimise the effects of the crankshaft misalignment as well as reducing static loading on the crankshaft, illustrated in Figure 5.5.

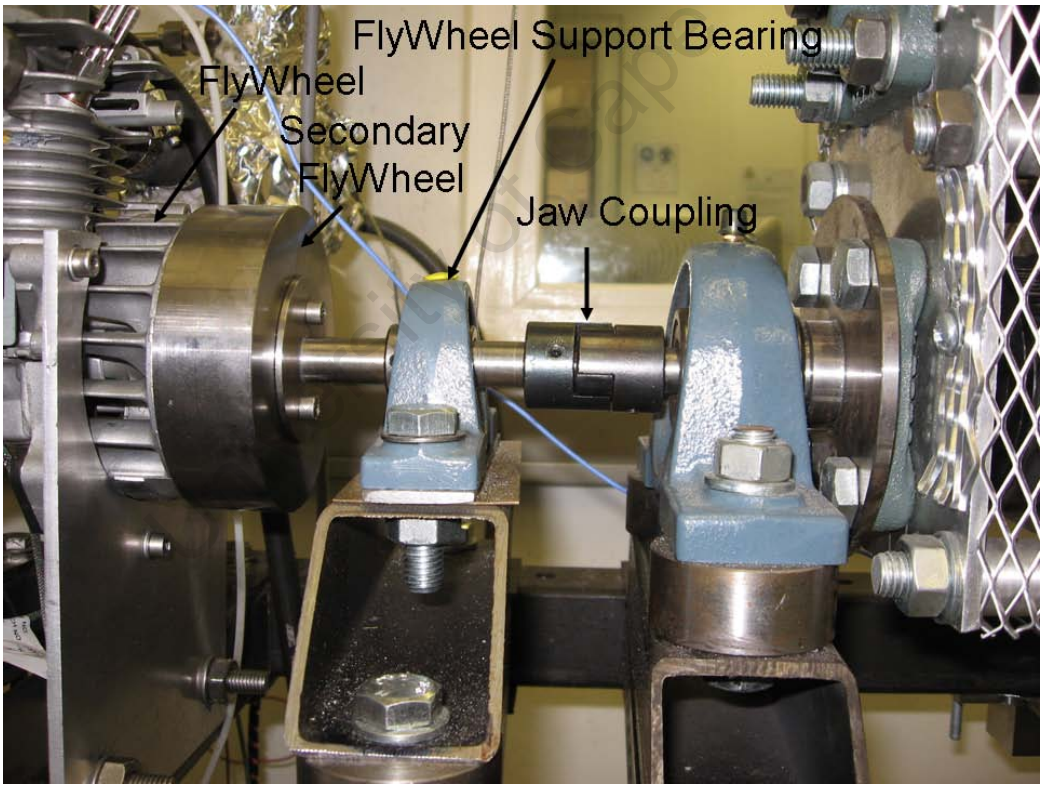

Figure 5.5: Power Transmission Mechanism

Figure 5.5 also illustrates the path of power transmission from the engine to the dynamometer with the aid of a Fenner™ Jaw Coupling. This coupling

allows for incidental misalignment (max 1^0 angular and 0.38mm radial), absorbing of shock loads as well as dampening of small vibrations which, due to the nature of the engine being a high speed single cylinder engine was seen as an ideal installation prerequisite (see section B for coupling specifications).

Power from the engine is transmitted to a Leeson^{TM} Regenerative DC motor (specifications in Table B.1), shown in Figure 5.6. Engine speed control is achieved using a Phantom DC Motor Controller (specifications in Table C.6). A TDC crank angle encoder (specifications in Table C.5), installed on the engines shaft controls the dynamometer speed with engine speed being monitored and set on the Electronic Control System (ECS).

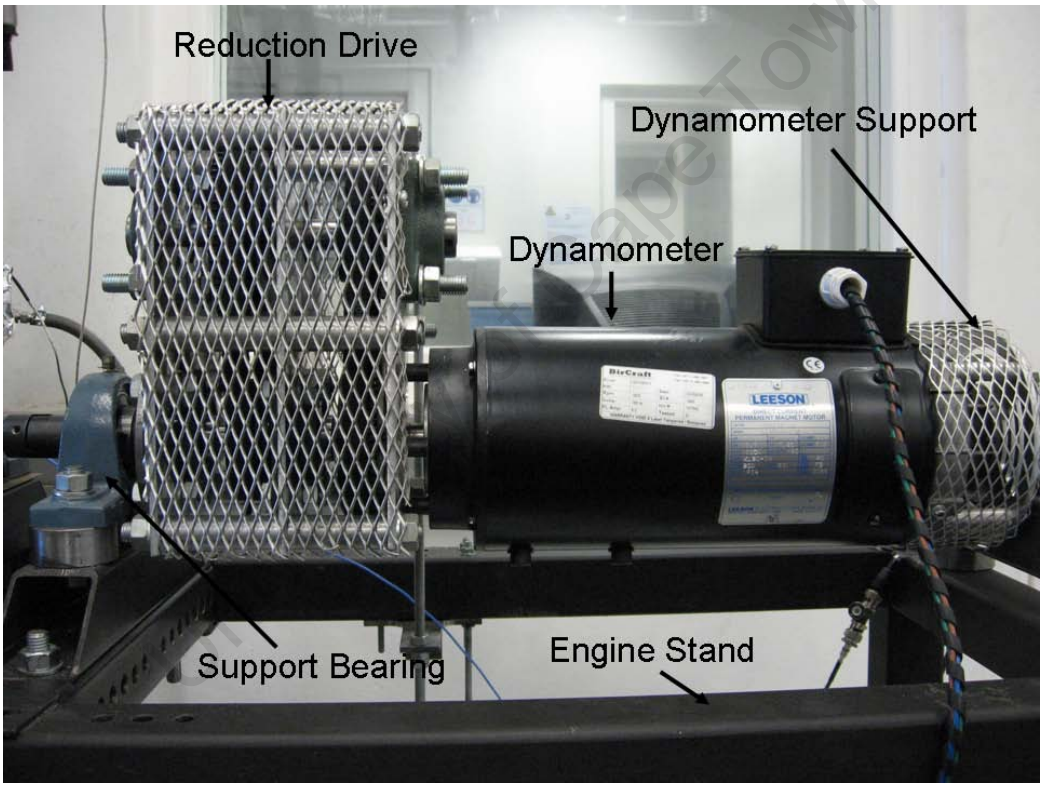

Figure 5.6: Reduction Drive and Dynamometer Setup

Operational speed differences between the engine (maximum operational speed of 9000 rpm) and dynamometer (maximum operation speed of 3000 rpm) resulted in a speed reduction requirement. A toothed belt reduction drive with an overall reduction ratio of 3:1 was installed. Two pulley sets, shown in Figure 5.7, one pair mounted on the flywheel output shaft and pulley shaft and second pair mounted on the pulley shaft and dynamometer shaft,

provide the desired reduction. Each pulley shaft is supported by bearings located on three separate slotted stainless steel plates, with spacers being used to provide correct distances between plates. The slotted plates allow for setting of required belt tension and ensuring the correct shaft alignment. One of the support plates is mounted onto the dynamometer, while the other is supported by a self-aligning bearing using a hollowed support shaft.

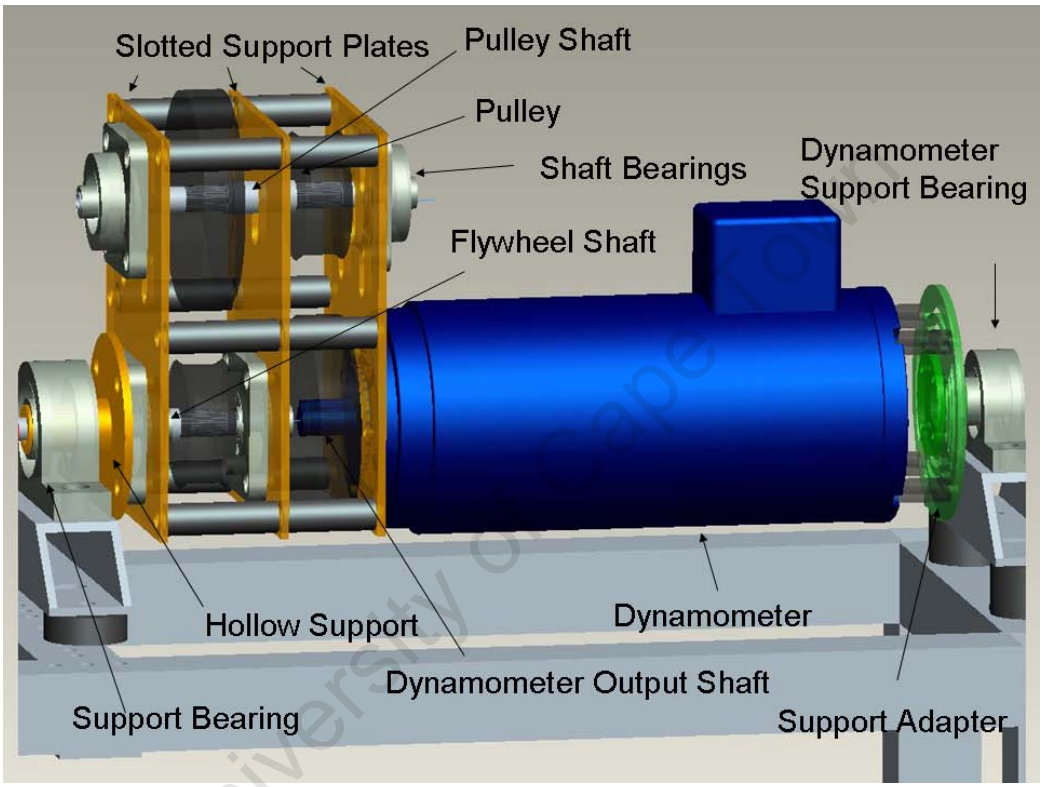

Figure 5.7: Reduction Drive and Dynamometer Assembly

The reduction drive and dynamometer are assembled as a 'freely' rotational system, between two non-rotating trunnion bearings, to facilitate the installation of a simple strain gauge to monitor engine load. This was achieved by running the flywheel shaft inside a hollow support shaft used to mount the reduction drive and dynamometer assembly, with the dynamometer possessing a separate support at the rear.

5.1.5 Measurement Equipment

Various measuring devices were installed for data capturing purposes as well as monitoring of engine operation. Below is a list of all installed instrumentation and their location:

Table 5.4: Location of Measurement Equipment

Signal	Description
P_1	Cylinder Pressure
T_{AR}	Air Reservoir Temp
$T_{mixture}$	Post Injector Mixture Temp
T_{exh}	Exhaust Gas Temp
T_{EGR}	EGR Line Pre-injector Gas Temp
T_{HE}	EGR Heat Exchanger
T_{cyl1}	Cylinder Wall Temp 1
T_{cyl2}	Cylinder Wall Temp 2
λ_1	Exhaust λ
λ_2	Inlet EGR λ
P_2	Air Reservoir
P_3	Exhaust Back-Pressure
Torque	Reduction/Dyno Assembly
Crank Angle	Engine Rear - Speed
FTIR Analyzer	Exhaust
$\dot{m}_{air}$	Laminar Flow Meter (Roots Blower)

Cylinder pressure transducer. Cylinder pressure was measured with a water-cooled piezo-electric pressure transducer mounted into the existing spark-plug hole, without the need for any modification. The pressure transducer used was calibrated for a pressure up to 250 bar. See Table C.3 for pressure transducer specifications.

Pressure sensor. The pressure sensors measuring the inlet and exhaust manifold pressures were GEMS pressure sensors having measuring ranges of 0 - 2.5 and 0 - 6 bar respectively. Both pressure sensors measure gauge pressure. See Tables B.4 and C.1 for sensor specifications respectively.

Temperature sensors. K-type and J-type thermocouples were used to measure various temperatures on the rig. These sensors measure absolute temperatures. T_{cyl1} and T_{cyl2} measure temperature in the cylinder wall. These temperature measurements are used to create a linear temperature extrapolation through the cylinder wall, based on their relative placements in the cylinder wall. The extrapolated temperature measurement is then utilised in heat loss modeling of the engine. Locations of thermocouple installation can be found in Section 8.1.

Emissions Measurement. NOx, CO_2 and CO exhaust emissions sampling measurements were measured using a NICOLET^{TM}Protege 460 Spectrometer Fourier Transform Infra-Red (FTIR) analyzer connected to the exhaust manifold. All emissions data was monitored using a PEUS-Systems^{TM} integrated FTIR management programme.

5.1.6 HCCI Engine Control Methods Utilised

Combinations of control systems were chosen that could be utilised during operation to facilitate control over HCCI combustion phasing and investigate the implemented control strategies on the engine's operational envelope. Selection criteria for the various control methods were considered according to their necessity in being able to achieve HCCI combustion with respect to the engines characteristics.

Fuel Injection

Fuel injection was added, as part of a PFI injection system, to a designed inlet manifold. The injector is housed downstream of a throttle approximately 200mm from the inlet valve, allowing for evaporation and mixing time of the air/fuel mixture. The injector, currently used on Honda's Zoomer 50cc scooters, is controlled by the ECS utilising a digital crank angle signal obtained via a TDC marker.

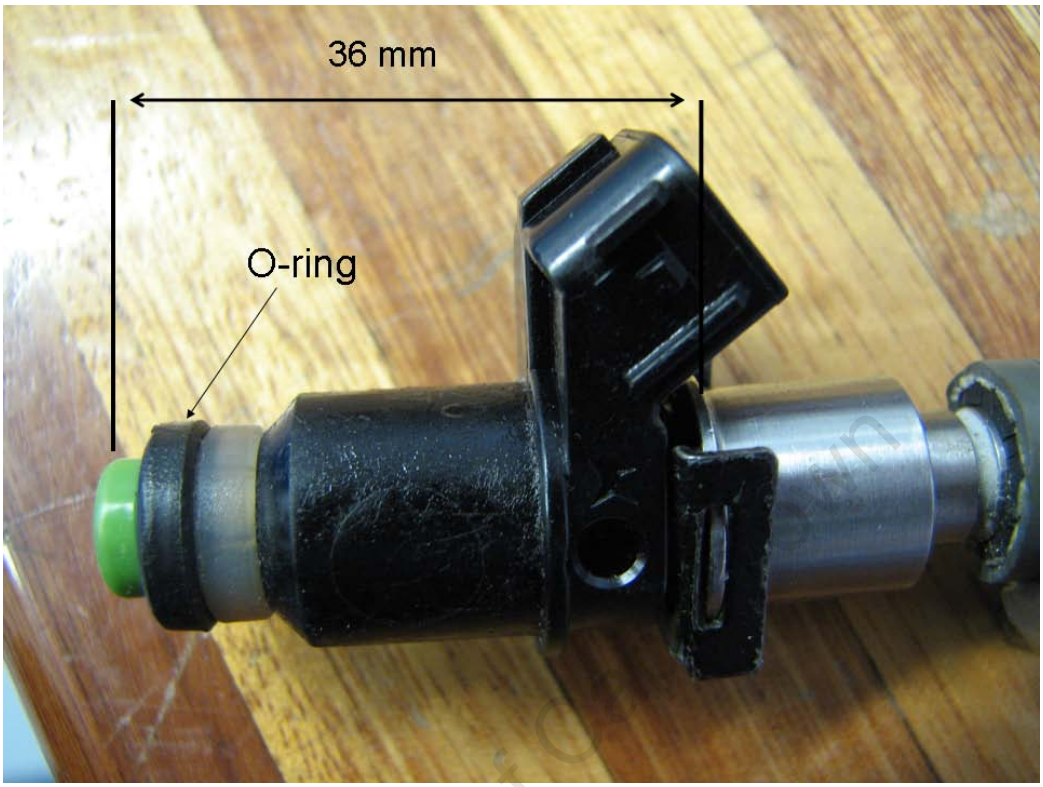

Figure 5.8: Commercially Available Fuel Injector

A single injection event occurs with respect to a CAD position BIVO (Before Inlet Valve Opening) using a preset injection duration. The preset injection duration is set to a desired value on the ECS. An injector calibration graph (see section C.2.2) utilises injection duration to obtain mass flow rates at the set injection pressure of 5 bar. Injection calibration was conducted at atmospheric conditions, making injection calibration valid for naturally aspirated operation.

Inlet Manifold Boosting

Supercharging has shown to broaden the HCCI operating range over a variety of operating conditions. **Inlet charge boosting** is provided by a roots blower and reservoir located in the test cell, allowing for boosting of up to 1.0 bar (gauge).

The blower is connected to the inlet manifold using a series of piping and control valves. Manifold pressure is altered using a control valve connected to the blower, with boosted air pressure being monitored in two separate locations as to ensure accurate manifold pressure measurements. Pressure measurements are recorded at the original reservoir located at the roots blower, as well as at a secondary reservoir located near the engines inlet using an absolute pressure sensor.

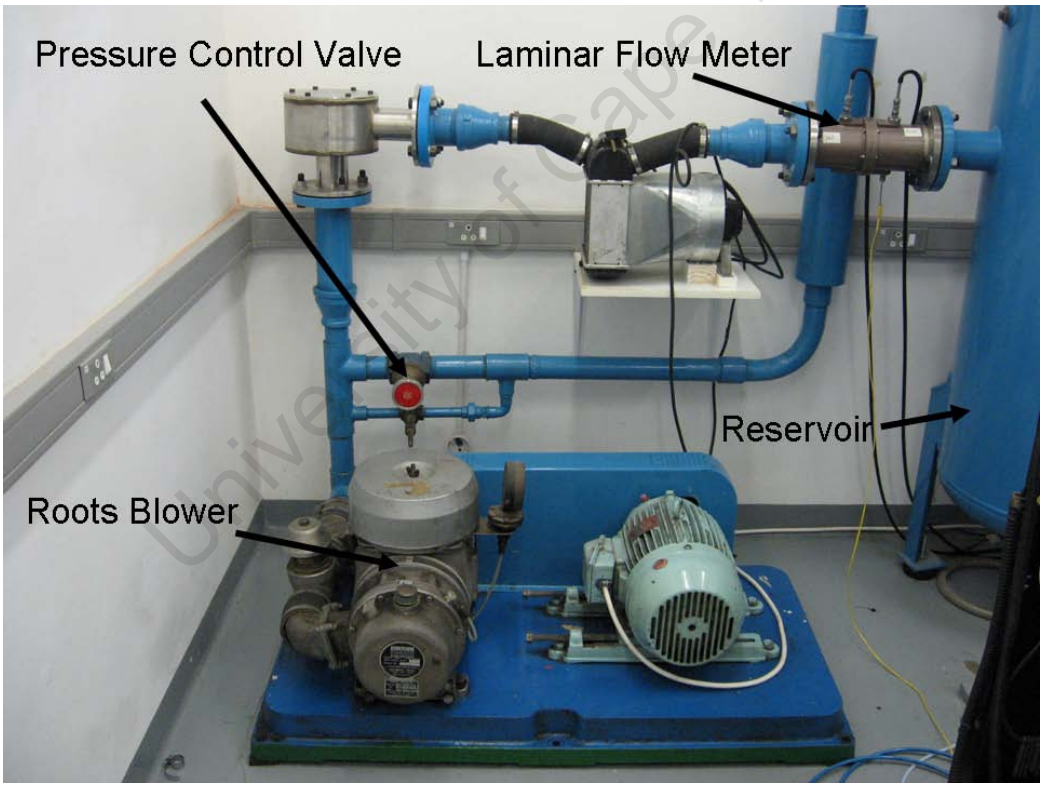

Figure 5.9: Roots Blower Used For Inlet Manifold Boosting

Inlet Manifold Temperature Control

A specially designed 0.8 kW cartridge air heating element was installed upstream of the throttle into a reservoir for inlet air heating control, shown in Figure 5.10. Air temperature is set in the control room and controlled using a K-type thermocouple and heating element control unit. Maximum designed air temperature is 453K with temperature being monitored at three locations in the inlet manifold:

1. Air temperature in the air reservoir used for the temperature control unit
2. Pre-injector temperature as to monitor effects of heat loss along the manifold
3. Inlet valve to monitor temperature of the air/fuel mixture temperature for experimental comparison purposes

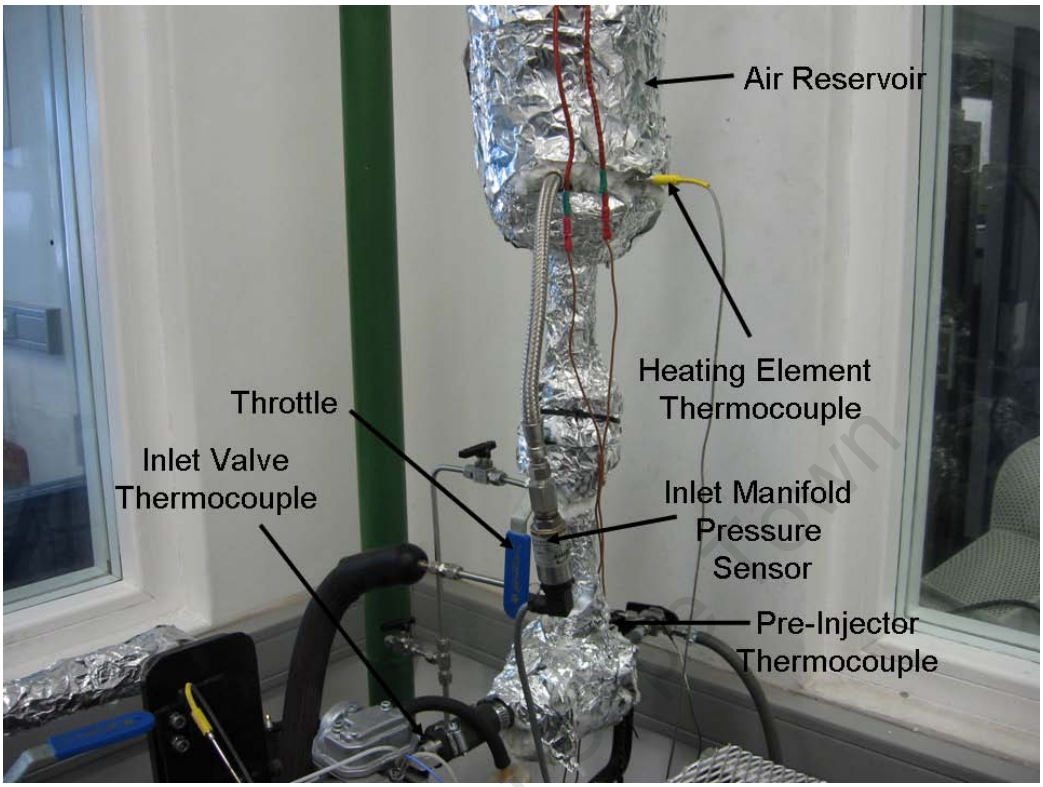

Figure 5.10: Inlet Manifold Temperature Control Setup

Temperature Controlled Exhaust Gas Recirculation

Exhaust Gas Recirculation (EGR) was installed by linking the exhaust manifold and inlet manifolds using stainless steel tubing (Figure 5.11). EGR is circulated through a temperature controlled heat exchanger to the inlet manifold. Flow control is achieved by controlling the pressure differential between the inlet and exhaust manifolds. This is achieved using two valves, one which controls exhaust back pressure (backpressure valve) and hence also varies in-cylinder residual exhaust gas (REG), and either EGR control valve 1 or 2, for coarse or fine adjustments respectively.

The heat exchanger is supplied with temperature controlled water fed from a reservoir. The water temperature is controlled using a heating element and temperature control unit.

EGR flows into the inlet manifold downstream of the throttle. EGR temperature is monitored by two thermocouples, one located at the exit of

the EGR Heat Exchanger and the other located at the inlet port to monitor exhaust gas mixing effects on inlet mixture temperatures.

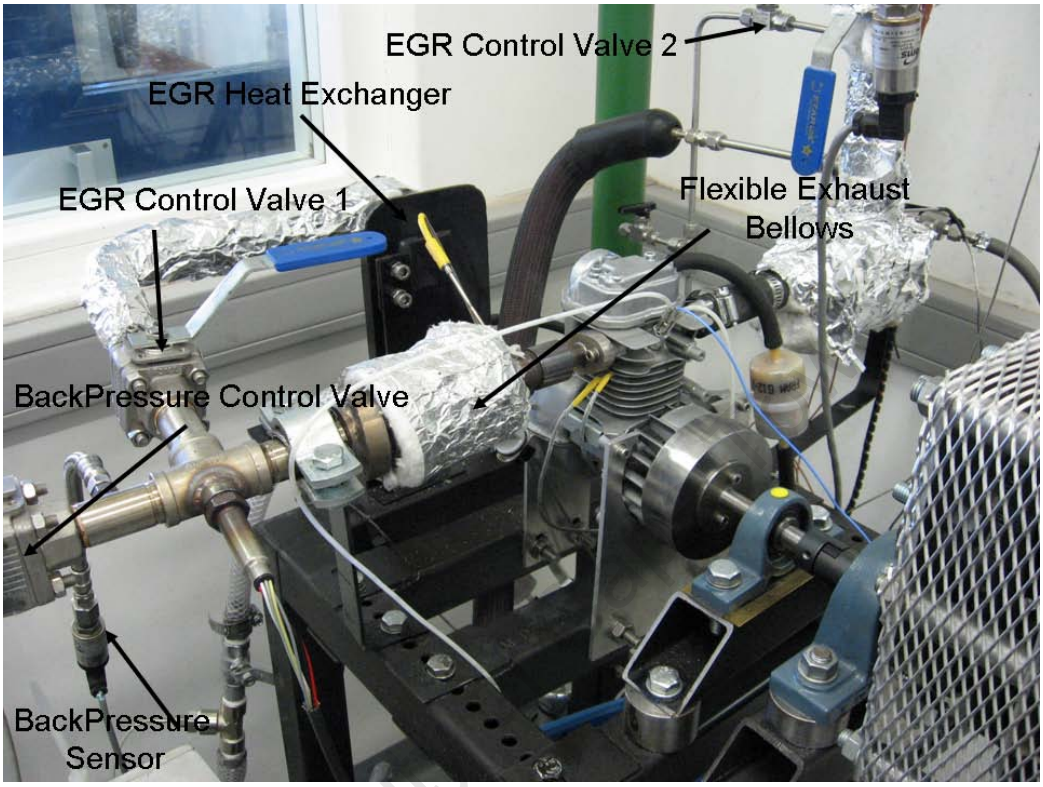

Figure 5.11: EGR System

A non-sampling method was required to predict EGR % being introduced into the inlet manifold due to the small volumes of exhaust gas being circulated. The volume ratio of O_2 content between the inlet and exhaust manifolds were compared, using two broadband Lambda sensors, to obtain EGR % using Equation 5.1 below.

$$EGR(\%) = \frac{\%O_{2intake} - \%O_{2Environment}}{\%O_{2Exhaust} - \%O_{2Environment}} * 100 \tag{5.1}$$

5.1.7 Data Acquisition

Engine control is achieved via an in-house developed Electronic Control System (ECS) using National Instruments™ LabView and a National Instruments™ Field-Programmable Gate Array (FPGA) card. This allows for constant monitoring of engine operation as well as basic control.

The ECS is able to directly control the following operating parameters:

- Engine Speed
- Injection Timing
- Injection Duration

A realtime data acquisition system is used to monitor cylinder pressure, manifold pressures, ϕ, temperatures, engine torque, injection control and engine speed. The ECS calculates CAD at 50% heat release as well graphing relative cylinder pressure, heat release rates and cumulative heat release rates. Analysis of the pressure trace is used to obtain pressure rise rates, peak pressures and locations of peak pressure. Figure 5.12 is a schematic of the entire engine and data acquisition (DAQ) systems layout.

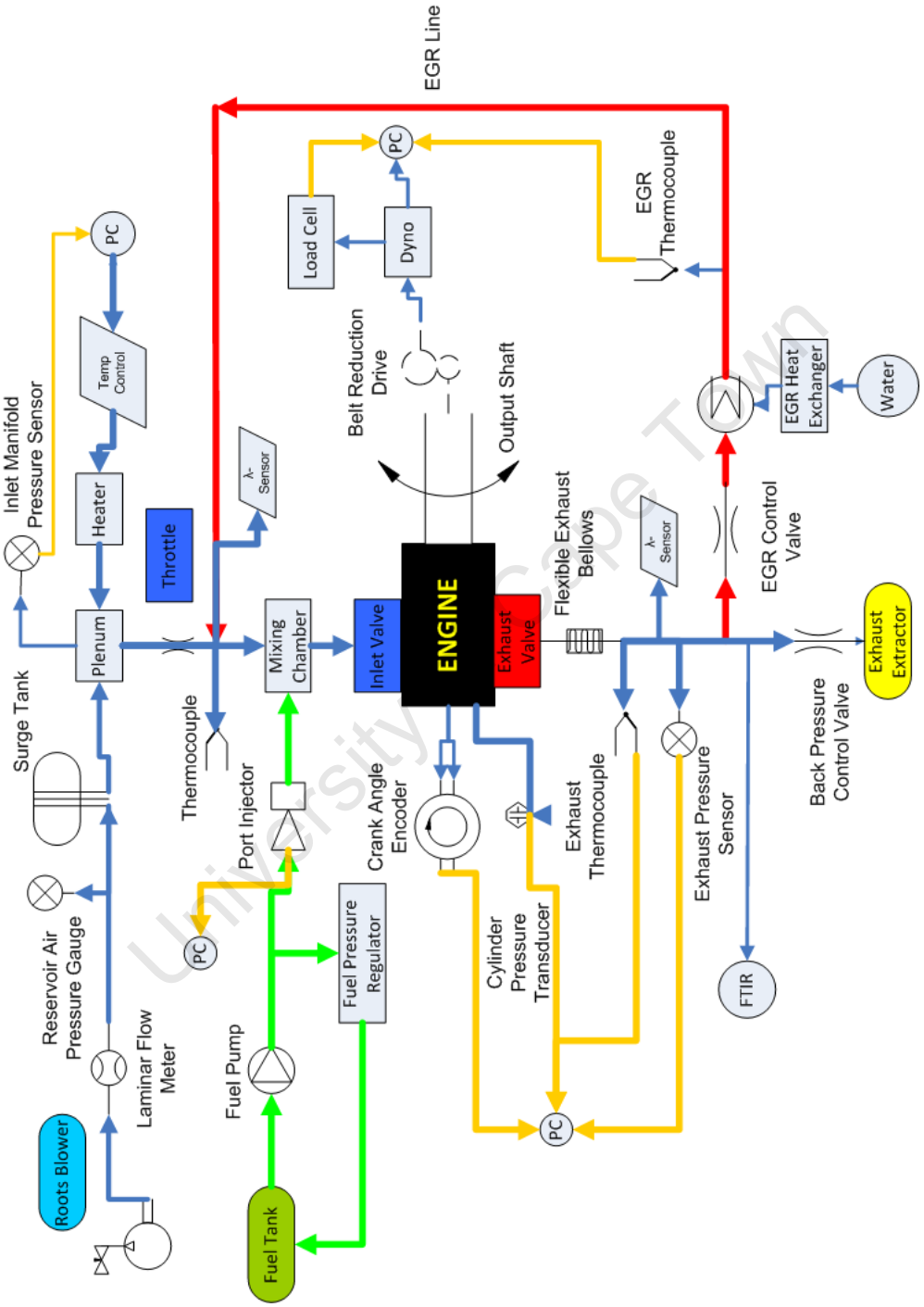

Figure 5.12: Experimental Setup with DAQ System Layout

The pressure trace is used to calculate various operating characteristics:

Pressure vs. CAD:

As mentioned previously, a crank angle encoder is used as a TDC marker. This marker is used to convert the time between TDC intervals into crank angle degrees to which a corresponding pressure measurement is recorded and placed in an array for display and output.

- P = cylinder pressure (kPa)
- V = cylinder volume (m^3)
- V_d = displaced cylinder volume (dm^3)
- W = Work (J)
- ω = engine angular velocity (rad/s)
- n_r = is the number of crank revolutions for each power-stroke (2 for a 4-stroke)

Work:

$$W = \frac{P_1 + P_2}{2}(V_2 - V_1)$$

Power:

$$Power = \frac{W}{dt}$$

Where dt is the time between cycles which is obtained from an engine speed measurement.

Torque:

$$T = \frac{P}{\omega}$$

Mean Effective Pressure (BMEP):

$$mep(kPa) = \frac{6.28 n_r T(N.m)}{V_d(dm^3)}$$

Heat Release Rates [11]:

$$\frac{dQ_n}{dt} = \frac{\gamma}{\gamma - 1} p \frac{dV}{dt} + \frac{1}{\gamma - 1} V \frac{dp}{dt}$$

Where γ is the ratio of the specific heats of the charge. This relationship is used to calculated cumulative heat release rates by integration over the engine cycle.

Exhaust Gas Recirculation:

The percentage of EGR rate is determined using a O_2 comparison between the inlet and exhaust Lambda sensor measurements using the following equation:

$$EGR(\%) = \frac{CO_{2intake} - CO_{2Environment}}{CO_{2Exhaust} - CO_{2Environment}} * 100$$

5.2 Experimental Test Method

Standard engine compression ratio of 8:1 was used for this research and is typical for a small Spark Ignition Engine. However this compression ratio is too low for auto-ignition of gasoline in HCCI engines, whose compression ratio is in the range from 12:1 - 21:1. Thus a fuel with high volatility and ignition quality was required to allow compression ignition in an engine with a compression ratio of 8:1. Diethyl Ether (DEE) was used as the primary testing fuel to obtain all required testing data. This allowed for reduced inlet mixture temperature requirements in obtaining engine operation.

Testing procedure began by motoring the engine with a controlled inlet manifold temperature of 300 K. The engine was required to be started at high speed, allowing for the engine to warm up, at which point engine speed could then be reduced. This operational characteristic was a result of the engines heat loss characteristics resulting in excessive heat transfer at low speeds and thus cold starting at low speeds proved to be difficult. Fuel delivery commenced once desired inlet temperatures were stable, at which time all fuel injection parameters had been set on the ECS. Inlet mixture temperatures were monitored and adjusted accordingly using inlet air heating to obtain the desired operating point.

Fuel metering was used to alter engine load over the engine's operating range, with engine speed being set on the ECS. The ECS constantly monitored cylinder pressure rise rates to prevent engine damage. The maximum allowable pressure rise rate was set at 10 bar/CAD. If pressure rise rates were exceed, fuel delivery was automatically stopped on the ECS and only allowed to recommence once the warning on the ECS was acknowledged.

Various HCCI combustion control methods were used to obtain fuel auto-ignition as well as explore the engines operational range. Additionally, the effects of the various control strategies on engine operation and combustion phasing were investigated. Phasing was maintained at 10^0 ATDC, as this combustion phasing has been shown to produce optimal combustion quality [67]. Once stable operation was attained, the effects of inlet mixture temperature, inlet manifold boosting, both internal and external EGR rates and valve timing on HCCI heat release rates and combustion phasing were investigated with their effects on HCCI operating characteristics examined and discussed.

Emissions measurements were captured at various operating points. A

Fourier Transform Infra-Red (FTIR) exhaust gas analyser was used to measure NOx, CO_2 and CO exhaust emissions. Emissions were compared and the effects of the various control strategies analysed and discussed.

Effects of engine characteristics such as size and combustion chamber heat loss parameters as well external engine cooling effects were incorporated into a single-zone combustion model using measured average cylinder temperatures. The resultant measurements were incorporated into an engine model to obtain a modified heat transfer correlation that could accurately predict engine operation, by matching the engines heat transfer characteristics.

Chapter 6

Control Strategy Effects on Engine Operation

6.1 Mixture Temperature Effects

Mixture temperature effects on engine operation were investigated by controlling mixture temperature at the inlet valve to a range of setpoints. Control of the mixture temperature in the inlet port, allowed the ability to compare inlet mixture requirements when operating at various ϕ's. Combustion peak pressure phasing was maintained at 10^0 ATDC, as this combustion phasing has been shown to produce optimal combustion quality [67]. Experimental inlet temperature and fueling swings were conducted at this constant combustion phasing, with the results shown in Figure 6.1.

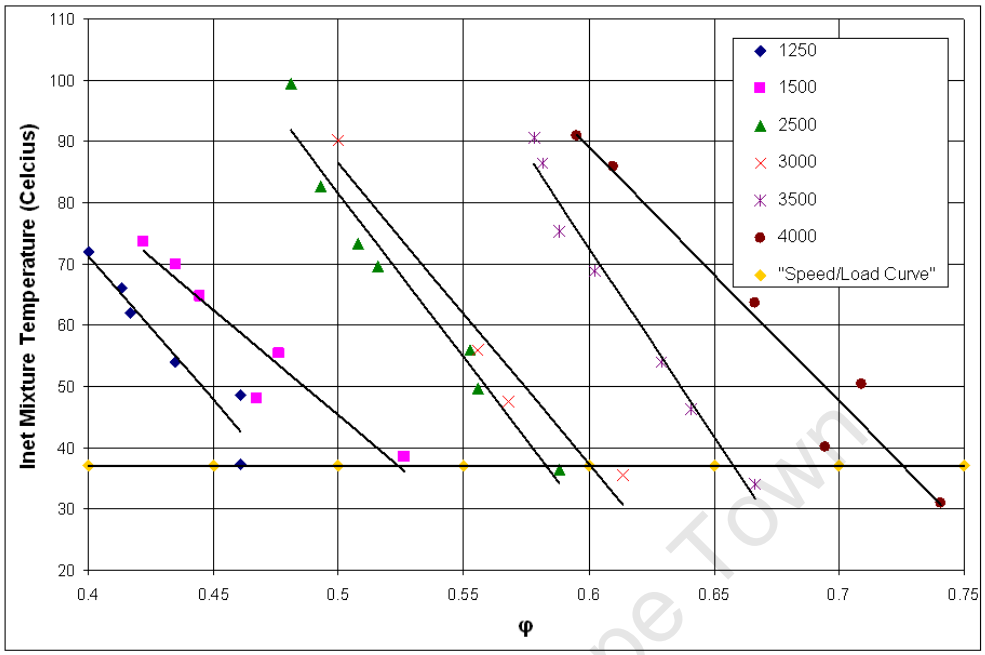

Figure 6.1: Inlet Mixture Temperature vs Fuel Equivalence Ratio for Constant Phasing with External Cooling Fan

When examining the graph above, several clear trends are visible.

- Operational speed range is 1000 - 4000 rpm.
- Increased mixture temperatures are required for a ϕ reduction at a given engine speed.
- Increased speeds require significantly increased inlet heating for a given ϕ value. The increased mixture requirement is to allow for the increased mixture temperature to advance the ignition timing, thus producing a similar advancing effect as a reduction in engine speed.
- Minimum operational ϕ was 0.4
- Maximum operational ϕ was 0.74 when operating without REG or EGR. This was due to excessive pressure rise rates when operating at increased engine speeds. Operation using REG or EGR would result in in-cylinder charge dilution and reduced cylinder pressure rise rates, allowing for operation at increased speeds with increased fueling resulting in an increase in operational ϕ.

- Minimum obtainable mixture temperature was 30^0C. This was due to inlet manifold heating effects as a result of engine operation.
- Maximum attainable mixture temperatures were 100^0C. Increased pressure rise rates are observed when reducing ϕ at constant speed and utilising an increase in the mixture temperature to maintaining combustion phasing. Although a reduction in ϕ increases the ignition delay [60], the increased mixture temperatures allows for constant combustion phasing by reducing the ignition delay. The maximum mixture temperature was a result of excessive pressure rise rates (greater than 10 bar/CAD) when operating at high speeds.
- Low speed maximum mixture temperatures of $\pm 70^0$C was an inlet manifold design limit. This limit was result of excessive manifold heat transfer and reduced manifold flow rates reducing the maximum attainable mixture temperatures.
- The steepness of the curves in Figure 6.1 indicates that the engine could be controlled to run with constant inlet air temperature through the indicated speed range, using fueling to maintain constant combustion phasing. This could result in a similar ability to run along a speed load curve as demonstrated by the model "diesel" aeroplane engine in [4]. An example of a potential speed/load curve is illustrated in Figure 6.1, such that operation is possible across the engine's operational speed range, using only fueling to maintain combustion phasing at a constant inlet mixture temperature.

Engine operation at constant ϕ requires increased inlet mixture temperatures to maintain combustion phasing, when operating through the engine's speed range. This is due to the reduction in time available for fuel auto-ignition. An increase in operating speed results in a retarding of the combustion phasing similar to that experienced in [36]. In order to maintain combustion phasing and operational ϕ, an increase in T_{inlet} is required, as increased mixture temperatures reduce the ignition delay [60]. A reduction in speed will therefore advance the ignition timing and allow for a reduction in required mixture temperatures.

Engine operation at reduced speeds advances the combustion phasing and requires a reduction in fueling to maintain combustion phasing. However, operation at reduced speeds increases overall heat transfer to the cylinder walls when in compared to heat transfer at increased engine speeds. This

results in reduced post-compression pressures and temperatures and a retarding of the combustion phasing. Engine operation was attempted at 1000 rpm, however operation proved to be difficult when attempting to maintain combustion phasing at 10^0 ATDC, resulting in engine misfire. Engine operation was possible at 1000 rpm, if combustion phasing was moved closer to TDC, while still maintaining conservative pressure rise rates. It must be noted maintaining combustion phasing at 10^0 ATDC, as suggested by Sjoberg and Dec [67], was performed on a larger more conventional engine, with a trade-off between combustion quality, pressure rise rates and Coefficient of Variance (COV). Results from their research produced optimum phasing at 10^0 ATDC. However, this phasing may present a problem when operating a smaller engine, where combustion chamber heat loss especially at reduced engine speeds becomes a major factor in combustion phasing. The increased combustion chamber heat loss of a small engine reduces cylinder pressures at a greater rate ATDC, when compared to conventional engines. This results that optimum combustion phasing for the GX25 may be closer to TDC, when operating at reduced engine speeds, than that suggested by Sjoberg and Dec [67].

Increased operational speeds were possible, however this resulted in increased pressure rise rates. Therefore, to prevent engine damage and prolong engine life, increased speeds were not explored. The engines maximum speed was 4000 rpm when operating without REG or EGR. Further significant speed increases resulted in pressure rise rates in excess of 10 bar/CAD.

The engines small displacement results in significant combustion chamber thermal gradients and the ability to run close to stoichiometric air/fuel mixtures. This is possible while still achieving conservative pressure rise rates of 10 bar/CAD without the use of EGR. The expected heat loss characteristics associated with small engines was investigated by operating without the use of any external cooling as provided by a fan. Combustion Peak Pressure Phasing was again maintained at 10^0 ATDC and experimental inlet mixture temperature and fueling swings were conducted as shown in Figure 6.2 below.

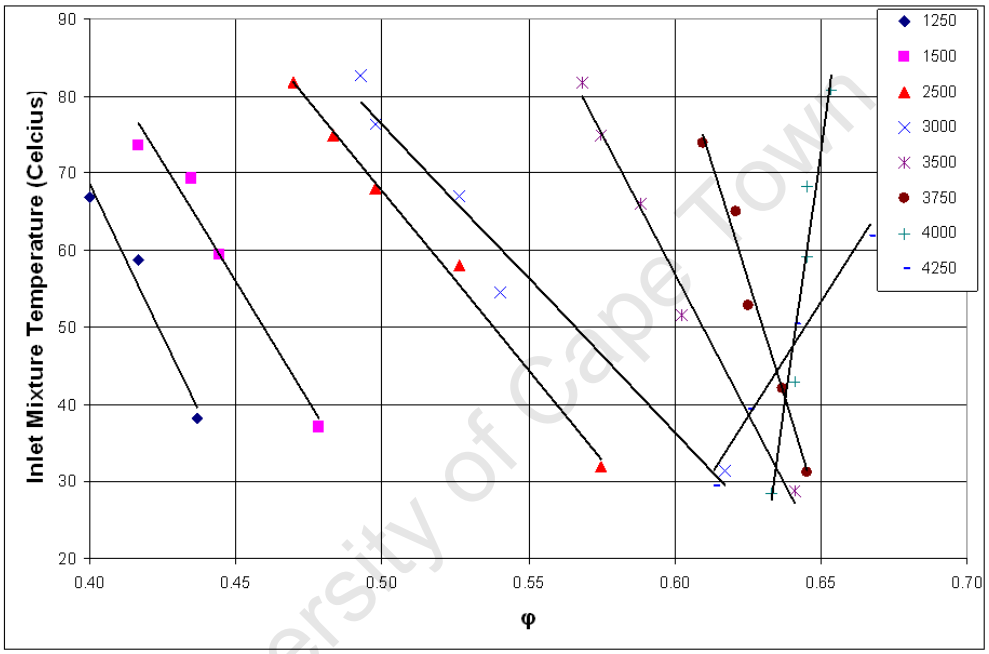

Figure 6.2: Inlet Mixture Temperature vs Equivalence Ratio for Constant Phasing - No Cooling Fan in Operation

Operation at a fixed ϕ required a reduction in inlet mixture temperature when operating without the external cooling fan. Engine operation without the external cooling fan resulted in an increase in recorded cylinder temperatures T_{cyl1} and T_{cyl2}, indicating that cylinder temperatures increased as expected.

A reduction in required inlet mixtures was prevalent across the entire speed range although the operational variance in ϕ reduced with each speed as compared to engine operation with the cooling fan. The minimum operational ϕ was 0.4, which was the same when operated with a cooling fan. This reoccurring lower limit reaffirms the suspected engine heat transfer characteristics on engine operation.

There is a distinct reduction in operational ϕ variances at increased engine speeds, suggesting that engine heat transfer characteristics and possible suspected fuel characteristics play a major role in engine operation. Slopes of the high speed bracket (4000 - 4250 rpm) change drastically when operated without external cooling. The slopes illustrate that an increase in operation ϕ required increased inlet mixture temperatures. This trend suggests that operation in this zone accesses the fuel's NTC region where phasing is independent of inlet mixture temperature. This is unusual, as comparison to other studies which have not shown such trends [8, 36, 44].

This was investigated further by examining Pressure (Figure 6.3) and Heat Release Rate (Figure 6.4) curves at a speed such that a clear advancing in the cool-flame was visible. Pressure traces were captured at 3800 rpm and $\phi = 0.62$, where various inlet mixture temperatures were possible at constant ϕ and constant phasing.

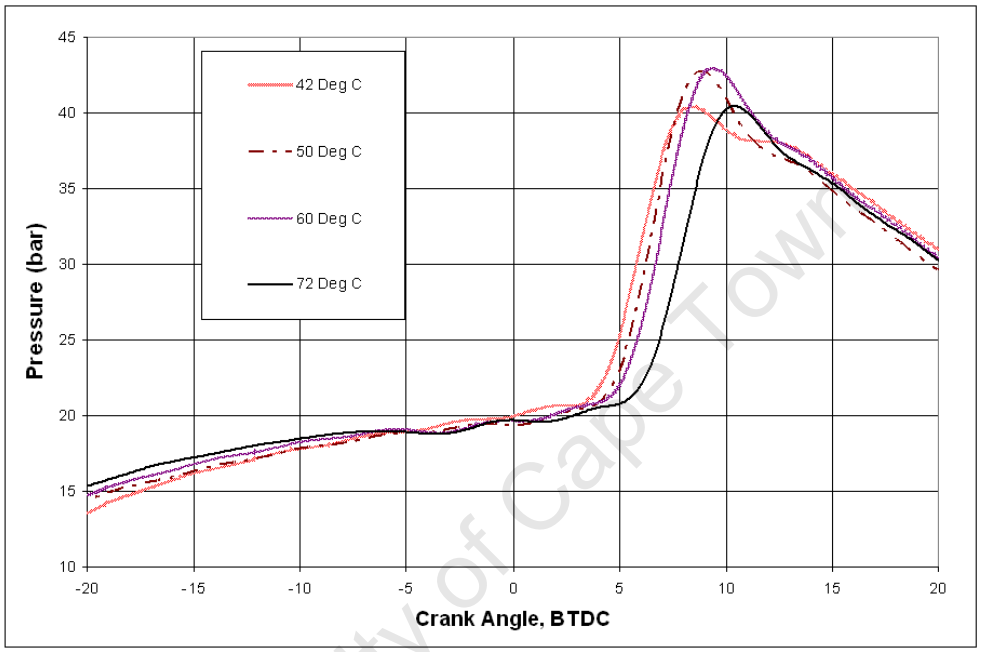

Figure 6.3: Inlet Mixture Temperature Effects on Cylinder Pressure at 3800 rpm and $\phi = 0.62$

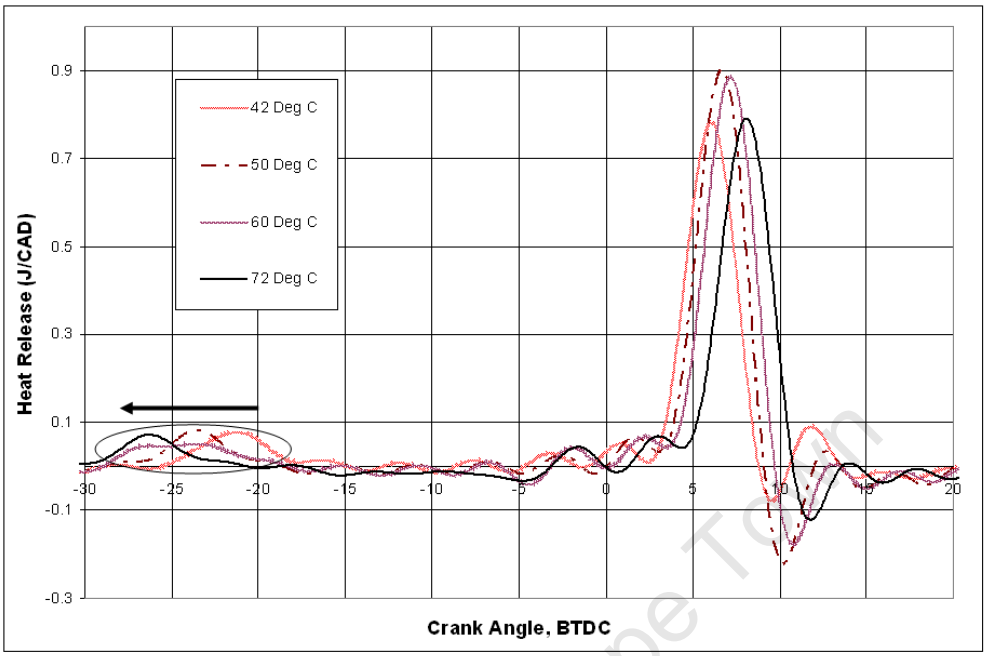

Figure 6.4: Inlet Mixture Temperature Effect Heat Release Rates at 3800 rpm and $\phi = 0.62$

Heat Release Rates plots confirm that an increase in inlet mixture temperature results in a reduction (advancing) in the cool flame ignition delay as illustrated in Figure 6.4. The fuel exhibits NTC behaviour such that the main Heat Release ignition delay is independent of inlet mixture temperature. Operation of the engine within the fuel's NTC region can be used to explain the changes that occur when operating without external engine cooling.

6.2 Exhaust Gas Effects

6.2.1 Cooled Exhaust Gas Recirculation

To compare effects of exhaust gas temperature on engine operation, cooled EGR was introduced into the cylinder via the EGR line. EGR circulates through the heat exchanger, supplied with circulating water temperature controlled to 20^0C to obtain cooled EGR. Inlet mixture temperature was used to maintain constant combustion phasing at 10^0 ATDC when increasing the % EGR. Results obtained while examining the effects of varying % EGR can be seen in Figure 6.5 below.

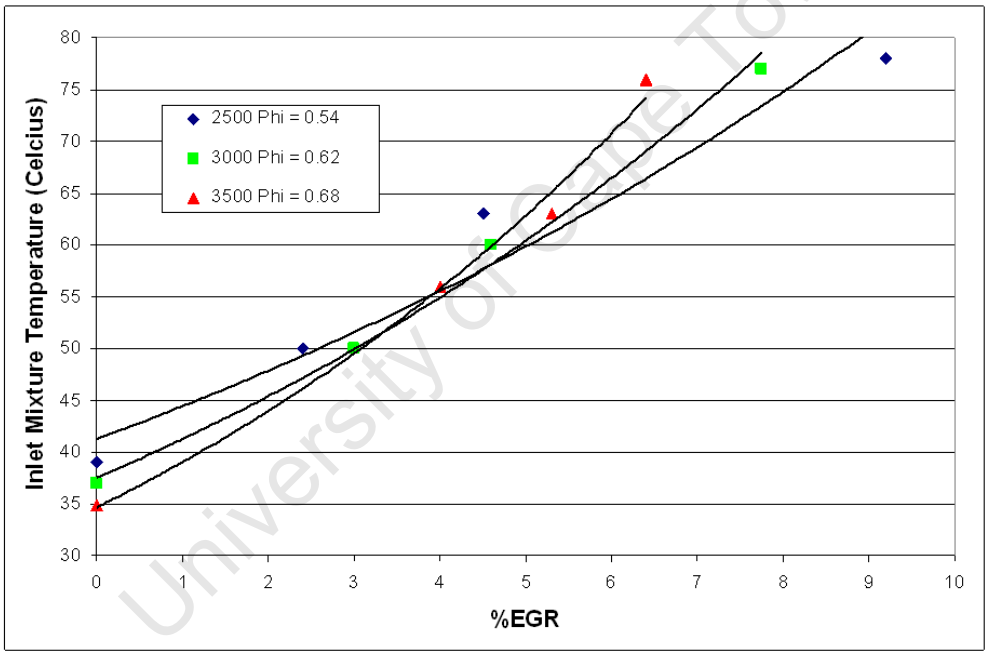

Figure 6.5: Effects of Cooled EGR on Engine Operation

Figure 6.5 shows engine speeds of 2500, 3000 and 3500 rpm operating at constant ϕ, while using inlet mixture temperatures to maintaining combustion phasing when increasing EGR %. An increase in EGR rate requires an increase in inlet mixture temperature to maintain constant phasing and ϕ. This trend is as result of the dilution and heat capacity effects of EGR on combustion phasing. Cooled EGR reduces compression pressures and temperatures resulting in a retarding of the auto-ignition timing which is then offset by an increase in inlet mixture temperature. EGR % reduces pressure

rise rates and allows for operation at increased mixture temperatures as well as increased ϕ, while avoiding pressure rise rate limits as experienced when operating without EGR.

The intersection point observed in Figure 6.5, indicates that an operating range exists where altering of speed has little or no effect on combustion phasing, which occurs at an EGR rate of $\pm$ 4%. The intersection point suggests 'sweet spot' similar to that suggested by Floweday [49] and Sjoberg [56].

6.2.2 Residual Exhaust Gas Effects as Result of Back-Pressure Control

The backpressure valve was used to control the backpressure in the exhaust stream. Changes in exhaust backpressure effect engine volumetric efficiency (η_v) by trapping residual exhaust gas (REG) in the cylinder. This results in reduced fresh charge induction. Two methods were used to illustrate the effects of backpressure on engine operation:

- Keeping a constant backpressure of 1.0 bar (gauge) at set speeds and noting the variances in ϕ at various mixture temperatures for constant phasing.
- Varying backpressure at various mixture temperatures to maintain constant phasing and ϕ when operating at fixed speeds.

When operating at a fixed backpressure, changes in ϕ with respect to inlet mixture temperature changes were noted and compared to data obtained when operating at zero backpressure and are shown by the graph below. Inlet mixture temperatures were used to maintain constant combustion phasing at 10^0 ATDC.

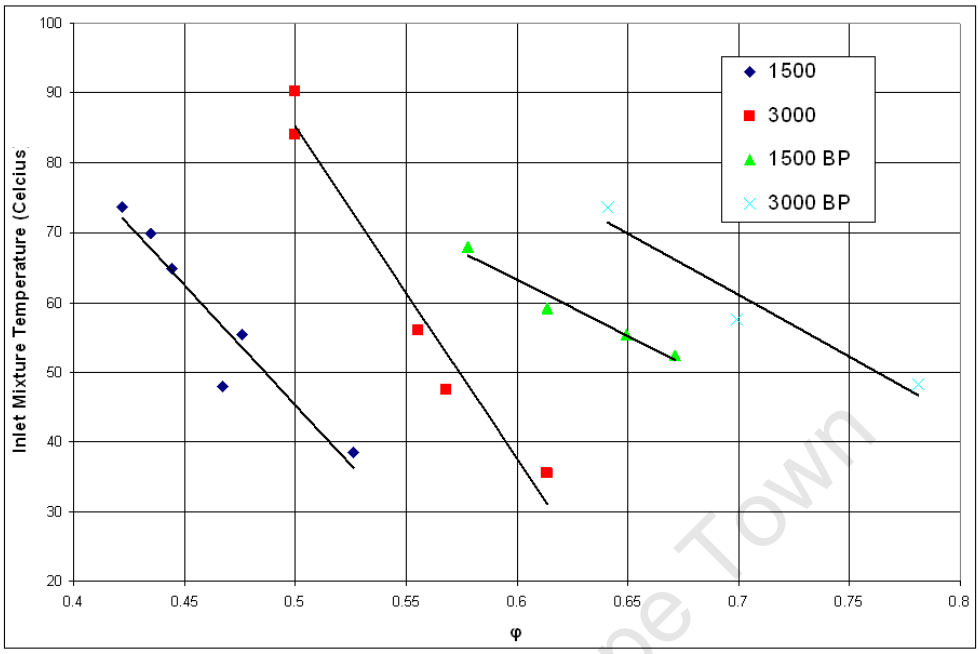

Figure 6.6: Inlet Mixture Temperature vs Eqvuivalence Ratio Comparing Operation With Or Without BackPressure

Operating at increased backpressure showed several trends:

- Operating at increased backpressure showed that an increase in inlet mixture temperatures is required when operating at a fixed ϕ. This is suspected to be a result of engine heat transfer characteristics and REG dilution effects negating the expected heating effects of REG.
- The steepness in the slopes of the backpressure plots shows an insensitivity of mixture temperature on combustion phasing when using REG. This trend suggests that engine load can be altered using fueling and REG without any affect on combustion phasing. This may produce a similar trend to that shown in Figure 6.1 and the ability to run along a fixed engine speed/load curve. However, further engine data is required to further investigate this operational characteristic.

Engine operation is possible at increased operational ϕ when using backpressure due to the increased REG mass fraction present in the cylinder at EVC. The dilution and heat capacity effects of REG reduce combustion

pressure rise rates (PRR), allowing for increased fueling and an increase in operational ϕ, while still maintaining combustion phasing.

The PAW engine's ability to operate at a stoichiometric AFR with conservative pressure rise rates [4], was thought to been due to the combination of high REG due to the two-stroke induction process and the engine's induced thermal gradients, which is a result of the small engine size. The use of REG in the Honda GX25 shows that engine operation is possible at conditions close to a stoichiometric AFR when using REG. The use of REG would produce a similar operational ϕ range to that observed by the PAW engine in [4]. A further increase in the operational speed range would also be attributed to the use of REG or EGR, as both reduce combustion pressure rise rates, allowing for an increase in the engine's operational speed while preserving conservative pressure rise rates.

The effects of backpressure on required inlet mixture temperatures to maintain combustion phasing was investigated. An initial base ϕ was obtained at reduced mixture temperature for the specified set speed. Inlet mixture temperature could then be increased and the backpressure altered as to obtain the preset required variables at speeds of 1500, 2500, 3000 and 3500 rpm. Results obtained from testing shown in Figure 6.7.

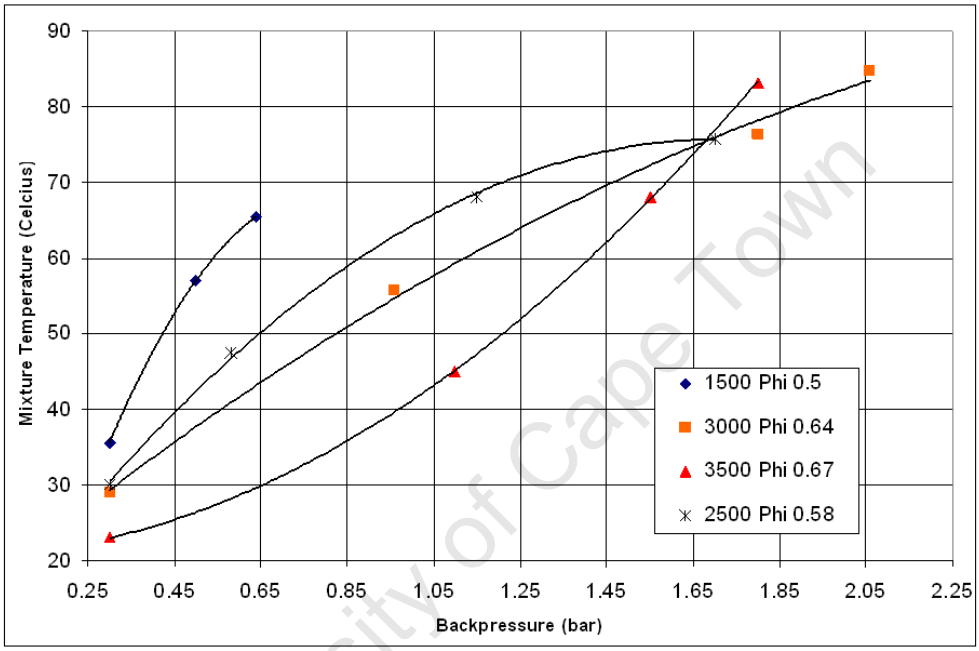

Figure 6.7: Varying Backpressure for Constant Phasing, Phi

A clear point of intersection exists in Figure 6.7. This intersection point describes a range at which the engine can vary speed without affecting the combustion phasing. This so called "sweet spot" operation suggests that engine operation with constant combustion phasing is possible under varying load conditions in this area, with no required altering of control strategies.

The relationship illustrated by Figure 6.7 suggests that an increase in Backpressure requires an increase in inlet mixture temperature. However, the expected relationship is such that an increase in hot REG mass would require an inlet mixture temperature reduction to compensate for the increased cylinder temperature as result of the hot residuals. However this doesn't occur, suggesting that engine characteristics such as cylinder heat transfer and breathing characteristics play a major role in small HCCI engine operation. This is a result of the combination of the dilution, chemical and

heat capacity effects of REG having dominant effect on combustion phasing over the expected preheating effects of the REG.

6.3 Inlet Manifold Boosting

Manifold pressure effects were investigated for inlet pressures (gauge) of 0.1, 0.15, 0.2 and 0.25 bar, by recording the change in ϕ as result of inlet pressure variations, while maintaining constant combustion phasing and inlet mixture temperature of 308K. Figure 6.8 below illustrates the recorded effects of altering inlet manifold pressures.

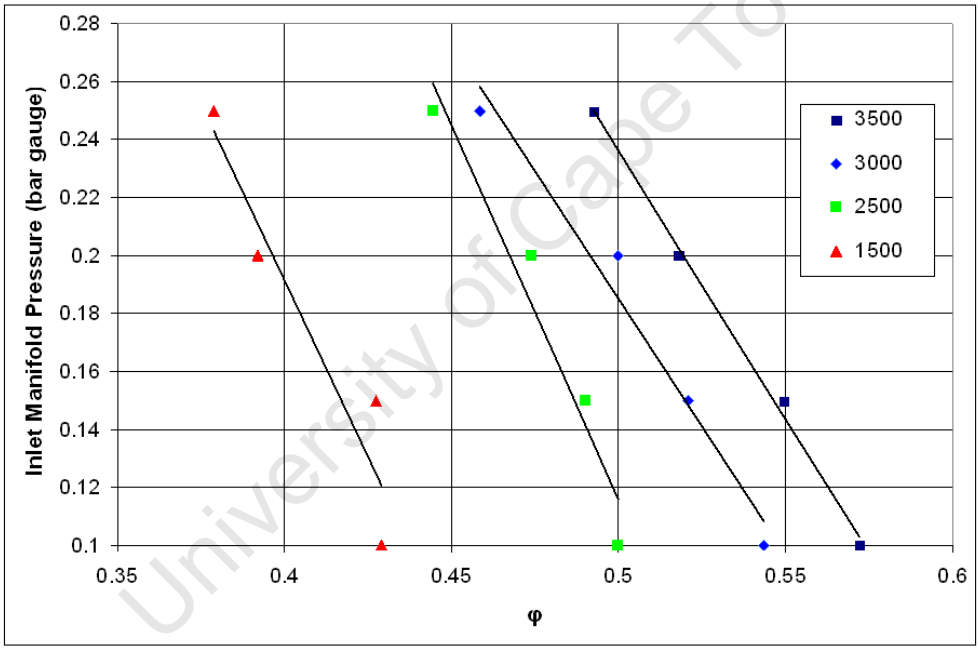

Figure 6.8: Effects of Inlet Manifold Pressure on Equivalence Ratio for Constant Phasing at $T_{inlet} = 308$K

Trends show that a reduction in operational ϕ requires increased manifold pressures across the speed range for constant combustion phasing. A reduction in fueling results in a retarding of the combustion phasing. This retarding of the phasing can then be offset by an increase in manifold pressure. This is result of increased post-compression cylinder pressures, reducing the ignition delay and advancing the combustion phasing.

6.4 Effects of Varying Relative Valve Timing

Valve timing plays a key role in engine breathing and is thus directly related to volumetric efficiency. Engine operating characteristics became apparent when engine operation was altered by varying relative valve timing. Valve timing was altered by adjusting the timing gear 1 or 2 teeth, corresponding to 24 deg/tooth, either forward or backwards with respect to the original timing, resulting in advancing or retarding of the relative valve timing respectively. Experimental Inlet Temperature and fueling swings were conducted at constant combustion phasing of 10^0 ATDC. Results shown in Figure 6.9 below illustrate the variances obtained, by retarding the valve timing by 1 tooth, as compared to the original fueling swings obtained at the original valve timing.

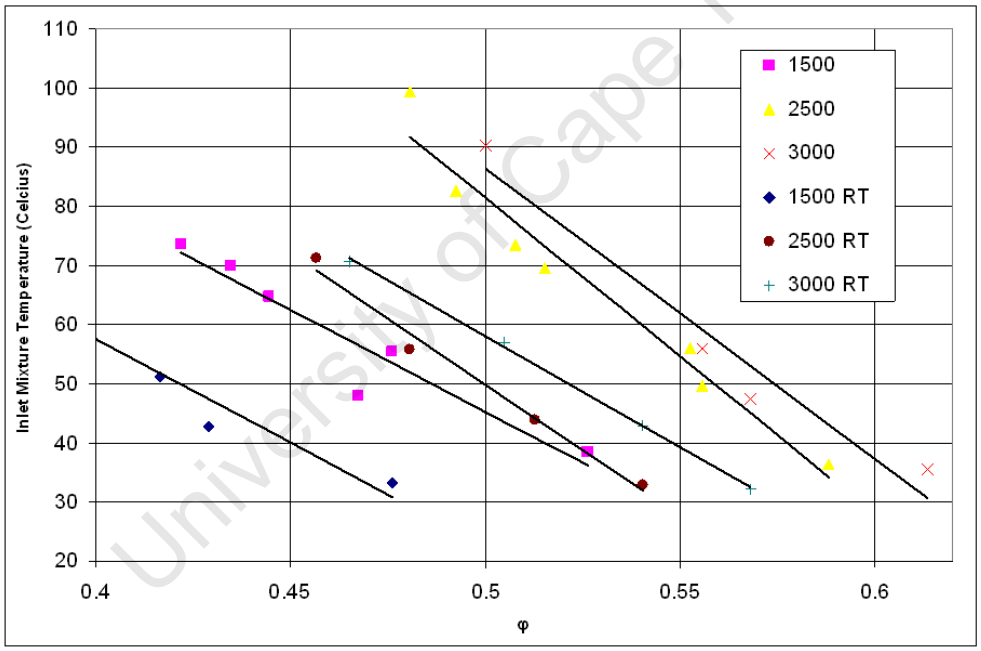

Figure 6.9: Effects of Retarding the Valve Timing by 1 Tooth on Required Inlet Mixture Temperatures for Constant Phasing

Retarding of the valve timing by 1 tooth produced interesting trends. Operational ϕ was reduced over the speed range as compared to that obtained at the original timing. This seemed to indicated that retarding of the timing increased the engine's volumetric efficiency. The increased volumetric efficiency leads to an increase in post-compression cylinder pressures as a result of the increased cylinder mass. As a result, a reduction in required inlet

mixture temperatures is necessary to maintain constant combustion phasing.

Further tests were conducted by further retarding the timing by 2 teeth, when compared to the original timing, however engine operation was not possible. This was result of a dramatic reduction in post-compression cylinder pressures and hence temperatures being too low to initiate fuel auto-ignition. The attempt was then made to advance the timing by 1 tooth as compared to the original timing. Operation was not possible at reduced speeds due to the reduction in cylinder compression pressure. Operation at increased speeds resulted in increased operational ϕ when the combustion phasing was maintained at 10^0 ATDC, however increased pressure rise rates proved to be a limiting factor in engine operation.

Effects of valve timing were further investigated by examining the engine's volumetric efficiency at various valve timings. This was achieved by motoring the engine and utilising a Laminar Flow Meter (see B.3 for specifications) to measure air flow. Volumetric efficiency η_v comparisons were calculated, using Equation 6.1 [11], across the engine's operating range as to evaluate the effectiveness of the engines induction process as affected by valve timing, where volumetric efficiency is defined as the volume flow ratio of air into the intake system divided by the rate at which volume is displaced by the piston:

$$\eta_v = \frac{2\dot{m}_a}{\rho_{a,i} V_d N} \tag{6.1}$$

Where $\rho_{a,i}$ is the inlet air density, m_a is the mass of air inducted into the cylinder per cycle, V_d is the displaced volume and N is engine speed. Experimental results are shown by Figure 6.10

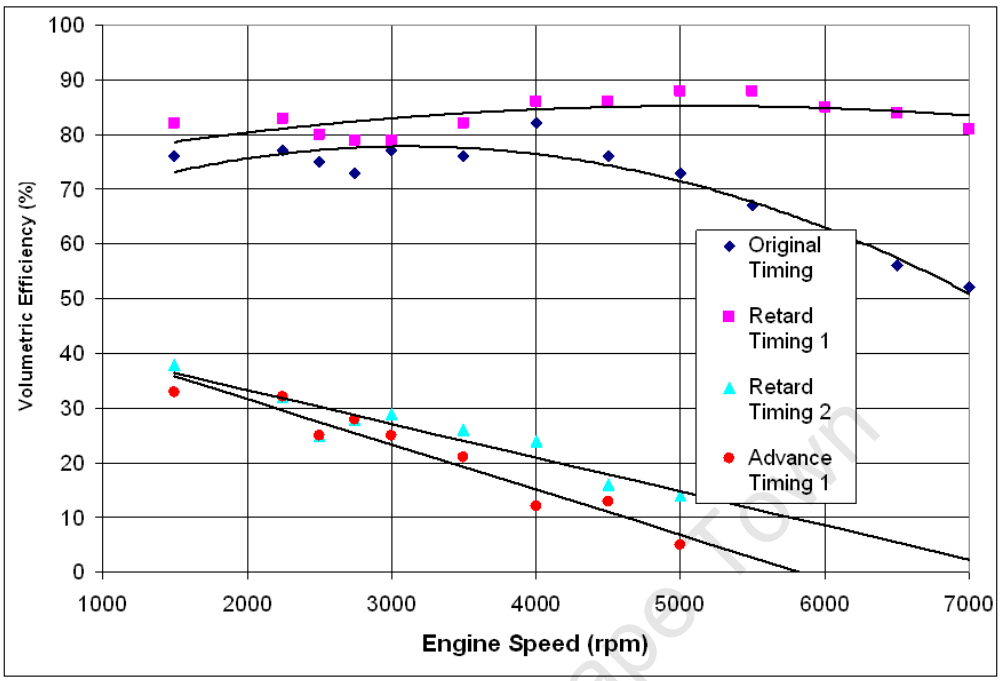

Figure 6.10: Volumetric Efficiency for Varying Valve Timings

Volumetric efficiency (Figure 6.10), torque plots (Figure 6.11) and power plots (Figure 6.12) affirm that retarding the valve timing by 1 tooth produces improved η_v and torque. This suggests the the valve timing is detuned by the manufacturer/supplier to improve engine durability. Note that the torque curves measured with this valve timing (Figure 6.11) matched the engines maximum specifications for the engine. This indicates that engine breathing performance can be significantly improved by retarding the valve timing as well as the effects that valve timing has on engine operation across a wide engine speed range.

The discrepancies between the "spec" plots are due to suspected errors in the engine manufacturer's performance specifications, as were obtained from power plots. Although, as previously stated maximum torque values corresponded to the correct engine speeds as supplied by the manufacturer. Further discrepancies were attributed to engine wear as a result of engine testing prior to obtaining the torque and power curves.

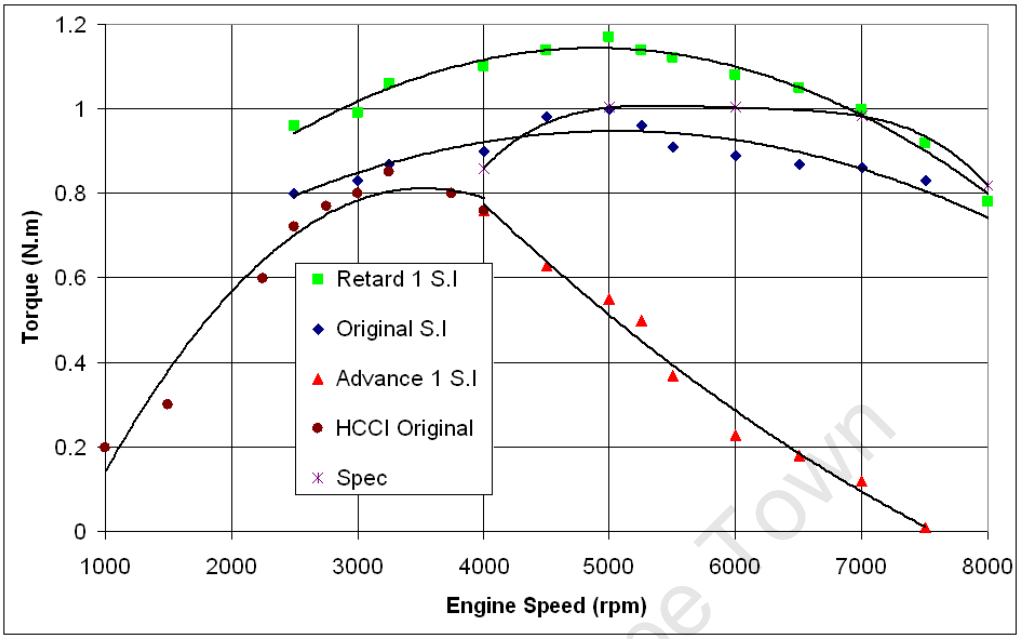

Figure 6.11: Effects of Valve Timing on Engine Torque (S.I fuel used was RON95 Gasoline and HCCI fuel used was DEE)

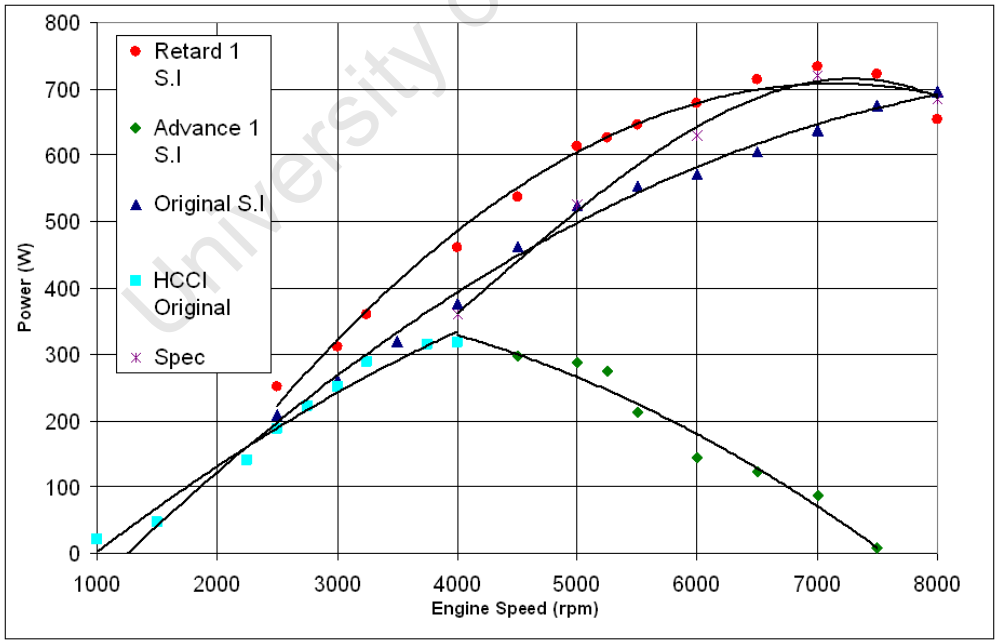

Figure 6.12: Effect of Valve Timing on Engine Power (S.I fuel used was RON95 Gasoline and HCCI fuel used was DEE)

Chapter 7

Exhaust Emissions

Table 7.1 below shows an overview of the effects of control strategies on engine exhaust emissions as will be discussed throughout this section. All trends are compared to emissions from standard HCCI operation with no heated inlet, no backpressure, no EGR and original valve timing strategy.

Table 7.1: Control Strategy Effects on Engine Exhaust Emissions

Emission	Engine Speed	↑ Temp.	↑ Pressure	Fixed Hot REG	Matched REG	Cooled EGR	Adv. Timing
NOx	4000	↓	↓	↑	↓	-	↓
	3500	↓	↓	↑	↓	-	↓
	3000	↓	↓	↑	↓	↓	↓
	2500	↓	↓	↑	↓	↓	↓
CO_2	4000	↓	↓	↓	-	-	↓
	3500	↓	↓	↓	↓		↓
	3000	↓	↓	↓	↓	Vary	↓
	2500	↓	↓	↓	↓	Vary	↓
CO	4000	↑	↓	↓	-	-	↑
	3500	↑	↓	↓	↓	-	↑
	3000	↑	↓	↓	↓	↑	↑
	2500	↑	↓	↓	↓	↑	↑

7.1 NOx Emissions

7.1.1 Inlet Mixture Temperature Effects on NOx Emissions

Engine operation showed reduced NOx emissions when increasing mixture temperature. This is result of the reduction in ϕ required for constant combustion phasing which although operation is at an increased mixture temperature the reduction in ϕ is the primary control parameter as it reduces peak cylinder temperatures and thus NOx formation. However the reduction in NOx was greater when operating at higher speeds due to the larger decrease in operational ϕ when increasing mixture temperatures. When operating at a speed of 4000 rpm, increased mixture temperatures allowed for NOx reduction from 400 ppm to 150 ppm. A reduction in NOx at low speeds was negligible due to the marginal differences in cylinder temperatures as a result of heat loss to the cylinder walls and was found to be in the region of 3 to 6 ppm, shown in Figure 7.1 below.

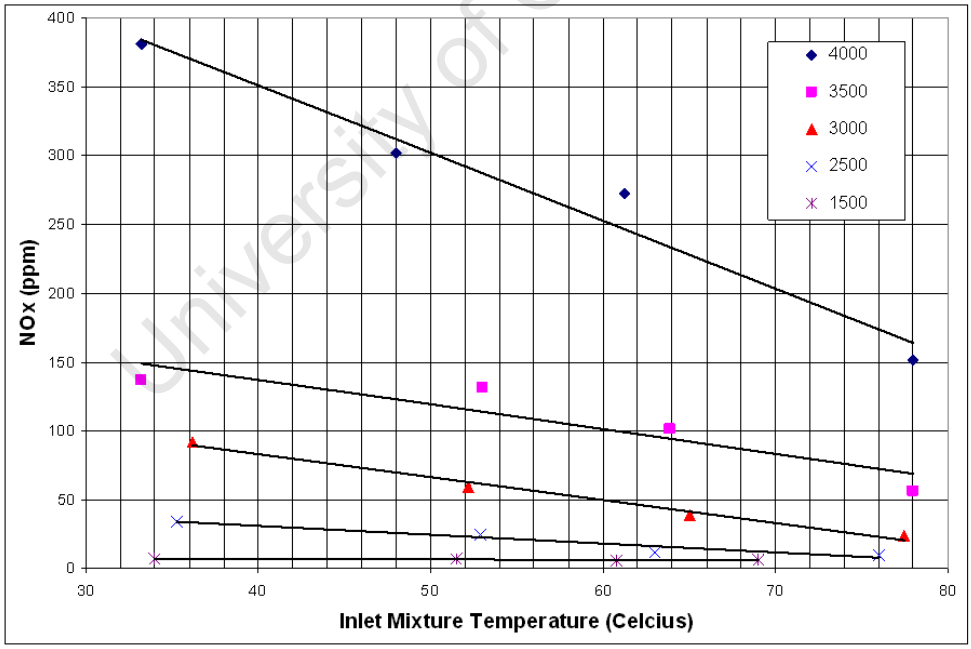

Figure 7.1: NOx Emissions vs Inlet Mixture Temperature at Constant Phasing

7.1.2 EGR Effects on NOx Emissions

EGR effects on NOx emissions were investigated by varying EGR rates and corresponding inlet mixture temperatures to maintain constant phasing at 10^0 ATDC as well as constant ϕ. Results obtained from the FTIR are shown in Figure 7.2 below for two speeds of 2500 and 3000 rpm. Visible trends show that increased EGR % reduces NOx emissions, which is as result of the dilution and heat capacity effects that EGR has on combustion phasing. Increased EGR results in further reduction in combustion temperatures, which are directly related to NOx formation during combustion and thus combustion temperature reductions result in reduced NOx emissions. Combustion temperatures were reduced as evidence by the reduction in exhaust gas temperatures with increasing EGR %.

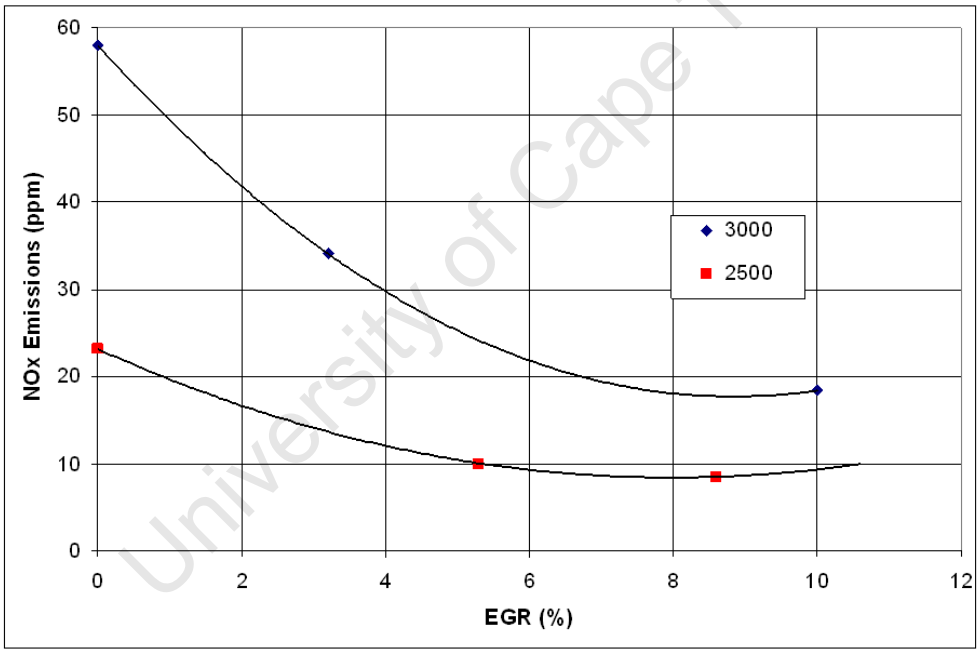

Figure 7.2: Effects of EGR Rate on NOx Emissions

7.1.3 Inlet Manifold Pressure Effect on NOx Emissions

Fueling was reduced and manifold pressure varied, between 0.1 - 0.25 bar (gauge), at constant inlet mixture temperature to investigate the effects on NOx emissions while maintaining constant phasing 10^0 ATDC. A reduction in fueling requires an increase in manifold pressure to maintaing combustion phasing. Increased manifold pressures result in increased inlet air density and thus mass flow into the cylinder. This increase in air mass results in increased post compression pressures, reducing the ignition delay. A reduction in operational ϕ results in a reduction of combustion temperatures and NOx formation. This trend is clearly visible in Figure 7.3 below. The magnitude of NOx formation is more apparent at higher speeds than at lower speeds. Lower speed reductions are less visible at 1500 ppm, where NOx emissions remain fairly constant due to the speed and heat loss relationship of the engine. Reductions in operational ϕ are offset by the heat loss experienced at low engine speeds.

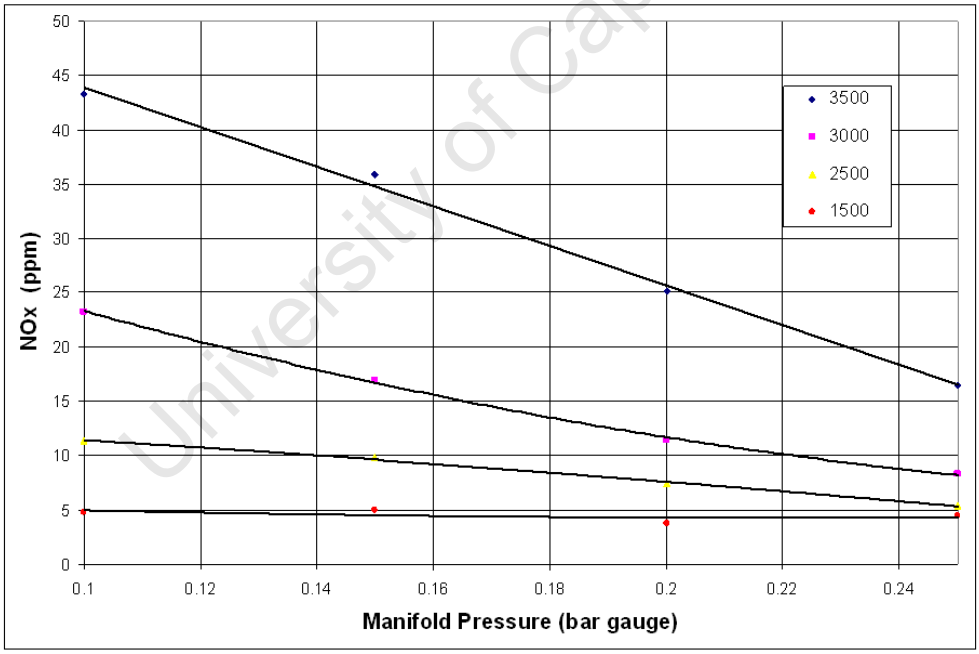

Figure 7.3: Effects of Inlet Manifold Pressure on NOx Emissions

7.2 CO Emissions

7.2.1 Inlet Mixture Temperature Effects on CO Emissions

Increased CO emissions result due to the inability for CO to oxidize to form CO_2 during low temperature combustion. This makes CO emissions directly related to ϕ [11], due to the variance in combustion temperatures when operating across a ϕ range, such that the temperatures required for CO oxidation to CO_2 is greater than 1300K [2]. A reduction in ϕ should reduce CO emissions, but in the case of HCCI engines, the low temperature combustion results in increased CO emissions as combustion temperatures may become too low for CO oxidation, especially at light loads.

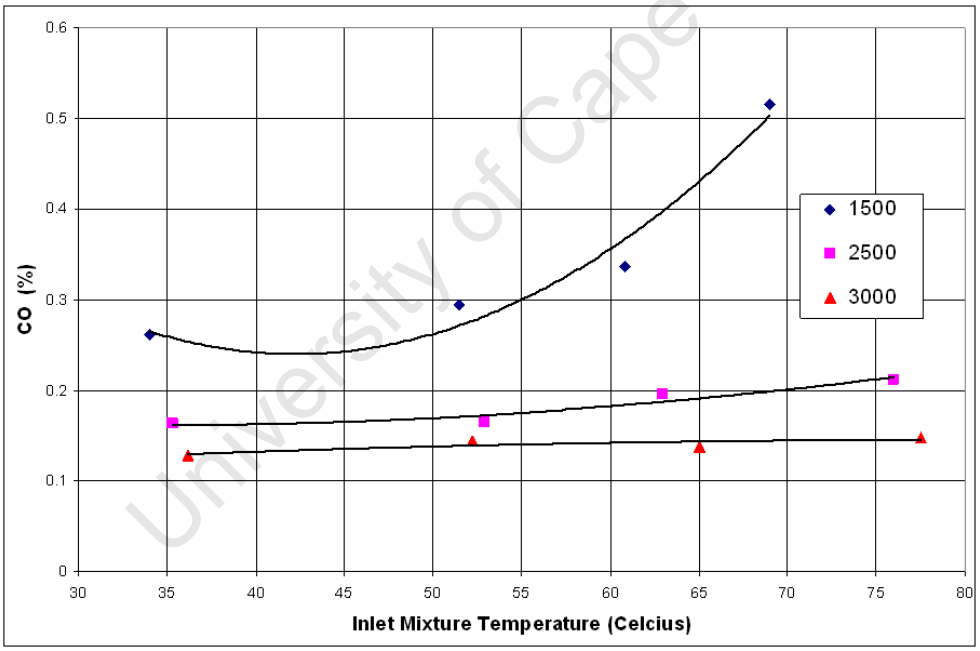

Figure 7.4: Effects of Mixture Temperature on CO Emissions

Figure 7.4 above, shows that inlet mixture temperatures increase CO emissions. Increased mixture temperatures should decrease CO emissions as a result of further oxidation to CO_2, however the reduction in operational ϕ as result of increased mixture temperatures, reduces cylinder combustion temperatures.

Additionally, experimental trends show CO emissions reduce with increasing speed, which is attributed to increased cylinder temperatures when operating at increased speeds. This is a result of increased operational ϕ when operating at increased speed while maintaining constant combustion phasing.

7.2.2 EGR Effects on CO Emissions

Figure 7.5 below shows the effects of increased EGR % on CO emissions. Results obtained during testing showed increased CO emissions similar when increasing the EGR %, similar to that recorded by [32].

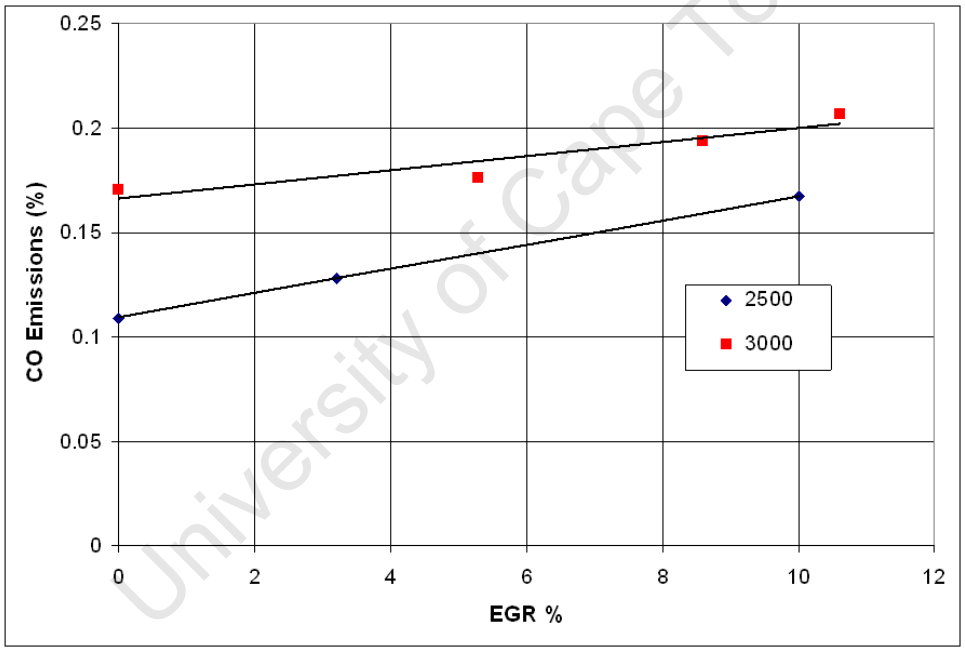

Figure 7.5: Effects of EGR % on CO Emissions

An interesting occurrence when examining the results is that CO emissions are higher at 3000rpm when compared to 2500rpm. This is trend in unexpected due to the apparent differences in operational ϕ (0.62 and 0.58 respectively) as well the reduced cylinder temperatures when operating at reduced speeds. However these differences could be explained by the possible chemical effects of EGR. The operational speed and ϕ variances may result in different EGR compositions, such that different chemical species may be

more prevalent between the two engine speeds. These chemical species may dominate the formation of CO and not operational speed and ϕ differences.

7.2.3 Manifold Pressure Effect on CO Emissions

CO emissions increased when increasing inlet manifold pressure, shown by Figure 7.6. Increased CO emissions are a result of the reduction in overall combustion temperatures due to the reduction in required ϕ to maintain constant phasing. When a mixture becomes overly lean, combustion temperatures are too low (below 1300K) and CO is unable to oxidize to form CO_2. This produces similar trends as to that shown by mixture temperature and EGR effects. This explanation is more apparent when examining the graph. CO emissions decreased with increasing speed, which is attributed to the inability of the CO to oxidize as a result of the decreased cylinder temperatures when operating at reduced speeds.

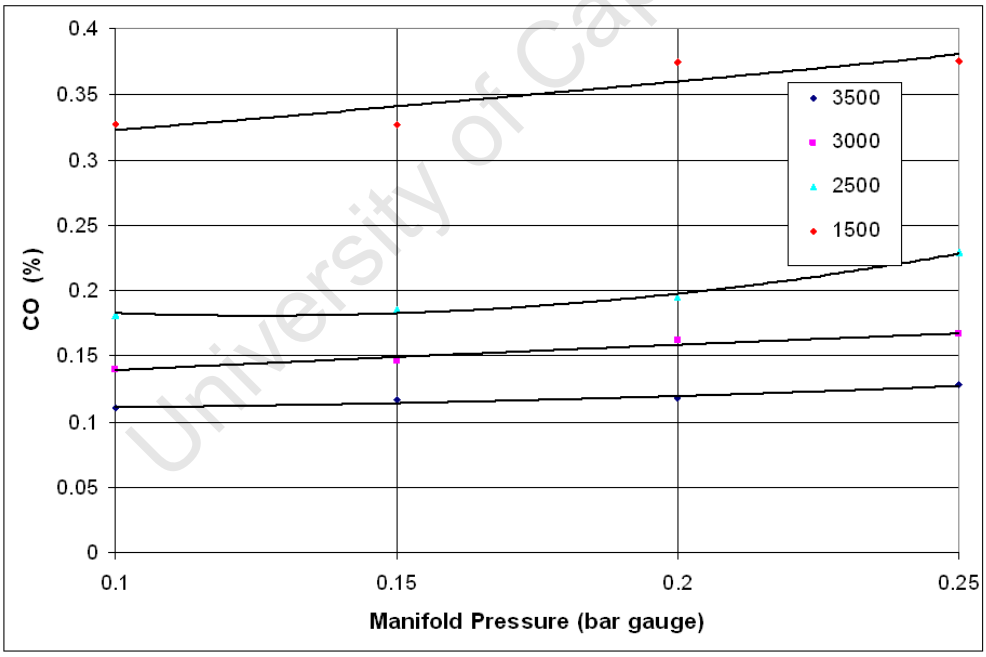

Figure 7.6: Manifold Pressure Effects on CO Emissions

Chapter 8

Experimental Engine Modeling

Experimental testing produced interesting results with respect to variances in engine operating characteristics. These variances were suspected to be as a result of high combustion chamber heat transfer. Signs of fuel NTC behaviour became apparent when operating around a speed of 4000 rpm with no additional fan cooling. A numerical engine model utilising measured engine characteristics was formulated, to model engine operating characteristics. The model was intended to gauge the effects of various heat loss terms on engine operation as well as their effects on peak pressure and auto-ignition.

The model was formulated in Microsoft Excel^{TM}to model in cylinder conditions with the aim to predict relevant cylinder characteristics as a function of Pressure vs. Crank Angle Degrees. This is achieved by separating the model into two separate components, namely a breathing model and combustion model (see Appendix A). Engine characteristics are used and incorporated with respect to Crank Angle Degrees (CAD), using a set engine speed, ambient conditions and fueling requirements to calculate desired outputs.

The breathing model runs between exhaust valve opening (EVO) and exhaust valve closure (EVC). This portion of the model calculates the breathing cycle of the engine with respect to fresh charge induced and residual exhaust gas (REG) remaining in the cylinder at IVC using inlet and exhaust manifold characteristics to accurately model the breathing cycle. A single-zone combustion model iterates the portion of the cycle between Inlet Valve Closure (IVC) and Exhaust Valve Opening (EVO) which includes the combustion portion of the cycle.

All required mixture properties are calculated using species property tables assigned to the breathing and combustion models.

Experiments were conducted in order to provide insight into effects of engine breathing and heat loss on engine operation. These results were utilised in the model as to more accurately predict engine operation.

8.1 Combustion Chamber Heat Transfer

High heat loss to the cylinder walls was expected due to the small volume to surface area ratio of the engine. As a result, heat transfer modeling would be an important factor in accurately modeling engine operation. In order to predict heat transfer to the cylinder walls, motored cylinder pressure traces were used to evaluate the heat loss to the cylinder walls from IVC to EVO, since there is no heat release from combustion and thus heat release analysis would show instantaneous heat loss from the cylinder [68]. A motored trace at 2500 rpm (shown in Figure 8.1) was chosen for Heat Release analysis purposes as it was the speed which indicated highest volumetric efficiency (n_v).

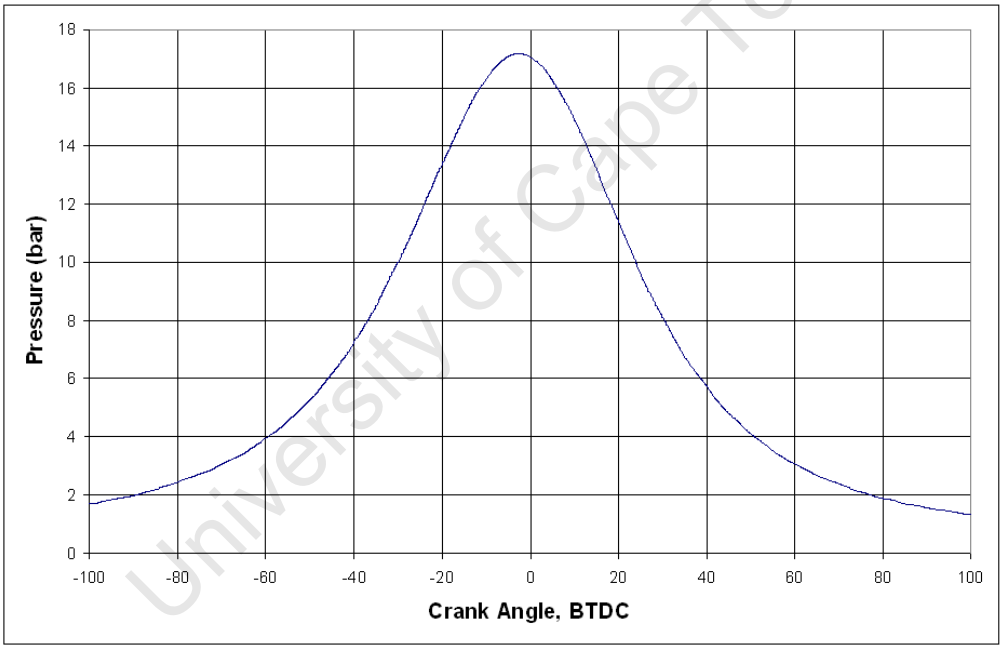

Figure 8.1: Motored Cylinder Pressure Trace at 2500rpm

A heat release analysis based on pure air with a temperature dependent specific heats was used to evaluate the heat release [11]:

$$\dot{Q}_w = \frac{\gamma(T)}{(\gamma(T)-1)} p \frac{dV}{d\theta} + \frac{1}{(\gamma(T)-1)} V \frac{dp}{d\theta}$$

The well known Woschni Heat Transfer correlation was used as a platform

for Heat Transfer modeling due its wide acceptance, robustness and simplicity in implementation. Errors were expected when using the correlation due to the nature of the original use of the correlations, where the model was used to describe heat loss in a four-cylinder water-cooled Direct Injection C.I engine.

$$\dot{Q}_{loss} = A_c h_c (T_c - T_w)$$

The Woschni Heat Transfer Correlation is shown by Equations 8.1, 8.2 below.

$$v = [C_1 S_p + C_2 \frac{V_d T_r}{p_r V_r}(p - p_m)] \tag{8.1}$$

$$h_c(W/m^2.K) = 3.26 B(m)^{-0.2} p(kPa)^{0.8} T(K)^{-0.55} v(m/s)^{0.8} \tag{8.2}$$

Where:

- B = Characteristic length usually cylinder bore
- v = Local average gas velocity
- p = Cylinder pressure
- S_p = Piston sliding speed
- p_m = Motored cylinder pressure
- V_d = Displaced volume
- p_r, V_r, T_r = Working fluids pressure, volume and temperature
- C_1, C_2 are constants depending on what part of the cylinders cycle is being considered

Inclusion of cylinder wall temperatures (T_w) for modeling purposes was provided using two thermocouples connected mounted on the cylinder. One thermocouple was placed on the outer wall and the other placed inside a hole drilled halfway between the cylinder and outer wall. These temperature

measurements are used to create a linear temperature extrapolation through the cylinder wall, based on their relative placements in the cylinder wall. The extrapolated temperature measurements are then utilised in heat loss modeling of the engine. Figure 8.2 and 8.3 below illustrate the positioning of the thermocouples on the exhaust side of the cylinder and the relative depth placements of each thermocouple on an engine cutout respectively.

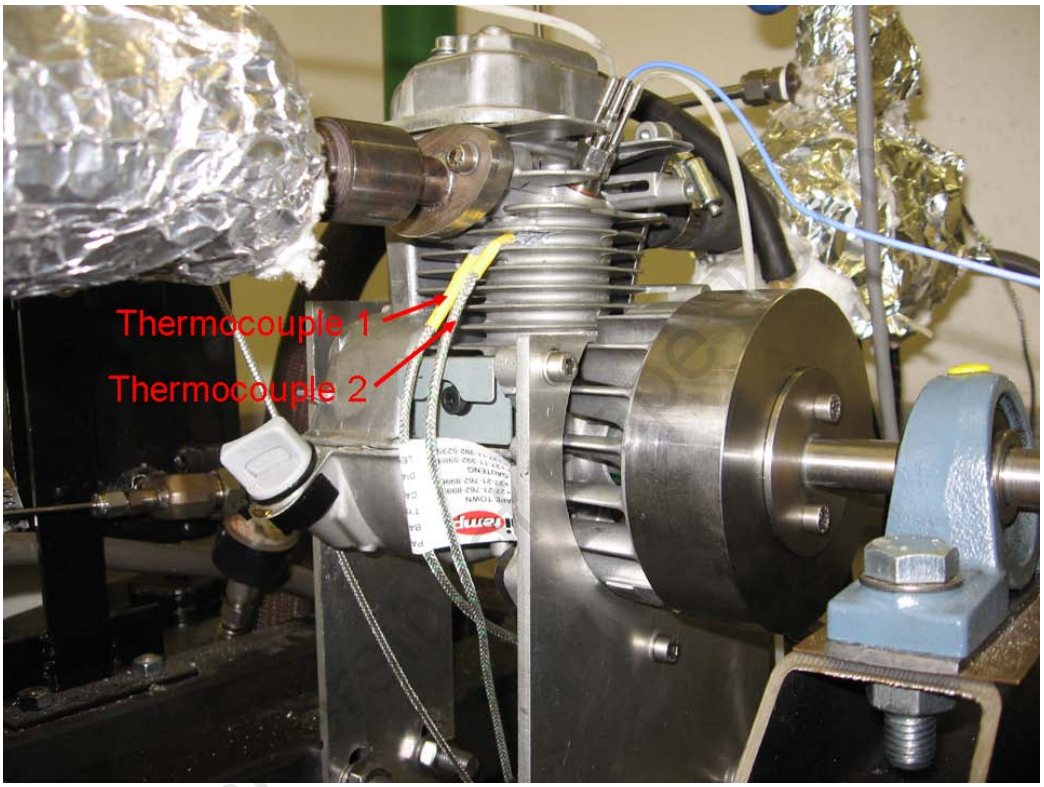

Figure 8.2: Side View of Thermocouple Placement for Cylinder Temperature Measurements

The thermocouples were installed on the exhaust side (Figure 8.2) of the engine approximately halfway up the cylinder. This position was chosen due to the spacial availability for the installation of two thermocouples within such close proximity without removing the cooling fins.

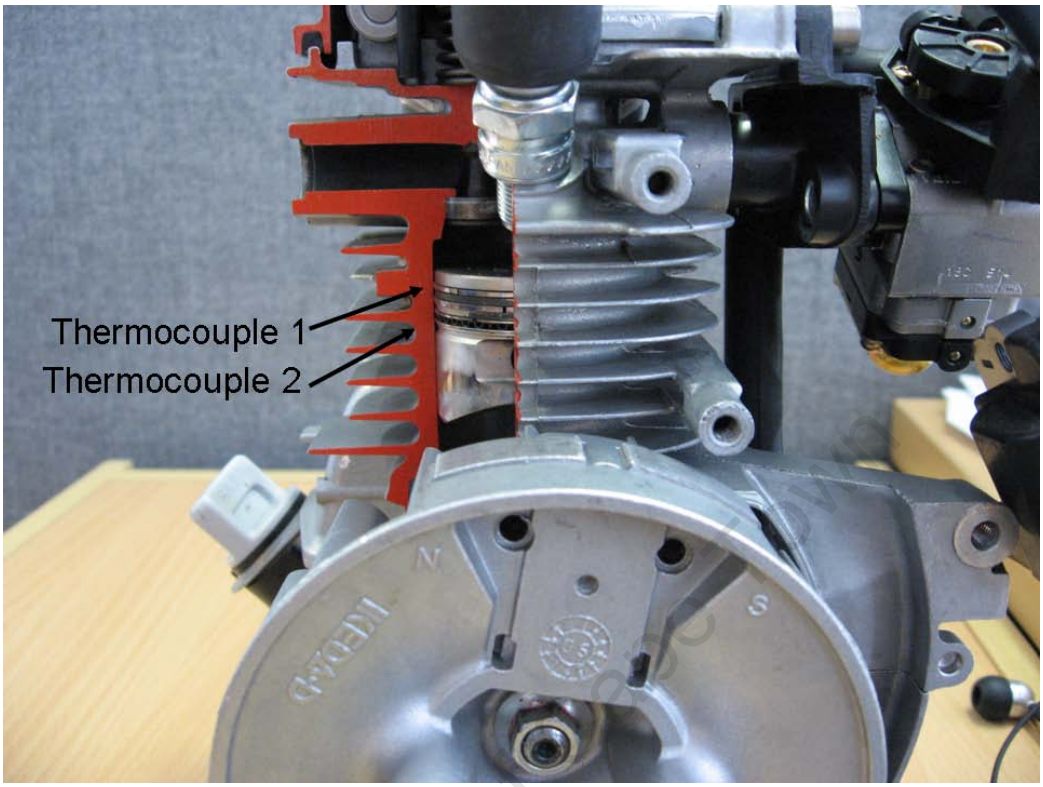

Figure 8.3: Relative Depth Placements of Thermocouples for Cylinder Temperature Measurements

The thermocouples were installed at different depths (Figure 8.3) to obtain a temperature profile across the cylinder wall as to extrapolate a time averaged combustion chamber temperature with which to use in heat transfer modeling.

A fitted heat loss model was formulated by modifying the Woschni Correlation's exponent to fit cumulative heat loss rates obtained from the experimental heat release analysis of the motored trace discussed above. Results from utilising heat release analysis as well as the thermodynamic engine model incorporating the Woschni Heat Transfer Correlation as well as a Fitted Heat Loss function are shown in Figure 8.4.

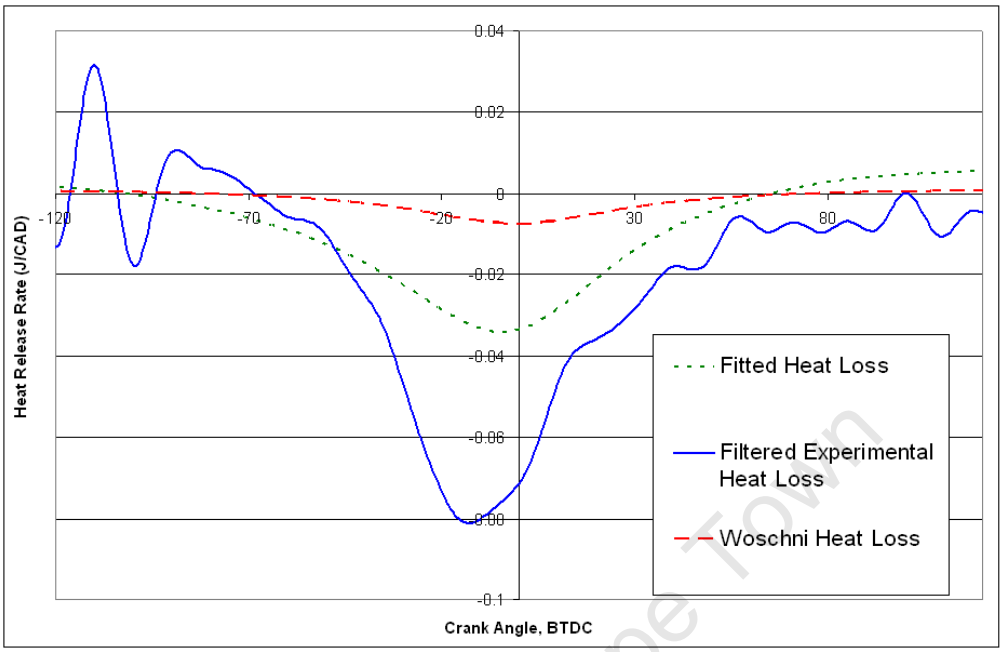

Figure 8.4: Heat Loss Rates for Motoring at 2500 rpm

It is clear that the Woschni Heat Transfer correlation doesn't accurately account for combustion chamber heat loss from the cylinder. However, the fitted heat transfer model is able to better predict heat loss over the compression and expansion strokes. The fitted heat loss function is able to more accurately predict the cumulative heat loss based on the heat release analysis, but still produces a reduced maximum heat loss rate experienced during motoring.

The fitted motored pressure trace was obtained by adjusting the **m** coefficient used in Woschni's Heat Transfer Correlation to m = 0.55. Modeling conditions remained unchanged when obtaining the original Woschni Heat Transfer Correlation's motored trace, such as cylinder wall temperatures as well as initial cylinder starting conditions.

8.2 Modeling of Proposed Adjustment to Heat Transfer Correlation

Motored pressure traces were simulated in the model to determine a fitted heat loss parameter. Figure 8.5 below is the result of the fitting of the heat loss parameters to the experimentally obtained motored trace.

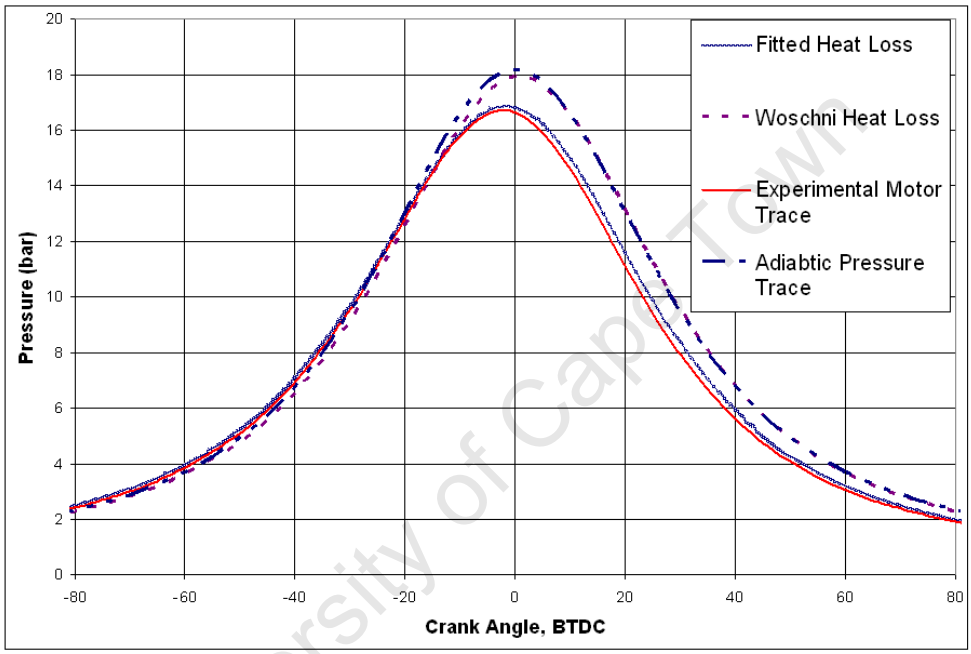

Figure 8.5: Modeled and Experimental Motored Traces Utilising Heat Loss Parameters at 2500rpm

In order to evaluate the effectiveness of the adjusted coefficient in predicting combustion engine operation during combustion, the adjusted coefficient Heat Transfer Model was iterated in the combustion model. The method of comparison was conducted by:

- Running the combustion model from IVC to EVO using:
  1. REG fraction as estimated by the breathing model which was 20%
  2. Inlet Port conditions as measured during operation where $T_{inlet} =$ 393 K
  3. Cycle averaged cylinder wall temperatures as provided by thermocouples. T_{wall} was calculated to be 220^0C.
- Utilise combustion timing obtained from the experimental combustion trace
- Use two Wiebe burn functions to describe burn progression of cool flame and main combustion
- Utilise auto-ignition modeling properties to estimate the cool flame temperature rise
- Utilise the Woschni Correlation as well as the proposed modified HCCI Woschni Correlation [5] and the fitted correlation as obtained from Motored Pressure Traces

Fuel auto-ignition was triggered manually to match experimental results for the purpose of heat transfer modeling development. However, once good thermal agreement was obtained, auto-ignition predictions could be obtained using the empirical auto-ignition model developed by Yates [60].

Figure 8.6 below shows the results as obtained from modeling of a n-Heptane experimental trace at 1500 rpm and $\phi = 0.6$ and $T_{inlet} = 393$ K. Both the original Woschni and Modified Woschni Correlations underestimated heat loss during combustion. It is clear from the plots that the fitted heat loss trace best describes the heat loss during the combustion cycle, although it seems to over estimate heat loss during the expansion stroke.

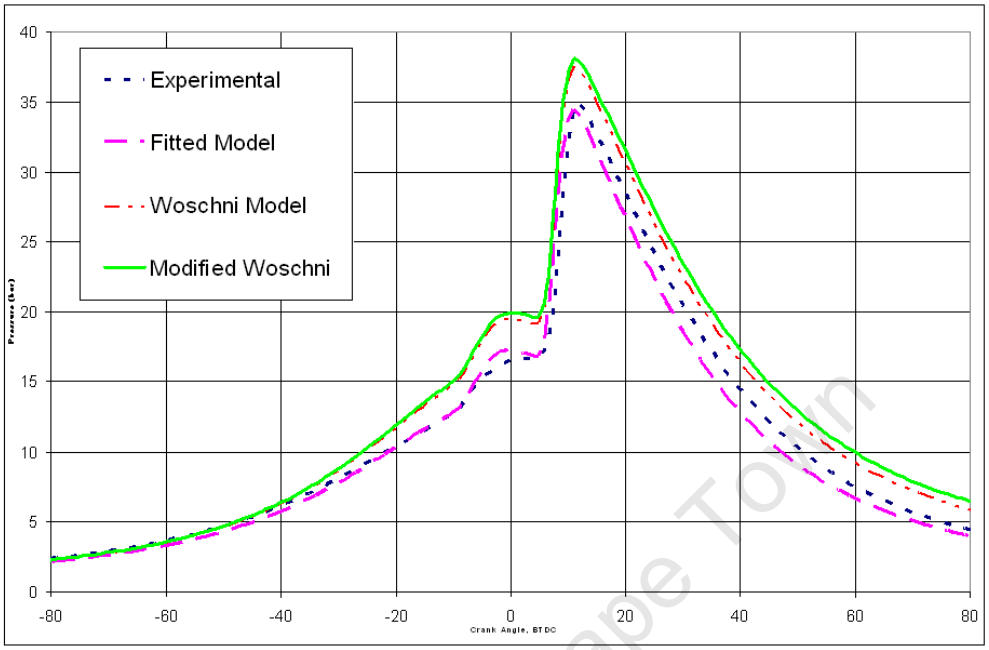

Figure 8.6: Effects of Various Heat Transfer Correlations on Predicted Cylinder Pressure Using n-Heptane at 1500rpm, $\phi = 0.6$ and $T_{inlet} = 393$ K

In spite of clear differences between HCCI, S.I and CI combustion dynamics, a change in the **m** coefficient of the Woschni model allows it to predict cylinder heat loss with surprising accuracy. When examining the equation for the heat transfer to the combustion chamber walls, shown by Equation 8.3:

$$\dot{Q}_{loss} = A_{b,w} h_{c,b} (T_b - T_w) \quad where: \tag{8.3}$$

1. $A_{b,w}$ is the cylinder area exposed
2. $h_{c,u}$ is the global heat transfer coefficient
3. T_b is the temperature of the combustion chamber
4. T_w is the cylinder wall temperature

The combustion chamber heat transfer in smaller engine's is critical due to the increased ratio of heat loss to in-cylinder internal energies and piston work. Effects of cylinder temperature chosen (T_w) with which to use in the modeling plays a major role in predicting overall heat loss from the combustion chamber. This thermal effect is further amplified due to the small engine size, such that the cylinder area exposed to heat transfer is much smaller when being compared to conventional engines. This results in relatively small changes in chosen combustion chamber temperature having a large scale affect on the overall heat transfer, especially since the wall temperature chosen is usually fixed during iteration of the model.

During the expansion stroke however the adjusted coefficient over-estimates the heat loss from the cylinder. This is as result of the wall temperature being used in the model as obtained from the thermocouples on the cylinder. The thermocouples only provide an estimate of the time averaged cylinder temperature. Over-estimation of heat loss during expansion suggests that measured cylinder wall temperatures are sufficient for the compression cycle but are underestimated during the expansion stroke as result of:

- Thermocouple placement obtains cylinder wall temperatures which may not be representative of the average combustion chamber wall temperature.
- Thermal inertia and associated delay.
- In-cylinder temperature variations due to engine operation variances.

Thermocouple placement is therefore critical in order to obtain cylinder wall temperatures which are representative of the bulk combustion chamber temperature.

Chapter 9

Conclusions

Engine Operation

General Operating Characteristics

It is possible to construct an inexpensive small scale HCCI test rig capable of performing various HCCI fuel and engine tests with a high degree of accuracy and repeatability. As a result of rig construction, stable HCCI operation was possible between 1000 - 4000 rpm similar to that in conventional HCCI engines. Engine operation was possible at 1000 rpm when operating with a combustion phasing closer to TDC. This was necessary as a result of engine misfire due to excessive heat transfer when attempting to maintain combustion phasing at 10^0 ATDC. This suggests that the proposed combustion phasing of 10^0 ATDC may be too retarded for small HCCI engine low speed operation. Upper speed limits are a result of excessive pressure rise rates (limits being set to 10 bar/CAD) defining the operational envelope.

Engine cold starting proved to be difficult, as is also experienced in conventional HCCI engines. This required the engine to be started at high speed. This operational characteristic was clearly a result of the engine's low compression ratio, resulting in reduced compression pressures, and heat loss characteristics resulting in excessive heat transfer at low speeds.

Maximum operational ϕ attained was greater than that in conventional HCCI engines. The GX25's maximum operational ϕ was 0.75 when operat-

ing without EGR. This was due to thermal gradients induced by the high surface area to volume ratio of the small engine size resulting in excessive combustion chamber heat transfer. The excessive heat transfer allows for increased fueling during operation while still producing conservative pressure rise rates (less than 10 bar/CAD).

Engine Exhaust Emissions

Engine out exhaust emissions were similar when compared to similar HCCI engine research. NOx emissions varied between 3 - 400 ppm, CO varied between 0.2 - 0.5 % and CO_2 5 - 12 % throughout the operating range. Emissions were able to be effectively controlled using the installed control strategies and can result in emission reductions.

Engine Sweet Spot Operation

Testing of the various control strategies seem to indicate points of optimal operation and so called "sweet spot" operation; where engine operation is possible under varying speed and load conditions with no required altering of control strategy conditions such that there is no effect on combustion phasing. These "sweet spots" are expected to be completely engine dependent and thus engine characteristics including heat-loss and breathing characteristics dominate in determining where inside the operational envelope they exist. This was shown by the effects of valve timing on volumetric efficiency as well as heat transfer modeling when operating over a speed range. For this reason, engine design parameters and operational characteristics in the form of breathing and heat loss are major factors in small engine operation and dictate the required control strategies and fuel selection. Such operational characteristics seem to further give proof of the existence of operational "sweet spots" suggested by similar studies.

Operational Differences Between the GX25 and PAW Engines

The ability to utilise smaller engines leads to cost reductions in performing HCCI engine research as well as defining the optimum size for full scale HCCI operation over an entire speed/load range. Below is a Table noting the operational differences observed in engine performance between the GX25 and PAW engines:

Table 9.1: Operational Differences Between the GX25 and PAW Engines

Defined Parameter	**GX25**	**PAW**
Engine Type	4-stroke	2-stroke
Cylinder Cooling Method	Air-Cooled	Water-Cooled
Fuel	Diethyl Ether	D1000
Operational ϕ Range	0.4 - 0.75 (No EGR)	0.71 - 1.05
Operational Speed Range (rpm)	1000 - 4000	2500 - 11300
Engine Compression Ratio	8:1	8 - 20.5:1
Max Operational PRR (bar/CAD)	10 (limited)	18
Max NOx Emissions	400ppm	830ppm
Max CO Emissions	0.5%	11.3 %
Max CO_2 Emissions	7.7%	15%

Operational differences between the GX25 and P.A.W engines are clear. Although the GX25 was unable to operate over such a wide speed range as compared to the PAW, it was able to operate within a large operating envelope, with the aid of combustion control strategies, from idle up to full load and speed conditions. GX25 operation was within a reduced operational ϕ range as compared to the PAW engine. However, the use of REG and EGR was shown to increase this range up to similar values to that obtained in [4]. The major differences between the GX25 and P.A.W occur due to:

- Differences in fuel's utilised between the P.A.W and GX25 engine determine the GX25's operational speed range. DEE's cetane number being higher than that of the D1000 utilised in the PAW engine testing.
- PAW's compression ratio is much high than that of the GX25, which if was increased in the GX25 would greatly improve performance. The ability to vary compression ratio was used extensively in [4] to vary engine operating conditions and extend the engine's performance. An

increase in the GX25's compression ratio would allow for operation at increased speeds as well as allow for leaner operation. Additionally the engine could be operated using a lower cetane fuel that is more representative of commercially available fuels.

- The PAW operates using a high REG % as a result of the engine's two-stroke operation. This results in the PAW engine possessing a higher operational ϕ as compared to the GX25. However, the use of EGR and REG in the GX25 does allow for a similar operational ϕ as the PAW engine.

- The PAW's high engine speed, high compression ratio and temperature controlled water-cooling system enhances the effects of engine heat transfer when compared to the GX25 engine. The PAW engine is also significantly smaller, which would also enhance it's comparative heat transfer. High combustion chamber heat loss characteristics of the GX25 is result of the engine size, speed range, four-stroke operation and air cooling strategy. This resulted in fuel NTC behavior when operating without any additional engine cooling as well as the unexpected trends observed when using REG in combustion phasing control.

Although the GX25 possessed a vastly different operational envelope, the GX25 did show signs of similar operational characteristics as that presented in [4]. The relative independence of fueling on required inlet mixture temperatures suggested that the engine could run through the operational speed range, when operating at a fixed inlet mixture temperature, using only fueling as a method of maintaining combustion phasing. This could result in the engine being able to operate along a fixed speed/load curve, similar to that demonstrated by the PAW engine. These operational similarities between the two engines are result of thermal gradients induced in the engine, result of their small size and associated high combustion chamber heat loss characteristics. This was further noted by the effects of backpressure showing an unexpected insensitivity of REG temperature on combustion phasing. This trend also seems to suggest that engine load can be altered using fueling and REG without any affect on combustion phasing, however further testing is required to clarify this hypothesis.

The so called "natural compensation" ability shown by the PAW engine was difficult to compare to the GX25 engine. Although the GX25 did show

signs of "natural compensation", as shown in Figure 6.1, the GX25's compensation is different to the PAW engine's compensation. The GX25 used fueling to maintain combustion phasing, when operating at a constant inlet mixture temperature, which altered the operational ϕ, whereas the PAW engine was able to maintain its operational ϕ and combustion phasing through the operational speed range.

Control Strategies as an Effective Means of Combustion Control

Combinations of the various control strategies can be used effectively to control HCCI combustion phasing throughout the operating range, although their effectiveness and response to transient operation was not investigated.

Installed combustion control strategies were effective in exploring and broadening the HCCI operational envelope of the engine such as allowing for increased speed range when utilising REG or EGR to reduce combustion pressure rise rates. A reduction in pressure rise rates allowed for increased operational speed at increased fueling and mixture temperature swings.

The effects of altering the relative valve timing were shown to greatly affect the engine's volumetric efficiency and thus engine torque and power. This affirms that the ability to vary the valve timing strategies, such as in a FVVT system could be used to great effect in the control of HCCI combustion phasing over a wide operating range. This would allow for the engine to operate at maximum volumetric efficiency across the engines operational speed range.

Maximum allowable mixture temperatures were approximately $\pm$340K in the lower speed range, as a result of engine misfire due to excessive combustion chamber heat transfer. An upper speed maximum temperature of $\pm$360K was obtained as a result of increased pressure rises rates when operating at increased inlet mixture temperatures. Mixture temperature control is difficult due to high thermal inertia and the associated delay in obtaining desired mixture temperatures, however this control method can be negated by utilising combinations of other control systems such as manifold pressure control and a temperature controlled EGR system.

Engine Modeling

The single zone combustion model and coupled breathing model were able to accurately predict engine operation when utilising a modified heat loss correlation. Thermocouple placement plays a major role in the modeling of heat transfer with thermal inertia affecting thermocouple measurement such that only the average cylinder temperature measurement is recorded. This was shown to have a large affect on calculation of the combustion chamber heat transfer. Results from the heat transfer modeling showed that it is possible to characterise small engine heat loss with a high degree of accuracy using motored pressure traces at one speed and transferring the correlation to combustion cycles at a different speed, while still maintaining a high degree of accuracy.

The adjusted correlation over-predicts heat loss during the expansion stroke, however accurate modeling of engine operation during the compression cycle is critical in modeling of fuel auto-ignition during engine operation. Having obtained good heat transfer correlations and modeling accuracy, auto-ignition can be accurately modeled as well as exploring the possibility of modeling engine sweet spots.

The major discrepancy between the different heat loss model correlations and the modified correlation as provided in this research, suggests that heat loss experienced in small engines during operation is primarily related to engine geometric characteristics and the method of engine cooling and not the mode of combustion.

Chapter 10

Recommendations

Further Testing

Additional Engine Testing

Engine testing must be conducted along fixed speed/load curves. This requires the construction of various speed/load curves by utilising the dynamometer in load control mode operation to construct various curves. A second option may be to utilise characterised propellers, similar to that used in the PAW testing. This would require the engine to be started using an electrical starter at high speed, due to the engine's inability to be cold started. If the engine is able to operate on fixed speed/load curves, the possibility of so called "natural compensation" operation can be investigated and the ability to possibly mimic operation of the PAW engine. Fueling can be used to construct the curves similar to that obtained in [4] and investigate whether the engine is able to produce similar operational characteristics. The ability to operate on a fixed speed/load curve can be used to extensively to characterise engine operational requirements as effected by differences between the GX25 and PAW engines.

The similar operational capabilities between the GX25 and PAW engine was expected to be the result of induced cylinder thermal gradients. If this factor is the key in operational similarities then this concept must be investigated using a larger scale engine and inducing large thermal gradients in the combustion chamber. This may then aid in operational load range extension

in large scale engines and help explain some of the operational limitations experienced by conventional HCCI engines.

Additional Fuels Testing

Fuels testing must be conducted as to characterise DEE as to provide auto-ignition data for modeling purposes by performing homogeneous combustion testing in either a combustion bomb or Rapid Compression Machine (RCM).

Hydro-Carbon (HC) Emissions Measurement

HC emission data is required to further investigate engine operation. This would require the rig to be routed to a more appropriate HC emission measurement equipment. HC emissions would provide better insight into the corresponding effects between the control strategies especially since HCCI engine are known to produce excess HC emissions.

Engine Modeling

In order to better characterise engine heat loss characteristics, the engine should be retrofitted with heat flux probes as to calibrate the heat loss function of the engine. This allows for improved accuracy in the prediction of engine heat loss as well as gauge the heat flux and temperature profiles throughout the engine. The increased modeling accuracy can be used in performing numerical "sweet spot" sweeps of engine operation before conducting experimental testing.

Test Rig Improvements

Although the test rig was able to perform all the required testing changes could be made to optimise testing and ease the testing procedure. These include:

- Installation of pneumatic control valves on the inlet and exhaust manifold control valves to provide easier method of flow control
- Adding additional control strategies such as compression ratio alterations
- Adjust the dynamometer control strategy as to allow for dynamometer load control as to aid in the construction of speed/load curves
- Install a temperature monitored engine water cooling system to replace the air-cooling system allowing for cold starting, allowing for the use of propellers for fixed speed/load curve experimentation
- Updating of the ECS to control and monitor newly implement systems
- Purchase of a spark plug/pressure transducer measuring device as to provide the possibility of exploring dual mode engine operation coupled with control strategies. This option may be difficult to implement as the octane and cetane requirements required to operate a dual mode HCCI engine. This is due to the ignition quality gap being smaller for small engines in comparison to larger engines, a result of the engine's heat transfer characteristics. This can result in misfire in HCCI mode and knocking when switching to S.I operation due to the choice of fuel.

References

[1] D. of Energy, E. E. R. Energy, and O. of Transportation Technologies, "Homogeneous charge compression ignition: (hcci) technology a report to the U.S. congress," *Report to Congress*, 2001.

[2] F. Zhao, *Homogeneous Charge Compression Ignition (HCCI) Engines: key research and development issues*. Society for Automotive Engineers, 2003.

[3] J. Bengtsson, *Closed-Loop Control of HCCI Engine Dynamics*. Lund University: Department of Automatic Control, 2004.

[4] K. Collair and G. Floweday, "Understanding hcci characteristics in mini hcci engines," *SAE 2008-01-1662*.

[5] J. Chang, O. Guralp, Z. Filipi, D. f, T.-W. Kuo, P. Najt, and R. Rask, "New heat transfer correlation for an hcci engine derived from measurements of instantaneous surface heat flux," *SAE 2004-01-2996*.

[6] S. B. Fiveland and D. N. Assanis, "Development of a two-zone hcci combustion model accounting for boundary layer effects," *SAE 2001-01-1028*.

[7] H. Yasar, H. Soyhan, H. Walmsley, B. Head, and C. Sorusbay, "Double wiebe function: An approach for single-zone engine modeling," *Applied Thermal Engineering 2007*.

[8] T. Aroonsrisopon, D. Foster, T. Morikawa, and M. Iida, "Comparison of hcci operating ranges for combinations of intake temperature, engine speed and fuel composition," *SAE 2002-01-1924*.

[9] D. Handford and M. Chekel, "Direct injection assisted hcci combustion of pre-mixed natural gas," *F2008-SC-007*, University of Alberta.

[10] M. Iida, M. Hayashi, D. Foster, and J. Martin, "Characteristics of homogeneous charge compression ignition (hcci) engine operation for variations in compression ratio, speed, and intake temperature while using n-butane as a fuel," *Volume 125, Pages 472 - 478*, Journal of Engineering for Gas Turbines and Power.

[11] J. Heywood, *Internal Combustion Engine Fundamentals*. Singapore: McGraw-Hill Book CO, 1988.

[12] R. Bartula, "A computational study of the effect of fuel type on ignition time in hcci engines," *Proceedings of the Combustion Institute*, 2007.

[13] gizmag, "Mercedes-benz unveils diesotto - the future of the gasoline engine," *gizmag*, 2007.

[14] S. Bickerstaffe, "Powertrain: Fire without a spark," *http://www.ae-plus.com/Keytopics/kt-Powertrain-news24.htm*, October 2007.

[15] E. Sippel, "First drive: Merc's high-tech diesotto engine," *http://www.wheels24.co.za/*, June 2008.

[16] S. Onishi, S. Jo, K. Shoda, P. Jo, and S. Kato, ""active radical" combustion in two-stroke cycle s.i engines," *SAE 790501*, 1979.

[17] R. Thring, "Homogeneous-charge compression-ignition (hcci) engines," *SAE 892068*, 1989.

[18] R. Craknell, J. Ariztegui, K. Barnes, P. Bessonette, W. cannella, F. Douce, B. Kelecom, H. Kraft, I. Lampreia, D. Reckeard, M. Savarese, and J. Williams, "Advanced combustion for low emissions and high efficiency: a literature review of hcci combustion concepts," *CONCAWE Report no. 4/08*, 2008.

[19] J. Allen and D. Law, "Variable valve actuated controlled auto-ignition: Speed load maps and strategic regimes of operation," *SAE-01-0422*, 2002.

[20] D. S. Kim and C. S. Lee, "Improved emission characteristics of hcci engine by various premixed fuels and cooled egr," *Fuel 85*, 2005.

[21] T. Urushihara, K. Hiraya, A. Kakuhou, and T. Itoh, "Expansion of hcci operating region by the combination of direct fuel injection, negative valve overlap and internal fuel reformation," *SAE 2003-01-0749*.

[22] Z. Zhenga and M. Yao, "Charge stratification to control hcci: Experiments and cfd modeling with n-heptane as fuel," *Fuel 88 (2009) 354365.*

[23] T. Amano, S. Morimoto, and Y. Kawabata, "Modeling of the effect of air/fuel ratio and temperature distribution on hcci engines," *SAE 2001-01-1024.*

[24] M. Richter, J. Engstrm, A. Franke, M. Aldn, A. Hultqvist, and B. Johansson, "The influence of charge inhomogeneity on the hcci combustion process," *SAE 2000-01-2868.*

[25] S. Aceves, D. Flowers, F. Espinosa-Loza, A. Babajimopoulos, and D. A. DN, "Analysis of premixed charge compression ignition combustion with a sequential fluid mechanics-multizone chemical kinetics model," *SAE 2005-01-0115.*

[26] K. Kumano and N. Iida, "Analysis of the effect of charge inhomogeneity on hcci combustion by chemiluminescence measurement," *SAE 2004-01-1902.*

[27] B. Walter and B. Gatellier, "Development of the high power nadi concept using dual mode diesel combustion to achieve zero nox and particulate emissions," *SAE 2002-01-1744.*

[28] P. D. et al (2004), "Progress in diesel hcci combustion within the european space light project," *SAE 2004-01-1904.*

[29] B. W. et al (2004), "Improvement of exhaust and noise emissions of the nadi concept using pre-mixed type combustion with multiple stages injection," *SIA International Congress: The diesel engine: today and tomorrow*, 12-13 May 2004.

[30] B. G. et al (2004), "New developments of the naditm concept to improve operating range, exhaust emissions and noise," *3th Aachen Colloquium Automobile and Engine Technology*, 12-13 May 2004.

[31] A. Maiboom, X. Tauzia, J.-F. Hetet, M. Cormerais, M. Tounsi, T. Jaine, and S. Blanchin, "Various effects of egr on combustion and emissions on an automotive di diesel engine: numerical and experimental study," *SAE 2007-01-1834.*

[32] X.-C. Lu, W. Chen, and Z. Huang, "A fundamental study on the control of the hcci combustion and emissions by fuel design concept combined with controllable egr. part 2: Effect of operating conditions and egr on hcci combustion," *Fuel*, 2005.

[33] S. Kook, "The influence of charge dilution and injection timing on low temperature diesel combustion and emissions," *SAE 2005-01-3837*.

[34] T. Ryan, "Hcci - update of progress 2005," *12th Diesel Engine-Efficiency and Emissions Research (DEER) Conference*, 2006.

[35] P. Aleiferis, "Autoignition initiation and development of n-heptane hcci combustion assisted by inlet air heating, internal egr or spark discharge: an optical investigation," *SAE 2006-01-3273*.

[36] H. Persson, M. Agrell, J.-O. Olsson, and B. Johansson, "The effect of intake temperature on hcci operation using negative valve overlap," *SAE 2004-01-0944*.

[37] Z. Chen and K. Mitsuru, "How to put the hcci engine to practical use: Control the ignition timing by compression ratio and increase the power output by supercharge," *SAE 2003-01-1832*.

[38] H. Machrafia and S. Cavadiasab, "An experimental and numerical analysis of the influence of the inlet temperature, equivalence ratio and compression ratio on the hcci auto-ignition process of primary reference fuels in an engine," *Fuel Processing Technology*, 2008.

[39] J. Hyvonen, G. Haraldsson, and B. Johansson, "Operating range in a multi cylinder hcci engine using variable compression ratio," *SAE 2003-01-1829*.

[40] Y. A. Cengel and M. A. Boles, *Thermodynamics: An Engineering Approach*. New York: McGraw-Hill Higher Education, 2002.

[41] H. Ogawa, "Dependence of ultra-high egr and low temperature diesel combustion on fuel injection conditions and compression ratio," *SAE 2006-01-3386*.

[42] T. C. et al, "Adapting the nadi^{TM}concept to heavy duty engines," *Oil & Gas Science and Technology, IFP 61*.

[43] M. Frackowiak, H. Xu, M. Wyszynski, J. Misztal, and J. Qiao, "The effect of exhaust throttling on hcci - alternative way to control egr and in-cylinder flow," *SAE 2008-01-1739*.

[44] M. Sjoberg and J. Dec, "Egr and intake boost for managing hcci low-temperature heat release over wide ranges of engine speed," *SAE 2007-01-0051*.

[45] X. cau Lu, W. Chen, Y. chun Hou, and Z. Huang, "Study on the ignition, combustion and emissions of hcci combustion engines fuelled with primary reference fuels," *SAE 2005-01-0155*.

[46] J. Yang, T. Culp, and T. Kenney, "Development of a gasoline engine system using hcci technology - the concept and the test results," *SAE 2002-01-2832*.

[47] J. Bengtsson, "Closed loop control of hcci engine dynamics," *Department of Automotive Control, Lund University*, 2004.

[48] J. Martinez-Frias, S. Aceves, D. Flowers, J. Smith, and R. Dibble, "Hcci engine control by thermal management," *Paper Submitted to 2000 SAE Conference in Baltimore*, SAE International.

[49] G. Floweday and A. Yates, "Integration of fuel auto-ignition characteristics and hcci engine operation," *SAE 2008-01-1661*.

[50] M. Christensen, B. Johansson, and P. Amnus, "Supercharged homogeneous charge compression ignition," *SAE 980787*.

[51] Morikawa and Ishibashi, "An experimental approach to the controlled auto-ignition," *SAE 2007-01-0173*.

[52] H. Kuzuyama, K. Inagaki, M. Ueda, and M. M. Kazuhiro Akihama, "A study on natural gas fueled homogeneous charge compression ignition engine - expanding the operating range and combustion mode switching," *SAE 2007-01-0176*.

[53] Y. Kodama, I. Nishizawa, T. Sugihara, N. Sato, T. Iijima, and T. Yoshida, "Full-load hcci operation with variable valve actuation system in a heavy-duty diesel engine," *SAE 2007-01-0215*.

[54] M. Shahbakhti, C. R. Koch, and R. Lupul, "Predicting hcci auto-ignition timing by extending a modified knock-integral method," *SAE 2007-01-0222*.

[55] C. Kyoungjoon, G. Lavoie, D. Assanis, Z. Filipi, and A. Babajimopoulos, "Analysis of load and speed transitions in an hcci engine using 1-d cycle simulation and thermal networks," *SAE 2006-01-1087*.

[56] M. Sjoberg and J. Dec, "Combined effects of fuel- type and engine speed on intake temperature requirements and completeness of bulk-gas reactions for hcci combustion," *SAE 2003-01-3173*.

[57] S. Aceves, D. Flowers, C. Westbrook, J. Smith, W. Pitz, R. Dibble, M. Christensen, and B. Johansson, "A multi-zone model for prediction of hcci combustion and emissions," *SAE 2000-01-0327*.

[58] G. Hohenberg, "Advanced approaches for heat transfer calculations," *SAE 790825*.

[59] W. Annand, "Heat transfer in the cylinders of reciprocating internal combustion engines," *Proc. Instn Mech. Engrs*, vol. vol. 177.

[60] A. D. Yates and C. L. Viljoen, "An improved empirical model for describing auto-ignition," *SAE 2008-01-1629*.

[61] J. Livengood and P. Wu, "Correlation of autoignition phenomena in internal combustion engines and rapid compression machines," *5th International Symposium on Combustion*, 1955.

[62] M. Murphy, J. Taylor, and R. McCormick, *Compendium of Experimental Cetane Number Data*. Colorado: National Renewable Energy Laboratory, 2004.

[63] M. Shukla, T. Bhaskar, A. Jain, S. Singal, and M. Garg, "Bio-ethers as transportation fuel: A review," *Indian Institute of Petroleum Dehradun*, 2007.

[64] J. Mack, D. Flowers, B. Buchholz, and R. Dibble, "Using biofuel tracers to study alternative combustion regimes," *Nuclear Instruments and Methods in Physics Research*, 2007.

[65] J. Mack, D. Flowers, B. Buchholz, and R. Dibble, "Investigation of hcci combustion of diethyl ether and ethanol mixtures using carbon 14 tracing and numerical simulations," *Proceedings of the Combustion Institute*, 2005.

[66] A. Yates, C. Viljoen, and O. Metcalf, "An accurate determination of the cetane number value of gtl diesel," *SAE 2007-01-0026*.

[67] M. Sjoberg and J. Dec, "Comparing late-cycle autoignition stability for single- and two-stage ignition fuels in hcci engines," *Combustion Institute*, 2007.

[68] K. Hansen, C. Nielsen, S. Sorenson, and J. Schramm, "A 50cc two-stroke di compression ignition engine fuelled by dme," *SAE 2008-01-1535*.

Appendices

Appendix A

Thermodynamic Engine Model

This Appendix describes in detail the method used in programming the Thermodynamic Engine Model used in this research project. The model was formulated in Microsoft Excel™ using Visual Basic™ to simulate relevant in-cylinder conditions as a function of Crank Angle Degrees (CAD). All relevant theory and equations are given with units being shown where necessary.

A.1 Introduction

Engine and auto-ignition modeling techniques are used to explore operating behavior with particular attention given to modeling of the engine's slightly unusual combustion heat transfer characteristics due to the engine's small displacement and air-cooled design. Modeling was completed using Microsoft Excel's Visual Basic ^{TM} and operated using a combination of Macros.

The model has been split into two separate components, namely a breathing model and combustion model, both utilising engine characteristics as well as experimental data captured to model engine operation with respect to crank angle degrees (CAD).

The breathing model entails the portion of the breathing cycle of the engine - between exhaust valve opening (EVO) to exhaust valve closure (EVC). This portion of the model calculates the breathing cycle of the engine with respect to fresh charge induced and residual exhaust gas (REG) remaining in the cylinder at EVC. The combustion model iterates the portion of the cycle between inlet valve closure (IVC) and exhaust valve opening (EVO) which includes the combustion portion of the cycle. All required mixture properties are calculated using species property tables linked to the breathing and combustion models. Each required property is calculated and sent to the relevant model.

The model provides the following characteristics of the engine on a cycle-to cycle basis:

1. Pressure vs. Crank Angle
2. Indicated Efficiency
3. Heat Release Rates
4. Work
5. Power
6. IMEP
7. Ignition Delay

*Refer to end of each section for flowcharts of the described model sections (see Figures A.1,A.3,A.5)

A.2 Species Property Tables

Properties of species listed below are calculated in the property tables. The reaction is split into reactants and products, with their relevant species properties being calculated and balanced for the combustion reaction.

Reactant properties are calculated for the following species:

- Equivalent hydrocarbon of the Fuel
- Air which consists of:
  - N_2 - Inert Gas that does not take part in the reaction
  - O_2

Product properties are calculated for the following species:

- Fuel - if rich mixture
- O_2
- CO_2
- H_2O
- H_2
- CO
- N_2

*Where CO and H_2 are products of the dissociation reactions for Water and CO_2 and are solved for by the model if dissociation reactions are required.

The model utilises property tables to calculate properties of either a motored cycle of air (for heat transfer modeling), exhaust gas (EGR/REG) or fresh charge depending what properties are required. Each zone has a dedicated Species Property Table to calculate the aforementioned species. Thus for this single zone model, the breathing model possesses motored (for heat loss calculation requirements) and breathing property tables and the combustion model has motored (for heat loss calculation requirements), fresh

charge properties and burned gas properties (either combustion products or EGR/REG).

Calculation of species properties begins with an input of fuel to produce an equivalent hydrocarbon of H, C and O using a volume blend of the components. An equivalent hydrocarbon is used to calculate phase change properties from unburned (reactants) to burned (product) gases at a chosen ϕ. Specific properties are computated based on an input of desired ϕ, thus controlling whether the mixture is Stoichiometric or Non-Stoichiometric and if the mixture is rich or lean.

Each species properties is tracked through the model (breathing and combustion) with reactions being completed according to mole based reactions for 1 mole of fuel. Species properties are solved based on the chemical equation for the reaction with a resulting mole balance required. A Gibbs Free Energy Balance is used to calculate resultant dissociated species if required. The balancing equations are shown for a non-dissociated reaction (Equation A.1) and a dissociated reaction (Equation A.2) used to calculate species properties:

$$Fuel + [3.773(O_2 + N_2)] \rightarrow aCO_2 + bH_2O + cN_2 \quad \text{(A.1)}$$

$$\rightarrow aCO_2 + bH_2O + cN_2 + dCO + eH_2 \quad \text{(A.2)}$$

Where coefficients a, b, c, d, e are solved for based on the mixtures ϕ and Gibbs Free Energy calculations (if dissociated species are required) when reacting with 1 mole of fuel.

Properties of enthalpy and internal energies are calculated at a desired temperature. The internal energy and enthalpy properties are computed using Equation A.3 below with respect to state, formation and sensible enthalpies and internal energies of each species.

$$\bar{h}_T^0 = \Delta hf_{298}^0 + \left(h^{-0} - \bar{h}_{298}^0\right)[J/mol] \quad \text{(A.3)}$$

Where:

- $\bar{h}_T^0$ = State enthalpy

- $\Delta h f^0_{298}$ = Formation enthalpy
- ($\bar{h}^{-0}$ - $\bar{h}^0_{298}$) = Sensible enthalpy

Equation A.3 is simplified using the relation that dh = CpdT, to include CHEMKIN references at a specific temperature (Equation A.4) of 298K used for convenience where constants cpa, cpb, cpc, cpd and cpe are obtained from CHEMKIN Table A.1 and Table A.2 to calculate state enthalpy:

$$\begin{aligned} &\text{If} \quad dh = CpdT \quad such \quad that \\ &Cp_{(T)} = a + bT + cT^2 + dT^3 + eT^4 \quad then \\ &\bar{h}(T) = cpaT + \frac{cpb}{2}T^2 + \frac{cpc}{3}T^3 + \frac{cpd}{4}T^4 + \frac{cpe}{5}T^5 + constant \\ &\bar{h}^0_T = \bar{h}(T)|^0_T \\ &\quad = \bar{h}(T)|_T + \Delta\bar{h}f^0_{298} - \bar{h}(T)|_{298} \end{aligned} \tag{A.4}$$

Calculation of the state internal energy is calculated by using the relationship between the enthalpy and internal energies, shown by Equation A.5

$$\begin{aligned} &\bar{u} = \bar{h} - \bar{R}T \quad \text{where} \quad \bar{R} = 8.3143[J/mol.k] \\ &\bar{u}^0 = \bar{h}T|_T + \Delta\bar{h}f^0_{298} - \bar{h}(T)|_{298} - \bar{R}T \end{aligned} \tag{A.5}$$

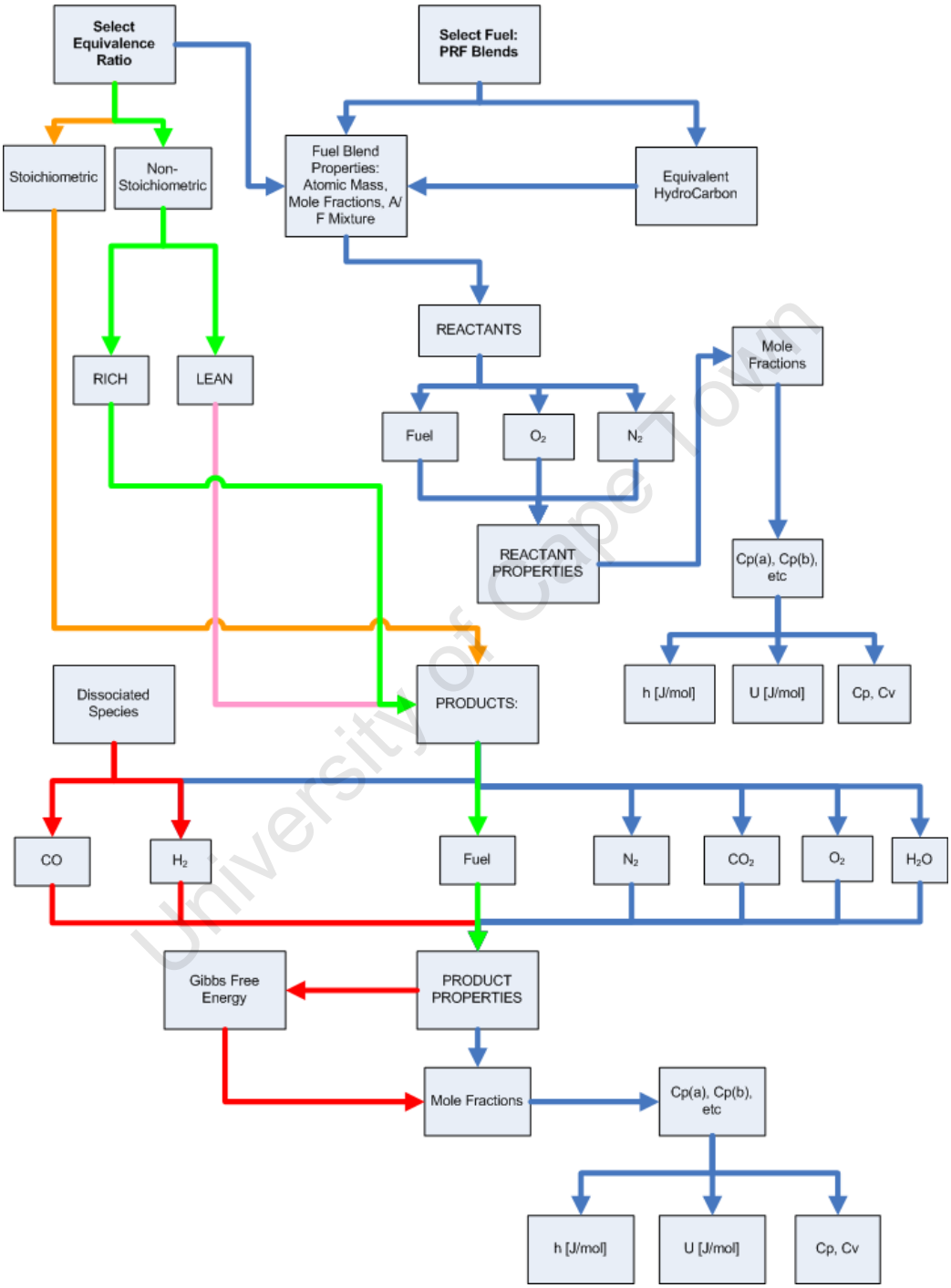

Figure A.1: Properties Schematic Layout

Table A.1: Low Temperature Thermodynamic Data for n-Heptane (300 - 1000K)

	cpa	cpb	cpc	cpd	cpe	(hf0298-h0298)	(sf0298-s0298)	hf0298	sf0298
CO_2	18.93	0.08255	-8.7E-05	5.71E-08	-1.8E-11	-402458.8824	84.76703	-393805	213.8770
CO	27.14	0.012579	-3.2E-05	4.64E-08	-2.1E-11	-119062.0152	40.3422	-110613	197.6779
H_2O	28.17	0.028911	-5.3E-05	5.8E-08	-2.1E-11	-251327.9516	21.5504	-242003.	188.839
H_2	27.44	0.006863	-6.8E-06	-7.9E-10	3.44E-12	-8424.055	-27.40647	2.450	130.680
O_2	26.73	0.009381	-4.8E-06	1.09E-08	-7.3E-12	-8363.554424	50.2083	-0.84820	205.178
N_2	27.44	0.011716	-3.3E-05	4.69E-08	-2E-11	-8493.768086	32.8666	1.430834	191.6370
Heptane	-5.146	0.6762	-0.00037	7.66E-08	0	-213098.0463	271.236	-187650	427.98

Table A.2: High Temperature Thermodynamic Data for n-Heptane (1000 - 5000K)

	cpa	cpb	cpc	cpd	cpe	(hf0298-h0298)	(sf0298-s0298)	hf0298	sf0298
CO_2	37.05	0.0261	-1.1E-05	1.99E-09	-1.4E-13	-407399.395	-7.948	-395280.74	210.50
CO	25.16	0.012003	-4.7E-06	8.47E-10	-5.7E-14	-118711.007	50.819	-110713.32	197.59
H_2O	22.23	0.0254	-7.3E-06	9.99E-10	-5.3E-14	-248757.939	57.097	-241061.51	191.03
H_2	24.88	0.0058	-4.7E-07	-7.7E-11	1.32E-14	-6947.38547	-11.274	727.64	132.24
O_2	30.76	0.00510	-1E-06	1.48E-10	-9.5E-15	-10266.154	26.533	-876.13	203.28
N_2	224.34	0.012	-4.7E-06	8.4E-10	-5.6E-14	-7677.569	49.757	92.26	191.97
Heptane	-5.146	0.6762	-0.00037	7.66E-08	0	-213098.046	271.236	-187650	427.98

A.3 Breathing Model

Due to the model being iterative, initial values are selected for pressure and temperature (see Equations A.7 and A.8). These values will be iterated and returned from the end of the combustion model and utilised as the new starting points for the following breathing cycle iteration.

Initial starting values provide initial values for the following:

- Cylinder mass (m) based on cylinder volume and cylinder Gas Constant properties (R)
- Internal energies (Obtained from property tables)
- Enthalpy (obtained from property tables)

Calculation of the current cylinder pressure is achieved by using Microsoft Excel's^{TM}Solver to alter cylinder pressure that will best satisfy an error term based on the First Law of Thermodynamics and the Conservation of Mass principle . The model is iterated for small CAD increments to try ensure model stability by minimising the error term shown in Equation A.6 below:

$$Energy \quad Error = \Delta U + \Delta W - \Delta Q - \Delta h \tag{A.6}$$

Basic breathing model columns layout are as follows:

$$\begin{aligned}
\theta \quad or \quad CAD = & \quad From \quad IVO \quad to \quad IVC \\
v_{cyl} = & \, Converted \quad using \quad engine \quad characteristics \quad (m^3) \\
P_{cyl} = & \, P@evo \quad (kPa) \quad Then \quad Calculated \qquad (A.7) \\
T_{cyl} = & \, T@evo \quad (K) \quad Then \quad T_{cyl} = \frac{PV}{mR} \qquad (A.8) \\
M_{cyl} = & \, M@ivo = \frac{PV}{RT} \quad (kg) \quad then \quad m_2 = m_1 + m_{port} \\
U_{cyl} = & \, m_2 u_{properties} \quad (kJ) \\
W = & \, \frac{P_1 + P_2}{2} dV \quad (J)
\end{aligned}$$

Where:

- v_{cyl} is cylinder volume at the current CAD
- P_{cyl} is cylinder pressure
- T_{cyl} is cylinder temperature
- M_{cyl} is cylinder mass, and m_{port} is mass entering or leaving the cylinder
- $u_{properties}$ is the internal energy from the property table

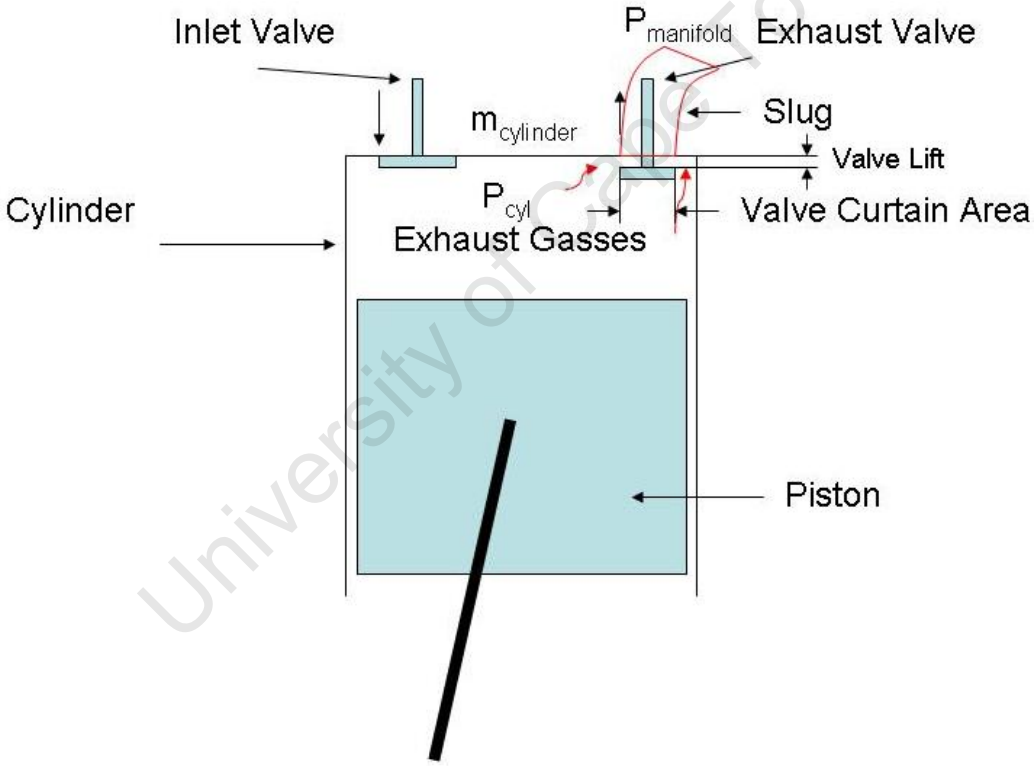

Figure A.2: Slug Movement Principle

A slug movement principle (see Figure A.2 above) is used to model dynamic pseudo compressible intake charge motion and cylinder exhausting. This principle assumes the inlet and exhaust manifolds to hold 'slugs' of mixture which interact with the cylinder as a result pressure differentials between the cylinder and manifolds. The mass either entering or exhausting from the cylinder is calculated using the pressure differential between

the cylinder and manifold (Equation A.9) coupled with the relative valve lift (Equation A.10) and valve curtain area (Equation A.11). Friction around the valve and through the manifold is specified and included as a friction factor ($F_{friction}$) using the manifolds characteristic length, diameter and the number of bends. The summation of these factors is used to obtain a resultant force on the slug (Equation A.12).

F_{total} can be used with manifold characteristics to obtain the acceleration through the port and thus a velocity (v_{port}). Velocity through the valve is limited to the sonic velocity of the mixture, simulating choking flow through the valve (Equation A.17). The direction of flow through the valve is determined by comparing the pressures between P_{cyl} and $P_{inlet/exh}$.

$$F_{port} = (P_{cylinder} - P_{manifold}).A_v \tag{A.9}$$

$$L_v = L_{max}[\frac{1}{2}(1 - cos(2\pi\frac{\theta - \theta_{ivo}}{\theta_{ivc} - \theta_{ivo}}))]^m \quad (m) \tag{A.10}$$

$$A_v = \pi D_v.L_v \quad (m^2) \tag{A.11}$$

$$F_{total} = F_{port} - (F_{loss} + F_{friction}) \quad (kN) \tag{A.12}$$

$$a_{port} = \frac{F_{total}}{m} \quad (m^2) \quad Where \tag{A.13}$$

$$v_{port} = u_{initial} + a_{port}.t \quad (m/s)$$

$$\Delta m_{port} = \rho A v_{port} \quad (kg) \quad Where$$

$$\Delta h = \Delta m C_p T \quad (J) \tag{A.14}$$

$$\Delta W = \frac{1}{2}(P_2 + P_1)(V_2 - V_1) \quad (J) \tag{A.15}$$

$$\Delta U_{cylinder} = m_{cylinder} u_{properties} \quad (J) \tag{A.16}$$

$$v_{sonic} = \sqrt{\gamma R T} \quad (m/s) \tag{A.17}$$

Where:

- m = Valve Harmonic Lift Power (0.7)
- L_{max} is the maximum valve lift (mm)
- ρ is density (kg/m^3)
- v_{port} is velocity (m/s)

- $u_{initial}$ is the initial velocity (m/s)
- a_{port} is the acceleration through the valve (m/s^2)
- v_{sonic} is the sonic velocity through the valve
- γ is the ratio of the specific heat of the mixture (Cp/Cv)

The only remaining term left to calculate is the heat loss function, Q_{loss}. This heat loss term is calculated using a modified Woschni correlation as has been described in Section 4.2, with it's correlation coefficients better describing the heat loss experienced in an HCCI engine, because of operational differences between HCCI and Diesel Engines, for which the model was initially intended.

The application of the Woschni Heat Transfer Correlation is shown by Equations A.18, A.19 below.

Where if:

$$\dot{Q} = A_w h_c (T_c - T_w) t \quad [kJ/s]$$

Where from the equation above;

1. A = cylinder surface area
2. h_c = heat transfer correlation
3. T = Temperatures of Cylinder and Wall respectively

$$w = [C_1 S_p + C_2 \frac{V_d T_r}{p_r V_r}(p - p_m)] \tag{A.18}$$

$$h_c(W/m^2.K) = 3.26 B(m)^{-0.2} p(kPa)^{0.8} T(K)^{-0.55} w(m/s)^{0.8} \tag{A.19}$$

- B = Characteristic Length usually cylinder bore
- w = Local average gas velocity

- p = Cylinder Pressure
- S_p = Piston sliding speed (m/s)
- p_m = Motored Cylinder Pressure (kPa)
- V_d = Displaced Volume (m^3)
- p_r, V_r, T_r = Working fluids pressure, volume and temperature
- C_1, C_2 are constants depending on what part of the cylinders cycle is being considered. $C_1 = 6.18$ for gas exchange and 2.28 for rest of the cycle. C_2 is 0 except for the combustion and expansion period where it is 0.00324

Mixture mass either entering or exhausting from the cylinder results in changes to cylinder enthalpy (Equation A.14), cylinder work (Equation A.15) and internal energy (EquationA.16). As mentioned above the error term can then be minimised using Solver to iterate a new pressure term. With this new pressure term, cylinder properties will be correctly adjusted and moved to the proceeding CAD where the corresponding pressure and mixture properties can be calculated.

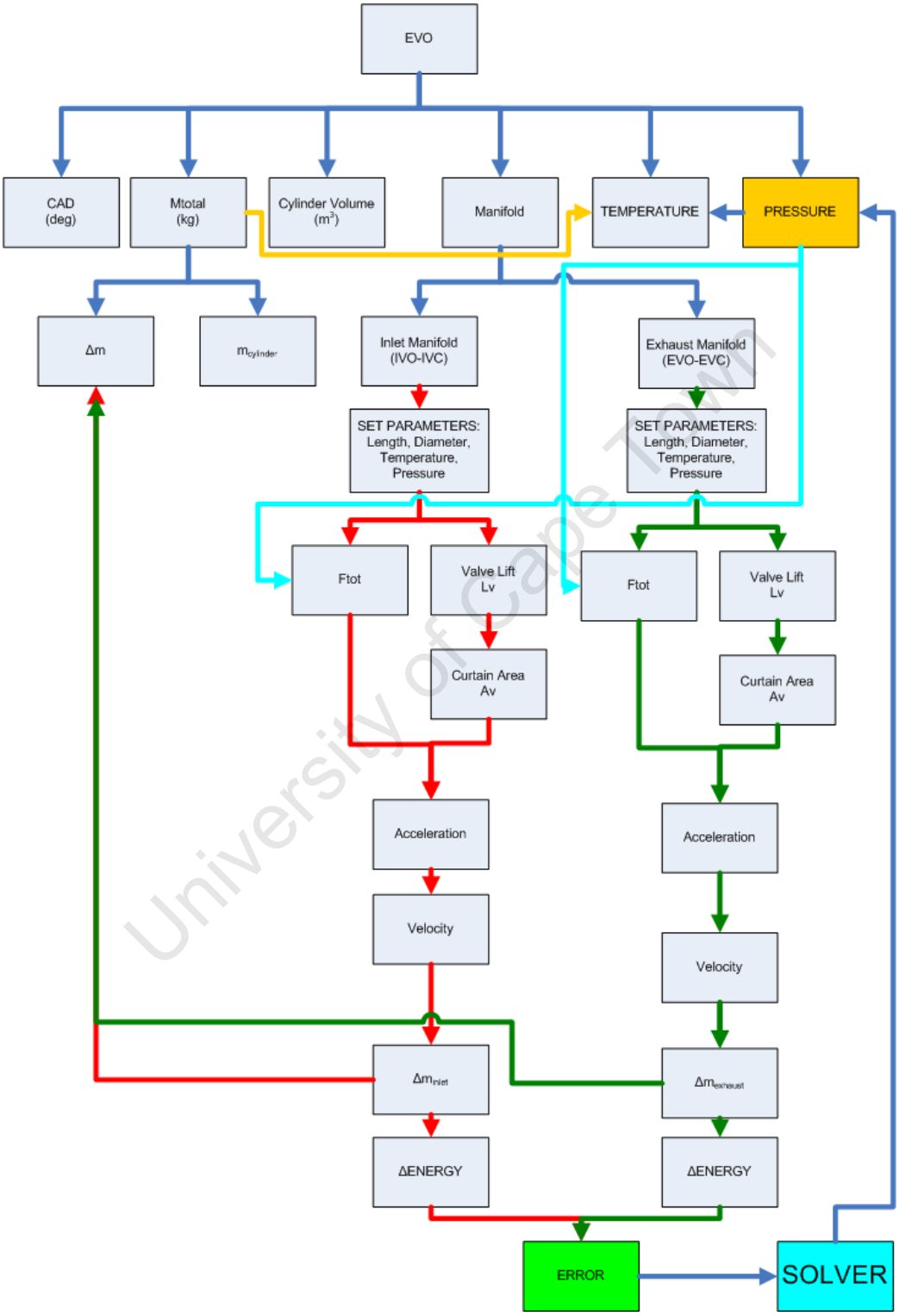

Figure A.3: Breathing Model Schematic Layout

A.4 Combustion Model

Initial combustion values are obtained from the breathing cycle, i.e IVC. Combustion is modeled using a single zone of the cylinder consisting of a mixture of fresh charge and REG. Similar to the breathing model, the combustion model also utilises a few basically defined values:

$$\begin{aligned}
\theta \quad or \quad CAD &= \quad From \quad IVO \quad to \quad IVC \\
v_{cyl} &= Calculated \quad using \quad engine \quad geometry \quad (m^3) \\
P_{cyl} &= P@evo \quad (kPa) \quad Then \quad Calculated \\
T_{cyl} &= T@evo \quad (K) \quad Then \quad T_{cyl} = \frac{PV}{mR} \\
M_{cyl} &= M@ivo = \frac{PV}{RT} \quad (kg) \\
U_{cyl} &= m_2 u_{properties} \quad (kJ) \\
W &= \frac{P_1 + P_2}{2} dV \quad (J)
\end{aligned}$$

In order to reduce computational time, the model solves using the same principle as in the breathing model, until the point of autoignition where the error is defined by:

$$EnergyError = \Delta U + \Delta W - \Delta Q$$

Ignition delay is an important parameter in the modeling of the combustion cycle. Fuel combustion can occur in two stages (if using a two-stage fuel), characterised by a preliminary reaction (Cool Flame) and then proceeded by a primary reaction (Peroxide Reaction). The cool flame reaction results in an initial pressure and temperature rise in the cylinder (see Figure A.4), affecting the ignition delay of the Peroxide reaction and phasing of maximum pressures and temperatures. This rise in Pressure and Temperature affects the ignition delay of the Peroxide reaction and cylinder heat release due to mass and cylinder energy balance changes as a result of the Cool Flame reaction. Modeling of the heat release is achieved using a double Wiebe function. One Wiebe function representing the Cool Flame Reaction and the second Wiebe function representing the Peroxide reaction.

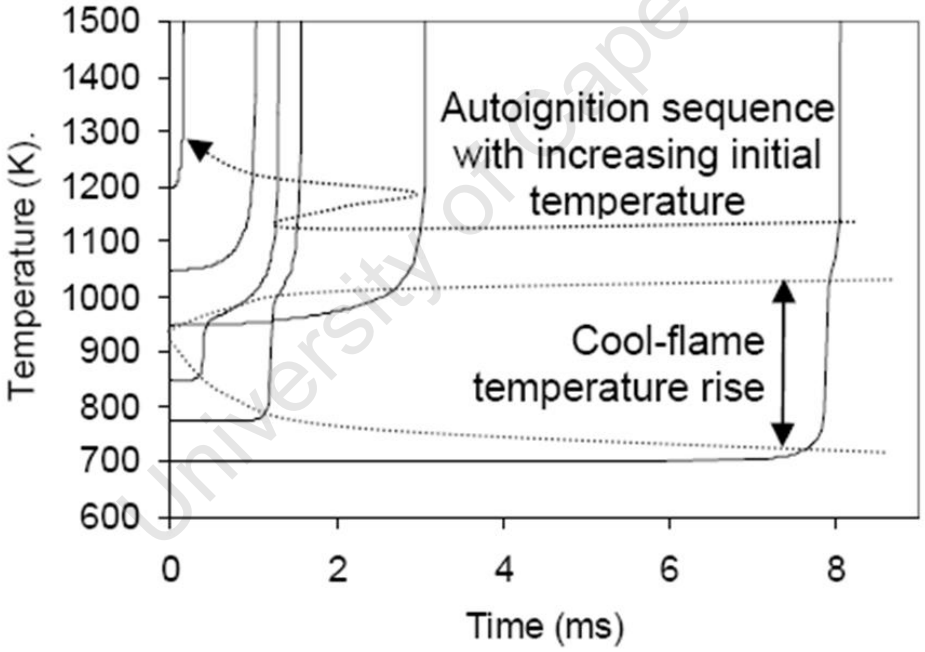

Figure A.4: Cool Flame Profile [60]

The overall ignition delay is undertaken in two stages such that: [60]

$$\int_{t_0}^{t_1} \frac{dt}{\tau_{h,i}} + \int_{t_1}^{t_2} \frac{dt}{\tau_{h,CF}} \tag{A.20}$$

Where:

- t_1 is the pre-cool flame delay
- t_2 is the overall ignition delay
- $\tau_{h,i}$ and $\tau_{h,CF}$ represent the characteristic exothermic reaction delay evaluated at the initial and post cool-flame conditions respectively.

Cool Flame autoignition criteria is defined as follows:

$$t_1 = \phi^{\beta_1} A_1 P^{n_1} e^{\frac{B_1}{T}}$$
$$\int_{t_0}^{t_1} \frac{dt}{\tau_{h,i}} = 1 \quad using \quad stage \quad 1 \quad coeff.$$
$$\tau_{h,i} = \phi^{\beta_h} A_h p_i^{n_h} e^{\frac{B_h}{T_i}}$$

Main (Peroxide) autoignition criteria is defined as follows:

$$\Delta T_{CF} = \omega \left(T_i - T_{EQ}.p^{\kappa}.\phi^{\mu} \left(\frac{100}{99+\phi} \right)^{\phi} \right) \tag{A.21}$$

$$\int_{t_0}^{t_{h,i}} \frac{dt}{\tau_1} + \int_{t_1}^{t_2} \frac{dt}{\tau_{CF}} = 1 \quad using \quad Peroxide \quad coefficients \tag{A.22}$$

$$\tau_{h,CF} = \phi^{\beta_h} A_h p_{CF}^{n_h} e^{\frac{B_h}{T_i + X\Delta T_{CF}}}$$

Coefficients (such as ln(A), n etc) are defined for n-Heptane (see Table A.3). Correct coefficient values are chosen in the Engine Models main programme by selection of the desired fuel, which will then utilise the corresponding input values.

Table A.3: Empirical coefficient values derived for n-Heptane [60]

Coefficients	N-heptane
$\mathrm{Ln}(A_1)$	-19.072
n_1	-0.065
B_1	14940
T_{equil}	816.8
ω	-1.263
$\kappa_{pressure}$	0.049
X	1.550
$\mathrm{Ln}(A_h)$	-11.41
n_h	-0.972
B_h	15474
μ_ϕ	0.0487
σ_ϕ	0.727
β_1	0.038
β_h	-0.357

The model continues iteration of the integral defined above up to the point of autoignition at which point utilisation of the current cylinder conditions are used to calculated a Cool Flame temperature rise (see Equation A.21) to determine the cylinder conditions post-Cool Flame. This temperature rise will then be used to calculate a required mass burned required to obtain post Cool Flame cylinder temperature due to the associated change in internal energy. The cool flame mass fraction burned utilises a cool flame Wiebe function as follows:

$$m_{cylinder} = m_{Unburned} + m_{Burned} + m_{EGR} \quad Where$$
$$m_{BurnedCF} = \sum_{i}^{1} Wiebe_{CF} m_{CF}$$

Mass will then be burned over a pre-determined duration using a Wiebe function defined below, which defines the mass burned as a fraction:

$$Wiebe_{CF} = 1 - exp[-b(\frac{\sigma - \sigma_0}{\Delta\sigma})^{m-1}]$$

Where:

- b,m are determined constants
- σ is the current CAD
- σ_0 is the CAD of start of Cool Flame reaction
- $\Delta\sigma$ is the Cool Flame combustion duration

All mixture properties defined by the species property tables are calculated in each section with specific reference to the specific mixture mass present in each section. At the point of the Peroxide autoignition, i.e Equation A.22 = 1, the same methodology of mass fraction burned used for the Cool Flame reaction is used to transfer mass during the Peroxide combustion event (see Equations A.23, A.24), using a newly calculated unburned mass.

$$\begin{aligned} m_{cylinder} &= m_{Unburned} + m_{Burned} + m_{EGR} \quad Where \\ m_{Peroxide}(TOTAL) &= m_{cylinder} - m_{CF} \\ m_{Peroxide} &= \sum_{i}^{1} Wiebe_{peroxide}(m_{cylinder} - m_{CF}) \end{aligned} \tag{A.23}$$

A Peroxide reaction which is the main heat release reaction ignites the remaining mixture mass according to a secondary Wiebe function (as has been described above) defined as:

$$Wiebe_{peroxide} = 1 - exp[-b(\frac{\sigma - \sigma_0}{\Delta\sigma})^{m-1}] \tag{A.24}$$

Where:

- b,m are determined constants
- σ is the current CAD
- σ_0 is the CAD of start of the Peroxide reaction
- $\Delta\sigma$ is the Peroxide combustion duration

The model is triggered to incorporate dissociated properties when cylinder temperature is above 1500 K, by solving two error terms separately and then a combination of the error terms for model stability and accuracy:

- First Error term is the Energy Balance
- Second Error term is the corresponding dissociated mole species based on Gibbs Free Energies

Incorporation of the species from dissociation reactions are achieved calculating the CO_2 (EquationA.25) and H_2O (EquationA.26) dissociation reactions, corresponding state energies associated with their formation with the aid of Gibbs free energy (EquationsA.27), formation energy principles coupled with the First Law and Second Law of Thermodynamics which define the criterion for chemical equilibrium. These energies are stored separately and used according to the dissociated species reactions property tables to calculate exact dissociated species mole fractions.

$$CO_2 \leftrightarrow CO + O_2 \tag{A.25}$$

$$CO + H_2O \leftrightarrow H_2 + CO_2 \tag{A.26}$$

Calculation of dissociated reactions relies on the chemical equilibrium principle. When considering a system of chemically reacting substances under-going a constant-pressure, constant-temperature process, in the absence of shear work the first law gives (see [11]):

$$\delta Q = \delta H$$

The second law gives:

$$\delta Q \leq T\delta S$$

Together they give:

$$\delta H - T\delta S \leq 0$$

Since the reaction is considered to be constant-temperature process, this equations becomes (where G is Gibb's free energy):

$$\Delta H - T\Delta S = \Delta G \leq 0$$

This allows the assumption that because the reactions occur at constant pressure and temperature Gibbs's free energy will equate to zero.

$$(\Delta G)_{p,T} = 0 \tag{A.27}$$

This relationship allows the computation of the various species of products which will satisfy Gibb's when dissociating. Moles of each species formed will be related to the pressure, temperature, ϕ of the mixture. Due to the computation utilising mole fractions, when looking at the mixture of ideal gases the general stoichiometric reaction can be given as, where v_i are the stoichiometric coefficients, where convention assigns positive for products and negative for reactants:

$$\sum_i v_i M_i = 0$$

This leads to an expression used to quantify the change in Gibbs's free energy of the mixture where v_i is the mole species and g_i is the chemical potential.

$$\Delta G^* = \sum v_i g_i \tag{A.28}$$
$$g_i = h_i - T_{s_i}$$

For an ideal gas and using Equation A.28 it follows that, where $\tilde{g}_i^0$ is Gibbs free energy of formation:

$$\tilde{\mu_i} = \tilde{g_i^0} + \tilde{R}Tln\frac{p_i}{p_0} \tag{A.29}$$

Simplification of the above produces two Equilibrium constants one at constant pressure K_{p1} and one based on concentrations K_{p2}. At equilibrium K_{p1} -$K_{p2} = 0$. Where K_{p1} and K_{p2} are defined as:

$$K_{p1} = e^{\frac{-\Delta G^*}{R_u T}}$$
$$K_{p2} = \left(\pi \left(N_i^{v_i}\right)\right) . \left(\frac{P}{\sum N_i}\right)^{\sum v_i}$$

The two Equilibrium constants coupled with atomic number balances are used as a basis for the secondary error term discussed earlier in this section.

Once each species properties have been defined correctly, mixture properties such as weights, Cp, Cv and molecular weights can be computated. All properties are calculated using the same method as described in Section A.3 with corresponding masses in each section used to calculate the mass specific properties and therefore satisfy the energy balance.

Iteration of the model continues to Exhaust Valve Opening. End model cylinder values and properties from the Combustion Model are transfered as initial values for the Breathing Model and the iterative process will continue until stable model operating is achieved, including final cylinder mole species with corresponding properties.

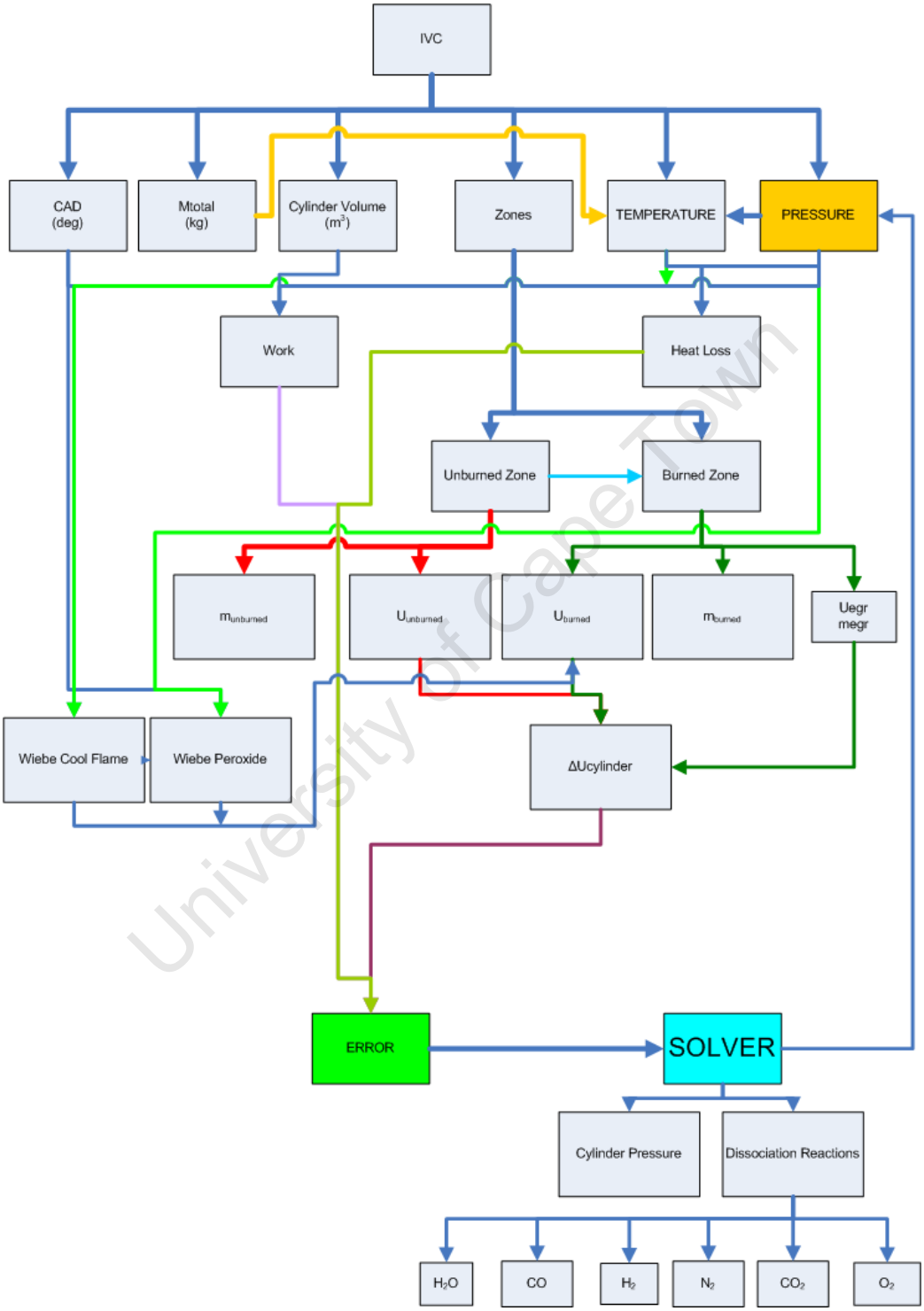

Figure A.5: Combustion Model Schematic Layout

Appendix B

Engine Test Bed Design

This appendix describes the design of the rig, including the inlet and exhaust manifold designs.

B.1 Introduction

The rig setup required that the engine be mounted such that the entire engine rig and equipment be:

- Easily accessible
- Mobile
- Easily operated
- Have maximum available control for testing
- Allow for testing of any small engine up to 1.1 kW

Constraints on the design of the rig are with respect to cost and spacial availability. Calculations are used where necessary, to ensure correct operation of the designed feature while ensuring rig safety.

B.2 Power Transmission and Engine Support

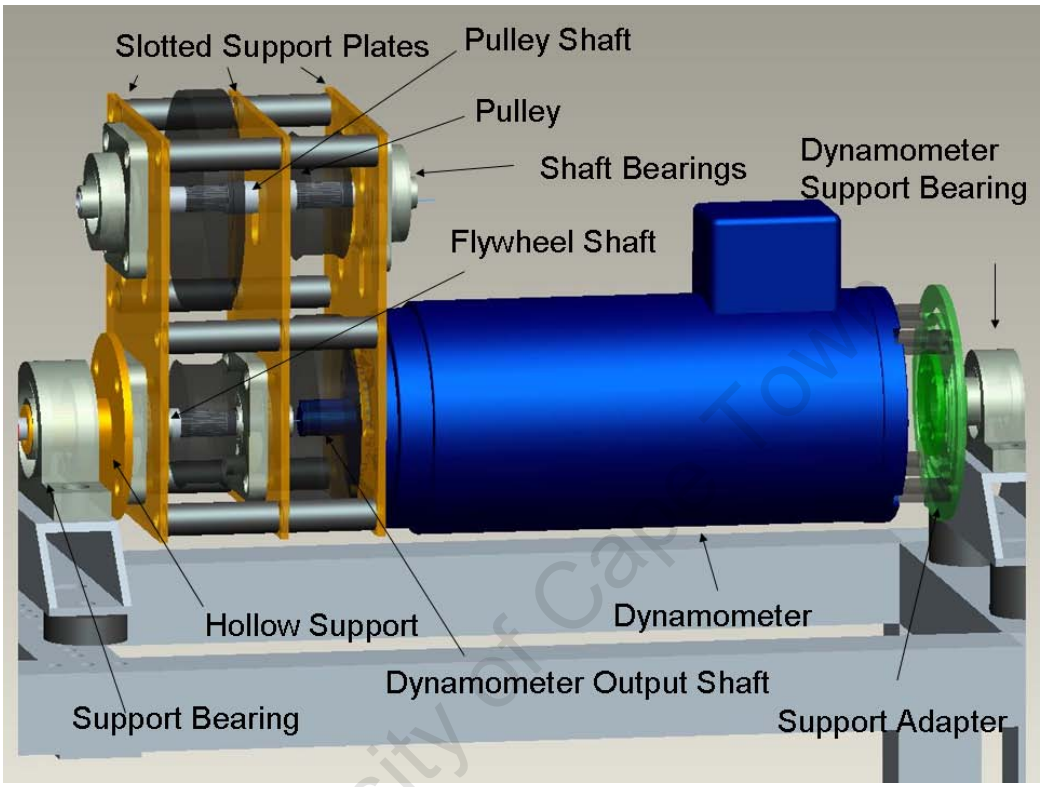

Figure B.1: Dynamometer and Reduction Drive Assembly

Figure B.2 above illustrates the Leeson™ DC Motor (specifications shown in Table B.1) and reduction drive assembly. Original design for the dynamometer and toothed belt reduction drive was completed by Mr. Kyle Collair. Minor changes were made to the design with respect to required dimensions, assembly and method of power transmission from the engine.

Table B.1: Leeson™ DC Motor Specifications

Rated Power	1.1 kW
Full Load RPM	3000 rpm
Full Load Amps DC	7.1 A
Supply Voltage	230 VAC
Thyristor Rated Voltage	180 V

A reduction drive was required due to the maximum operational speed differences between the dynamometer and engine. Speed reduction ratio

of 3:1 was used and is mounted directly onto the dynamometer with the dynamometer and reduction drive supported by two self aligning bearings mounted onto support beams. Spacers are used to ensure correct vertical alignment. Dynamometer support is achieved with a support shaft connected to the original fan cover at the rear while the front end is supported by a hollow shaft locating into a support bearing.

The reduction drive system was designed as to allow easy maintenance and interchangeability when utilising a different engine configuration. Two sets of gears are utilised for the reduction drive (see Figure B.2), one set is supported on the pulley shaft and dynamometer output shaft and the other set supported on the pulley shaft and flywheel output shaft. The pulley and flywheel shafts are supported by three slotted stainless steel plates using spacers to maintain correct horizontal distances.This design using slots are to allow for setting of the correct belt tension.

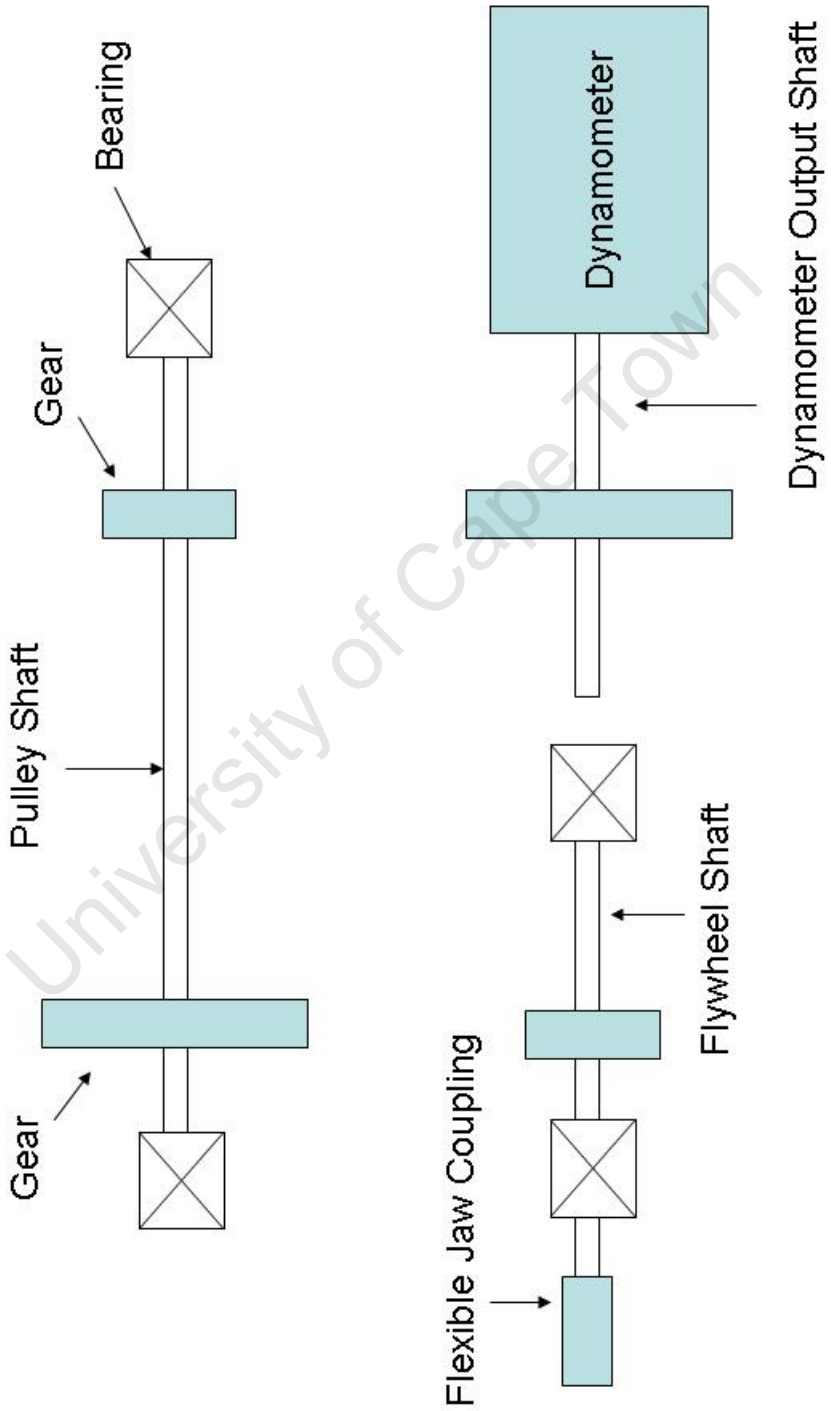

Figure B.2: Reduction Drive Schematic Layout

The reduction drive and dynamometer are assembled as a 'freely' rotational system, between two non-rotating trunnion bearings, to facilitate the installation of a simple strain gauge to monitor engine load. This was achieved by running the flywheel shaft inside a hollow support (see Figure B.1) shaft used to mount the reduction drive and dynamometer assembly, with the dynamometer possessing a separate support at the rear.

Original design of the power transfer system had a secondary flywheel mounted directly to the engines original finned flywheel. However, due to the engines inherent shaft misalignment, this concept proved to be unstable as a unbalanced eccentricity was clearly visible when running the engine at lower speeds and necessitated in a design alteration.

The new design consisted of a secondary flywheel connected to a shaft located in a self-aligning bearing. The self-aligning bearing acts as a running support for both flywheels during operation and provides static flywheel support as well as minimising the effects of the crankshafts misalignment. The secondary flywheel is mounted onto the finned flywheel and is located using two machined surfaces. This system of installation of a secondary flywheel with self-aligning bearing was chosen for several reasons:

- The original finned flywheel locates onto a tapered crankshaft. The tapered shaft makes it difficult to machine a single flywheel to locate on the shaft.
- The requirement for increased rotational inertia due to the low mass of the original finned flywheel.
- Method of assembly of the engines crankshaft causing an inherent misalignment along the crankshaft which results in a unbalanced force along the shafts axis thus requiring support to minimise the effects of the misalignment.

Figure B.3 below illustrates the method of power transfer as well and engine and reduction drive support. Two separate shafts connected by a jaw coupling transmit power throughout from the engine to the reduction drive and dynamometer. Two shafts allow for interchangeability when switching between engines. This reduces the time required when commissioning an engine, as the reduction drive assembly is fixed and does not require any adjustments, unless a change in speed reduction ratio is required. Engine

support is provided by two slotted stainless steel plates and located into slotted cross struts on the rig which are used for engine and shaft alignment.

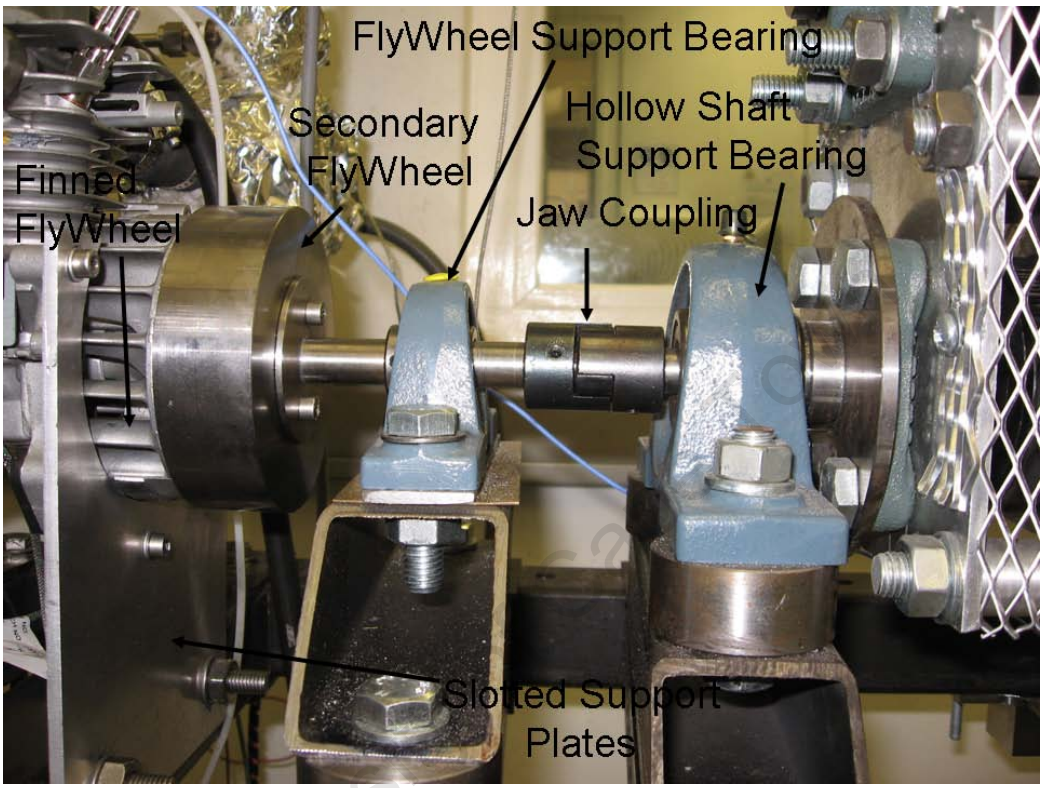

Figure B.3: Power Distribution and Engine Support

Power is transmitted from the engine to the dynamometer via a Fenner^{TM} Jaw Coupling. This coupling allows for incidental misalignment, absorbing of shock loads and dampening of small vibrations, which due to the nature of the engine being a high speed single cylinder engine was seen as an ideal installation prerequisite.

Coupling specifications are shown in Table B.2 below.

Table B.2: Coupling Specifications

Service Factor (Moderate Load)	1.5
Power Rating (kW)	1.32
Torque (N.m)	3.51
Max Misalignment (angular)	1^0
Max Misalignment (radial)	0.38mm
Element Material	Nitrile

System alignment is achieved by following several assembly steps to ensure correct alignment:

1. Dynamometer and reduction drive are assembled and placed within support bearings with flywheel shaft and coupling installed
2. Flywheel Support shaft and coupling are then connected and aligned within the support bearing
3. The engine can then be connected to the finned and secondary flywheels and aligned by utilising the slots in the supports and cross-strut supports

B.2.1 Strain Gauge Measurements

The strain gauge is mounted on the rig's frame and connected to the reduction drive using a Rod End connection and threaded bar. The strain gauge requires load introduction in a specified direction. This operating feature required a strain gauge support stand to allow for correct strain gauge alignment and load introduction while also allowing for overload prevention for safety reasons. Maximum load experienced by the strain gauge was calculated using the base engines maximum torque output of 1.0 N.m being converted to a mass output, which is achieved by using distance measurements expressed as torque arms from the centre of rotation acting through the load cell to obtain a correction factor for the load cell output. The method of load calculation is shown below with all required dimensions.

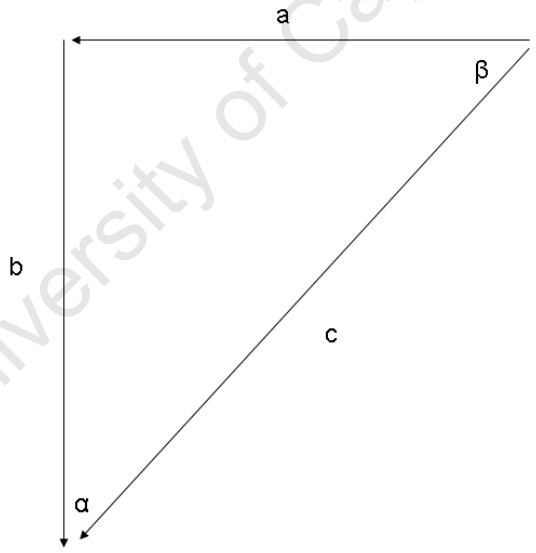

Figure B.4: Strain Gauge Distance Representation

Where:

- a = Load Measured by the strain gauge, with a distance of 100 mm

- b = 188 mm
- c = Resultant Force Vector

Using the Pythagoras and sine rules to obtain angles , α and β and .

$$\begin{aligned} \tan(\beta) &= \frac{a}{b} \\ \beta &= 61.9 \ \ degrees \\ Therefore \ \ c &= \frac{a}{\sin(\beta)} \end{aligned} \tag{B.1}$$

Therefore from the relationships above, the measured torque value must be converted using the conversion factor defined by Equation B.1 above.

The above relationship was used to estimate the maximum force experienced by the strain gauge.

$$\begin{aligned} T &= (F)(d) \\ 1.0 &= (F)(0.1) \\ F &= 10 \ \ N \\ F &= 1.02 \ \ kg \end{aligned}$$

A simple strain gauge is connected to a P-3500 Strain Gauge Amplifier which displays microstrains per strain and a $40\mu V/\mu\epsilon$ analogue output. The output voltage is sent to the ECS, from the amplifier, and converted into a load measurement using a calibration table. A strain gauge calibration graph shown below is used to convert the voltage output from the amplifier to a load, coupled with conversion factors. The strain gauge was calibrated using known masses used to generate a measured voltage using a variety of known masses.

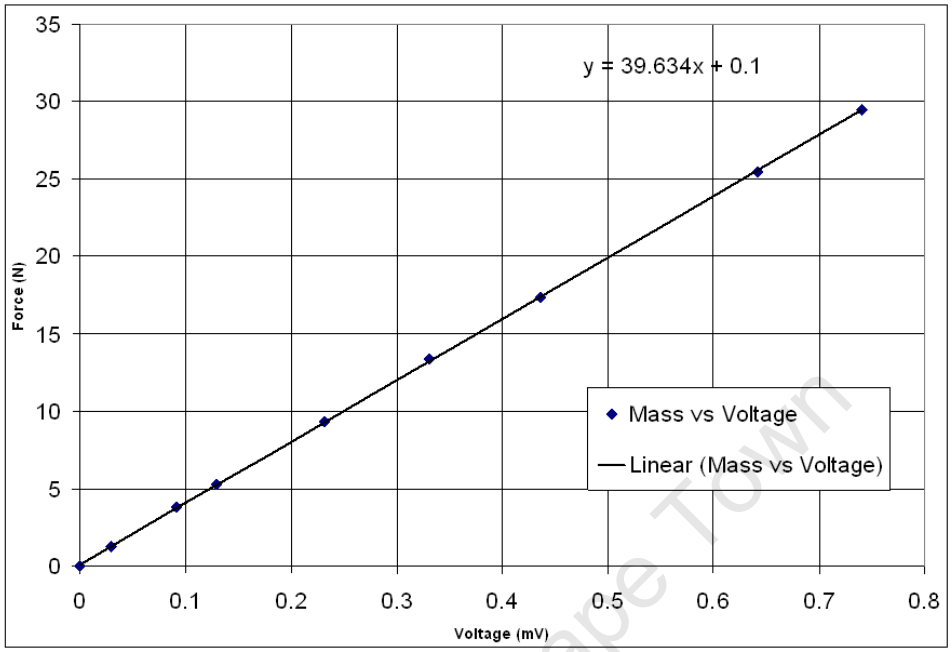

Figure B.5: Strain Gauge Calibration Graph

B.3 Inlet Manifold Design

Several design specifications for the inlet manifold were made:

- Incorporate boosting into the manifold
- Allow for control of inlet air temperature heating
- House fuel injector

The inlet manifold consists of:

- Galvanised Steel Piping for pressurised air flow
- Stainless Steel reservoir housing inlet air heater, thermocouple and pressure sensor
- Stainless Steel tubing with throttle control valve
- Injector Housing
- Flexible tubing to inlet valve

B.3.1 Inlet Manifold Boosting

Varying inlet pressure is seen as important control method for HCCI load expansion. Boosting was initially incorporated with inlet temperature control to simulate variances in compression ratio's as the engines compression ratio was only 8:1 which is seen as very low for HCCI combustion.

Boosting was provided by a roots blower (see Figure B.6) that is used for a Ricardo Hydra Single Cylinder Research Engine. The roots blower is connect to a pressure vessel which acts as a reservoir and is rated to 1.0 kPa gauge pressure. A control valve, coupled with a pressure gauge on the reservoir provides an accurate pressure measurement, and pressure control. A pressure "'tap"' was made from the Hydra's manifold line through the test cell to the Honda GX25's inlet manifold. A Cussons P7200 Laminar Flow Meter is connected to the roots blower prior to the reservoir and allows for air flow measurements to be used for mass flow measurements in the calculation

of engine volumetric efficiency. The manifold's boosting setup is shown by schematic Figure B.7 which illustrates positions of the various components in the air flow.

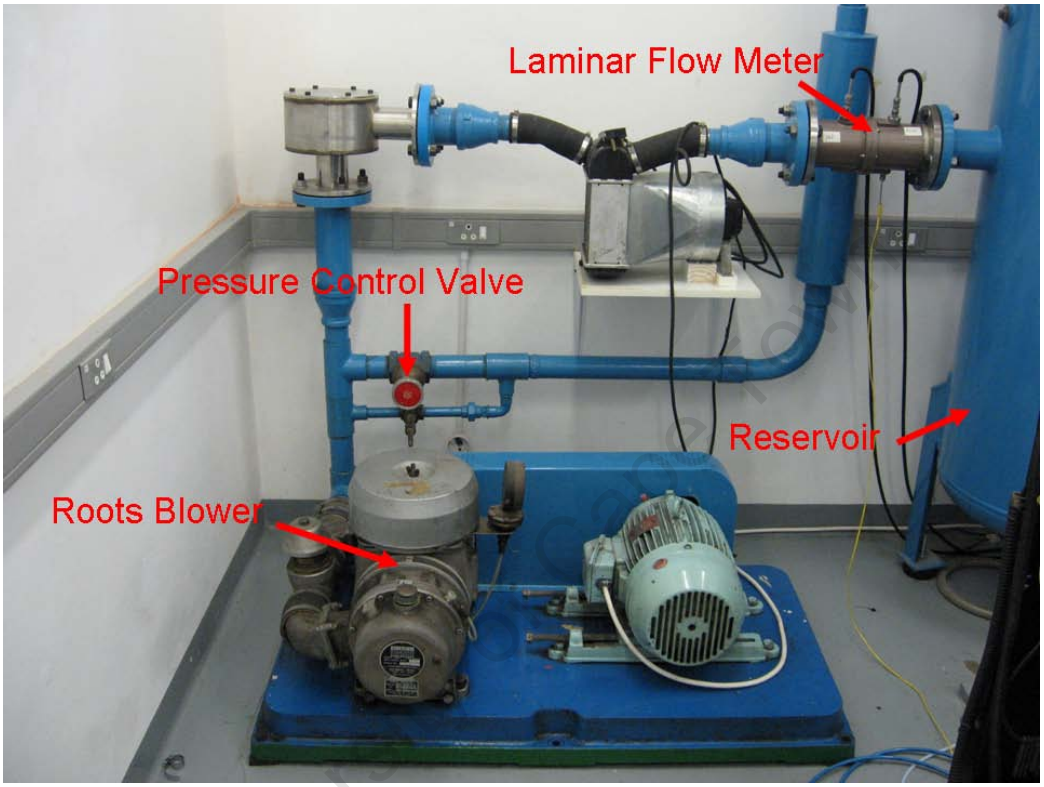

Figure B.6: Roots Blower Used for Inlet Boosting

Cussons P7200 Laminar Flow Meter specifications are shown in Table B.3 below:

Table B.3: Laminar Flow Meter Specifications

Nominal Range (smooth flow)	0 - 200 l/sec
Nominal Range (pulsating flow)	25 l/sec
Maximum Line Pressure	4 bar (gauge)

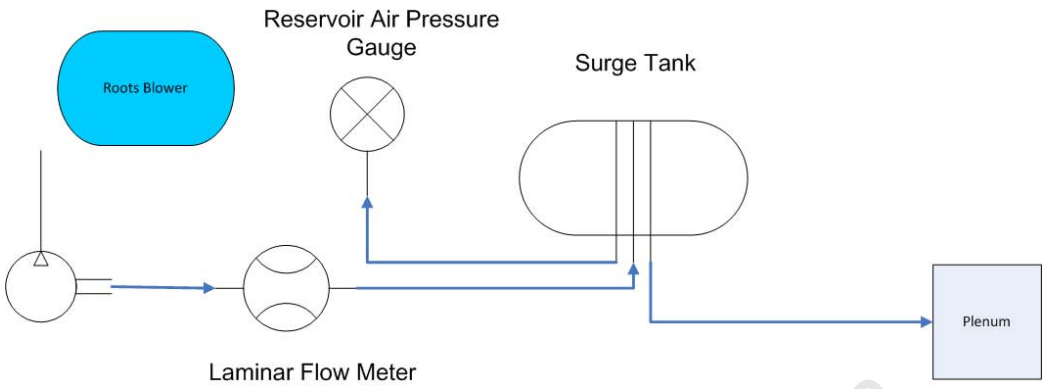

Figure B.7: Inlet Manifold Boosting Schematic

A air reservoir/plenum was added closer to the engine. There were several reasons for this addition:

- House the Inlet Air Heater
- Record Pressure and Temperature measurements for mass flow rate calculations
- Limit pressure waves on the heater to avoid possible damage
- Provide a buffer of heated pressurised air

The reservoir consists of a stainless steel tube, sealed with two designed stainless steel flanges. A third flange is used for placing of the heating element, with a groove for element placement location and support. Six holes located on the same PCD are used to seal, coupled with a gasket, the reservoir and hold the element in the correct orientation. Figure B.8 below shows an exploded view of the air reservoir, with designed flanges to house the heater and the location of airflow piping.

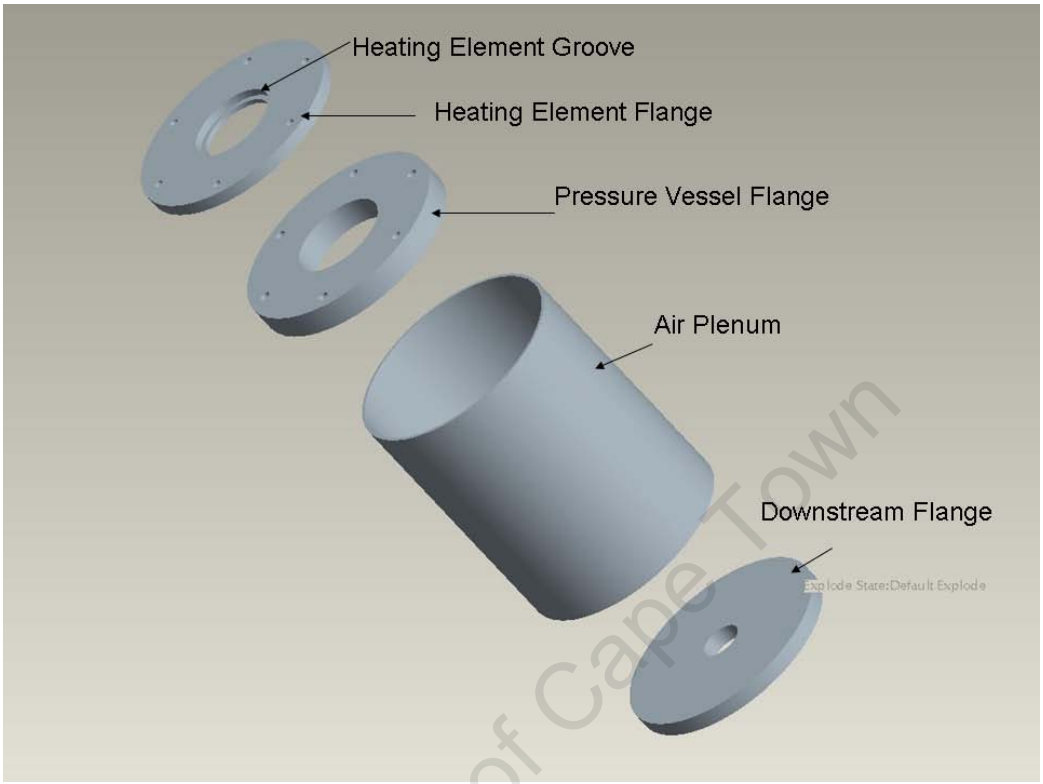

Figure B.8: Air Reservoir and Flanges

A second GEMS (0-2.5 bar) absolute pressure sensor was added to the reservoir. The aim of this sensor was to provide a second downstream measurement of the boosted air, to minimise errors due to losses through the piping. This could provide an accurate pressure reading at the point of temperature measurement, required to calculate air density used in the ECS control.

Table B.4: Inlet Manifold Pressure Sensor Specifications

Specification	**GEMS Absolute Pressure Sensor**
Current Output	0 - 20 mA
Supply Voltage	0 - 24 Vdc
Max Operating Temperature	125^0C
Max Pressure	2.5

B.3.2 Inlet Manifold Temperature Control

Inlet temperature control is a major control strategy in HCCI combustion. Altering of the inlet air temperature will affect gas temperatures at the end of compression, which will directly affect the combustion timing and heat release rates. For this reason, the ability to control inlet temperature was seen to be critical, accompanied with the fact that due to the engine's compression ratio being only 8:1, increased compression temperatures would be required in order to achieve autoignition.

Inlet temperature control was achieved with the installation of a specially designed 0.8 kW cartridge air heating located in the inlet manifold and housed in the reservoir as discussed previously. The heater is located in the reservoir in such a way that the entire air flow must flow through the heater. This ensures that the entire volume of air will experience some form of heating. The heating element is a 0.8kW heater chosen due to its required power capacity (based on Equation B.2 and Equation B.3). The heating element is controlled using a heating element temperature controller. The controller utilises a K-type thermocouple located in the reservoir which compares the reservoir temperature to a desired set temperature. The controller drives a relay control which switches the heating element on or off by comparing the desired and actual temperatues. This ensures safe operation of the element, preventing overheating of the element while still providing temperature control.

The element was selected based on engine operating conditions of:

- Initial Temperature @ 300K with maximum temperature change of 180K
- Pressure @ 2bar absolute
- 25cc of air @ max speed of 8000 rpm

The above parameters will provide initial air properties before the heating element and calculated heating requirements to obtain the desired temperature and a desired flow-rate.

$$\begin{aligned} \dot{m} &= \rho \dot{V} \qquad (B.2) \\ &= (2.322)(2.5exp^{-05})(75) \\ &= 0.00435 \ \ kg/s \\ \dot{Q} &= \dot{m} Cp \Delta T \qquad (B.3) \\ &= (0.00435)(1.005)(180) \\ &= 788W \end{aligned}$$

B.3.3 Fuel Injector

Fuel control is a critical parameter in the control of HCCI combustion. Originally, the engine utilised a diaphragm carburettor for fuel delivery, however this fuel delivery control method is not sufficient for HCCI combustion control. HCCI combustion phasing control requires exact fuel volume flow rates, which necessitates the need for fuel injection. A gasoline fuel injector was used to provide metered fuel delivery. The injector originated from Honda's Zoomer 50cc scooter and was the found to be the most appropriate injector due to its fuel flow rates.

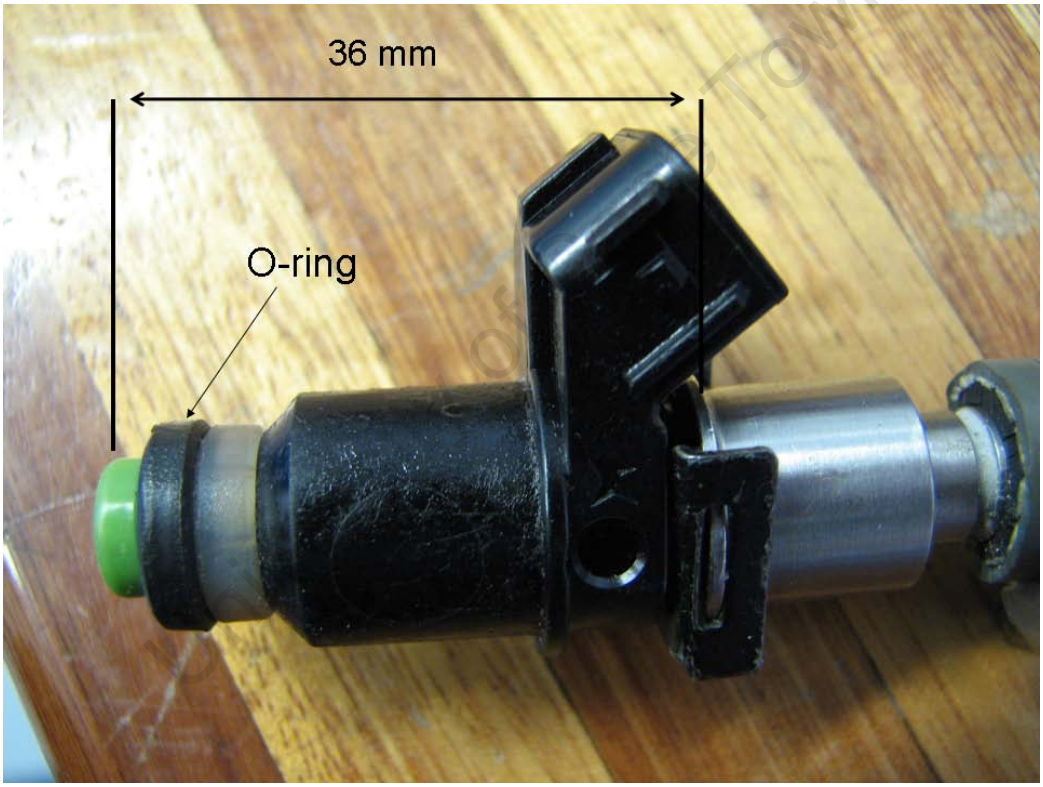

Figure B.9: 50cc Fuel Injector

Figure B.10 is a schematic of the fuel deliver system. Injection pressure for the fuel line was pre-set to 5.0bar. A high pressure Bosch Fuel pump boosted the fuel pressure to 8 bar and a check valve ensured constant pressure injection of 5 bar. A return line was required to achieve the desired pressure and return unused fuel back to the fuel tank. A pressure gauge is installed in the return line to monitor fuel pressure. A fuel filter is installed between the fuel pump and tank and a secondary high pressure fuel filter installed on the high pressure line of the fuel delivery system.

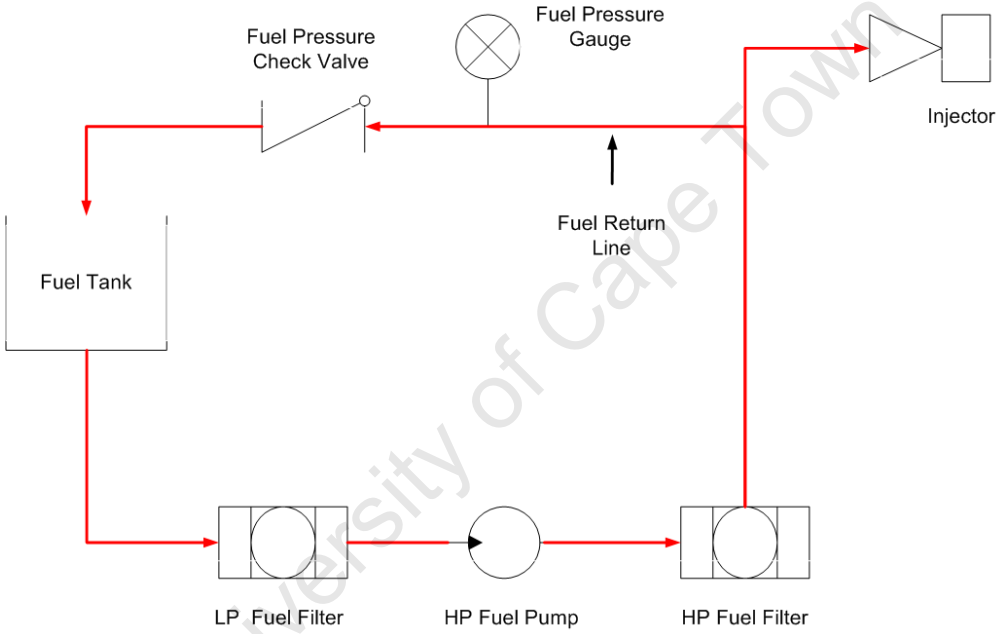

Figure B.10: Fuel Line Setup

The injector is housed in a specially designed stainless steel holder, designed to hold the injector and allow mixing between the fuel and air. Air enters the holder at 90^0 to the path of fuel flow. The air inlet port is slightly offset toward the exit side. This was done to ensure maximum fuel evaporation prior to the fuel mixing with the air. The injector and exit ports are conical in shape to minimise possible droplet pool formation. A cross-section of the design is shown by Figure B.11.

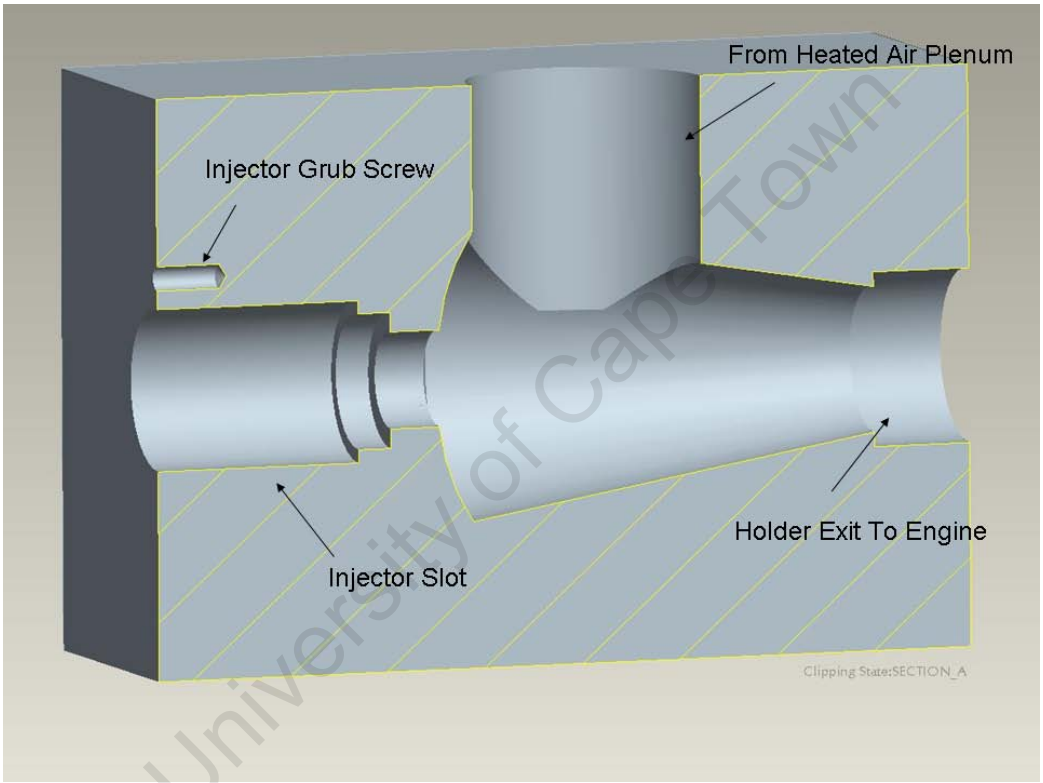

Figure B.11: Injector Holder

*See section C.2.2 information regarding the injector control circuit

B.4 Exhaust Manifold Design

Several design specifications for the exhaust manifold were made:

- Allow for exhaust gas temperature monitoring
- Control exhaust backpressure for Residual Exhaust Gas control
- Incorporation of Exhaust Gas Recirculation
- Allow for exhaust extraction
- Allow emissions measurement capabilities
- ϕ measurement

The exhaust manifold consists of:

- Stainless Steel tubing
- Stainless Steel bellows to allow flexibility of the exhaust and limit loading on the engine
- 2 x 3/4' Ball Valves for backpressure control and EGR flow rate control
- 2 x 1/4' Ball Valves for control of emissions flow rate and for inlet manifold switching
- Heat Exchanger for Exhaust Gas temperature control

Figure B.12 shows a schematic layout of the exhaust manifold with all added measurement equipment and control mechanisms. The exhaust manifold was designed with focus on attaining maximum control over engine operating conditions. The ability to control exhaust backpressure has a considerable effect on engine breathing characteristics. Exhaust backpressure is directly related to the volume of residual exhaust gas (REG) remaining in the cylinder after the breathing cycle. Additionally backpressure was to be used to control EGR flow rates in through the exhaust manifold system.

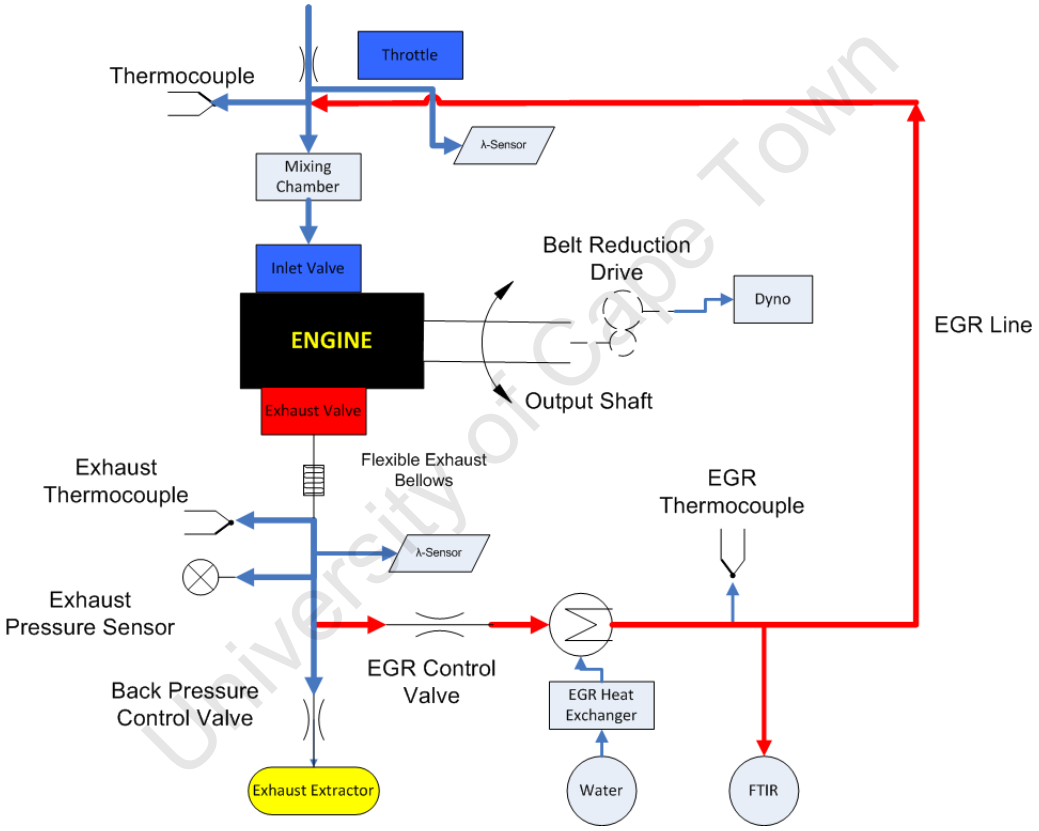

Figure B.12: Exhaust Manifold Schematic

Obtaining maximum control required several key aspects:

- Minimum REG when no backpressure is applied
- Ability to control and monitor backpressure
- Matching inlet and exhaust manifold pressure to ensure EGR flow directions

The volume of REG remaining in the cylinder at EVC is affected by the valve timing strategy as well as the exhaust manifold characteristics. Maximum exhausting from the exhaust will occur when minimal backpressure is applied, assuming a fixed timing strategy as in the GX25. This occurs when the differential pressure between the cylinder and exhaust manifold are at a maximum, such that if Pressure = Force/Area:

$$F_{Total} = F_{cylinder} - F_{losses}$$

Where:

- $F_{cylinder}$ is cylinder pressure related to a force
- F_{Losses} are result of exhaust friction and applied backpressure

Based on the aforementioned equation, maximum breathing control requires maximum control over F_{losses}. The result is that the addition of a backpressure control valve in the exhaust manifold results in maximum control over REG volumes and EGR flow rates. The backpressure valve causes a flow restriction in the manifold such that when the valve is closed, the volume of exhaust gas in the manifold increases and thus increases the manifold pressure. The increase in manifold pressure results in a decrease in differential pressure during the exhaust portion of the cycle and thus increases the REG mass at EVC. A 3/4' ball valve was used to control backpressure. Exhaust pressure was monitored by a GEMS (0 - 6 bar) absolute pressure sensor.

EGR was installed by linking the exhaust manifold and inlet manifolds using stainless steel tubing (Figure B.13). The difficulty in the design of an EGR system is the playoff between the piping sizes, EGR flow speeds as well as EGR system residence time required for temperature control. If large diameter tubing was utilised, EGR temperature control would improve due to the reduction in EGR flow speeds. The reduced flow speeds would increase the residence time in the heat exchanger. However reduced EGR flow speeds would increase EGR circulation time when switching between operating points. Due to the small volumes being circulated in the system as result of the small engine size, this would result in an undesirable increase in experimental time as well as difficulty in controlling heated EGR flow rates. Another potential issue is pulsating EGR flow due to the engine

being a single-cylinder engine. This would result in a difficulty in timing the introduction of the EGR into the cylinder. This can be overcome using a pressure differential between the inlet and exhaust manifolds, to ensure correct direction of flow.

1/4" tubing is used to connect the exit of the heat exchanger to the inlet manifold. EGR flows through a gas-water heat exchanger, to the inlet manifold. Water temperature is controlled using a heating element and K-type thermocouple temperature controller, used to set and control water temperature in the water reservoir. The water temperature is used as a method of controlling EGR temperatures into the inlet manifold with water being supplied from a water reservoir. The heat exchanger allows for the use of either hot or cold EGR depending on engine operating requirements. Water temperature and flow rates are adjusted according to the EGR exit temperature as monitored by a K-type thermocouples at the heat exchangers exit with a control valve on the water supply line from the reservoir controlling water flow rates. Flow control is achieved by controlling the pressure differential between the inlet and exhaust manifolds. This is achieved using two valves, one which controls exhaust back pressure (Backpressure valve) and hence also varies in-cylinder REG, and either EGR control valve 1 or 2, for coarse or fine adjustments respectively.

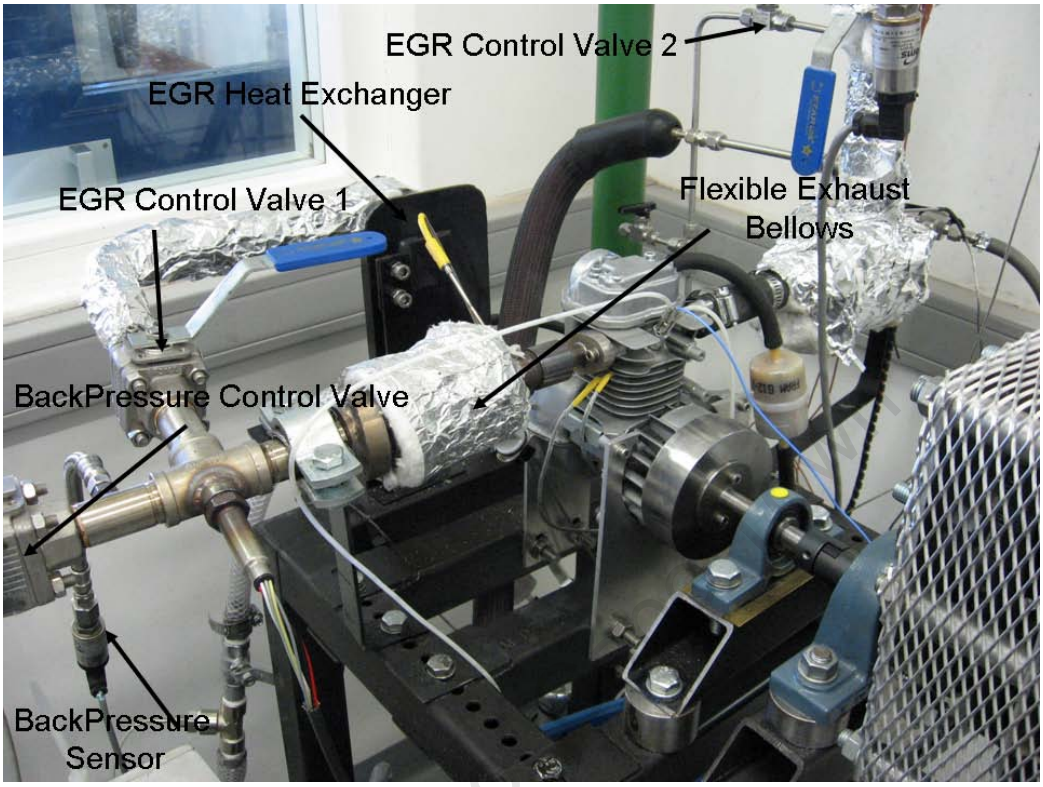

Figure B.13: Installed EGR System

A non-sampling method was required to predict EGR % being introduced into the inlet manifold due to the small volumes of exhaust gas being circulated. The volume ratio of O_2 content between the inlet and exhaust manifolds are compared, using two broadband Lambda sensors, to obtain EGR % using the Equation below:

$$EGR(\%) = \frac{\%O_{2intake} - \%O_{2Environment}}{\%O_{2Exhaust} - \%O_{2Environment}} * 100$$

B.5 Cost Analysis

A secondary goal for this research was to design an inexpensive HCCI rig able to perform research with good repeatability while occupying minimal space. Table B.5 below is an estimated cost analysis for setup of a miniature HCCI test rig based on the rig as was used for this research.

Table B.5: Mini HCCI Engine Test Rig Cost Analysis

Cost Analysis		
Engine Hardware	Engine	R2500
	Dynamometer	R10 000
	Dyno Control	R15 000
Measuring Devices	Load Cell and Amp	R20 000
	Cyl. Pressure Transducer	R30 000
	Transducer Amplifier	R20 000
	Lambda Sensors	R60 000
	Thermocouples	R2000
	Pressure Sensors	R4000
Data Acquisition	FPGA Card	R30 000
Control Hardware	PC	R10 000
	Injector	R1500
	Air Heater	R450
	Water Pump	R400
	Temperature Controller	R2000
Consumables	Materials	R10 000
	Fuel Line	R2000
TOTAL		± R226 000 ± $22 000*

*Note: Rand to U.S dollar conversion at R10.27

Appendix C

Data Acquisition Systems

This appendix details the data acquisition system as well as installed electrical component circuits as used in this research. Constraints on the control and data acquisition systems required that it allow for:

- Accurate capturing of all required data measurements
- Display all necessary data to ensure correct and safe engine operation
- Control of desired engine parameters such as engine speed and injection control
- Allow for exporting of all data captured
- Ease of operation to allow for further development and further research

C.1 Data Acquisition

A realtime data acquisition system is used to monitor cylinder pressure, manifold pressures, ϕ, temperatures, engine torque, injection control and engine speed. Data acquisition is achieved with the aid of a National Instruments Compact NI 7831-R FPGA card and connector box. All signals, digital and analogue, are connected to the connector box which acts as a signal distribution source with a FPGA card on the PC processing the signals. The signals are displayed and controlled by a LabView™ programmed Electronic Control System (ECS). The ECS was developed specifically for engine control and monitoring for this research project. All required control systems are programmed on the ECS with various display and control systems available to monitor and alter engine operation.

The ECS monitors the following:

- Engine Speed
- Cylinder Pressure from which is able to calculate:
  - Heat Release Rates
  - Cumulative Heat Release Rates
  - SOC
  - CA50
  - Maximum Pressure and CAD of Maximum Pressure
  - Power
  - Mass Flow Rates of Air and Fuel
- Inlet Manifold Pressure
- Exhaust Manifold Pressure
- Load Cell Torque Reading
- ϕ for Inlet and Exhaust (for EGR measurements)

In addition to monitoring various values, the ECS is able to vary several parameters:

- Engine Speed
- Injection Duration
- SOI with respect to TDC
- Desired number of injections (for fuel injector calibration)

Figure C.1 below illustrates the layout of the ECS in Labview™.

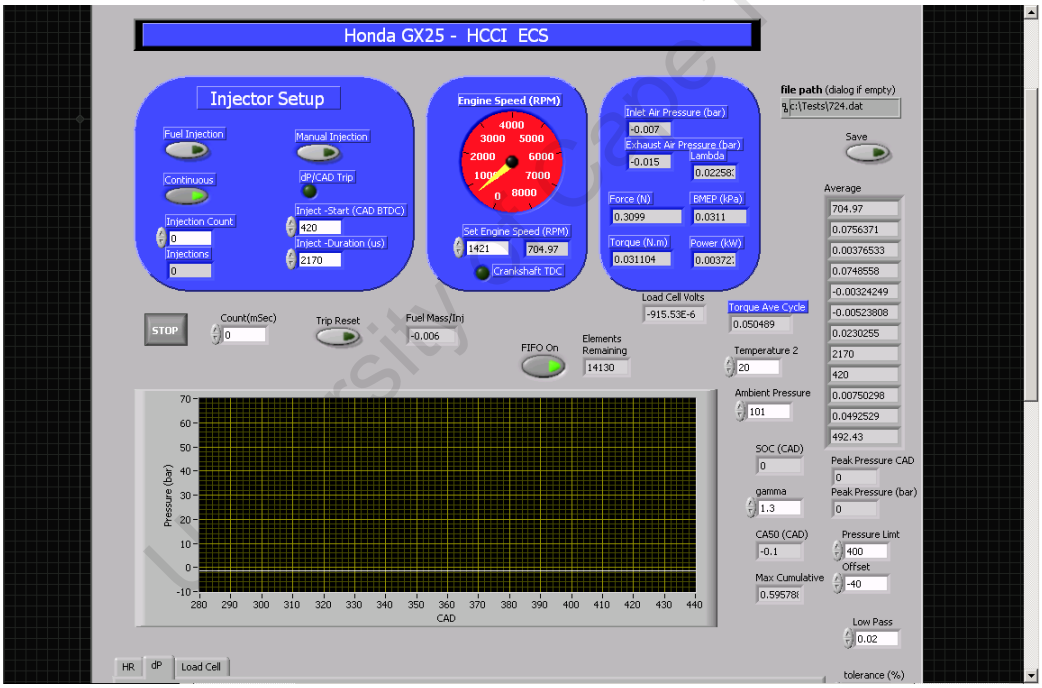

Figure C.1: Electronic Control System Layout

Exhaust, Inlet and Water temperatures are monitored on a separate digital thermocouple display. Inlet manifold boost pressure is controlled by a manual valve located on the roots blower in the test cell and monitored by the ECS using a GEMS (0 - 2.5 bar) absolute pressure sensor in the air reservoir (see Table B.4 for sensor specifications). Exhaust manifold pressure is monitored in the exhaust manifold using a GEMS (0 - 6 bar) absolute pressure sensor with specifications shown in Table C.1.

Table C.1: Exhaust Manifold Pressure Sensor Specifications

Specification	**GEMS Absolute Pressure Sensor**
Current Output	0 - 20 mA
Supply Voltage	0 - 24 Vdc
Max Operating Temperature	125^0C
Max Pressure	6

All valves including throttle, exhaust and EGR are manually operated with variances in engine operation monitored by the ECS. The Table C.2 below summaries the added measurement devices with their location and measurement requirements.

Table C.2: Location of Measurement Equipment

Signal	Description
P_1	Cylinder Pressure
T_{AR}	Air Reservoir Temp
$T_{mixture}$	Post Injector Mixture Temp
T_{exh}	Exhaust Gas Temp
T_{EGR}	EGR Line Pre-injector Gas Temp
T_{HE}	EGR Heat Exchanger
T_{cyl1}	Cylinder Wall Temp 1
T_{cyl2}	Cylinder Wall Temp 2
λ_1	Exhaust λ
λ_2	Inlet EGR λ
P_2	Air Reservoir
P_3	Exhaust Back-Pressure
Torque	Reduction/Dyno Assembly
Crank Angle	Engine Rear - Speed
FTIR Analyzer	Exhaust
$\dot{m}_{air}$	Laminar Flow Meter (Roots Blower)

- **In-cylinder pressure** is captured using a AVL QH33D Water-Cooled Pressure Transducer, installed into the original spark plug hole without the needs for any modifications. The pressure measurements are taken at 0.1 CAD with the traces being recorded on LabView^{TM}from which heat release rates, work, power and BMEP values are calculated as well as the location of CA50 to allow for fuel control. A crank angle encoder acting as a TDC marker is used to convert the time between cycles into CAD measurements, allowing for a pressure versus CAD output. Specifications for the Pressure Transducer can be seen below.

Table C.3: AVL QH33D Water Cooled Pressure Transducer Specifications

Specification	**QH33D**
Type	Water Cooled Quartz Pressure Transducer
Maximum Working Pressure	250 bar
Frequency	80 kHz
Nominal Sensitivity	17 pC/bar
Temperature Variance	0.02 $\%/^0C$
Transducer Mounting Size	M10
Charge Amplifier	Kistler Charge Amplifier type 5105

- **Temperature** measurements are achieved with the aid of K-type thermocouples to measure exhaust gas temperature as well as cooled EGR, inlet air, premixing chamber temperature and water temperatures. All temperatures are monitored and recorded either directly to the ECS or to a temperature controller which sets the desired temperature. Each measured temperature has a designated rated range which is monitored to ensure safe and optimum engine operation. Each thermocouple is able to operate up to temperatures of 1350^0C and were chosen due to the availability of K-type thermocouples digital display.

- **Emission analysis** equipment consists of a NICOLET^{TM}Protege 460 Spectrometer Fourier Transfrom Infra-Red (FTIR) gas analyzer. All emissions data was monitored using a PEUS-Systems^{TM}integrated FTIR management programme.

- ϕ is measured using a broadband lambda sensor located in the exhaust. An additional lambda sensor is located after the cooled EGR entrance to the inlet manifold after the throttle but before the fuel injector. These Lambda sensors are used for their ability to measure lean mixtures stoichiometry which is a necessity for this research, as the engine

is operated using lean air/fuel mixtures. To allow for calculation of the cooled EGR rates, using the two installed lambda sensors the formula below is used:

$$EGR(\%) = \frac{\%O_{2intake} - \%O_{2Environment}}{\%O_{2Exhaust} - \%O_{2Environment}} * 100$$

Table C.4: Lambda Sensor type and Display Unit Specifications

Lambda Sensor	BOSCH LS17025 Broadband Lambda
Measurable Lambda Range	0.7 to 32.767
Measurable O_2 Concentration	0 to 20.41%
Display Unit	ETAS LA4 Display Unit

- Fuel mass flow is determined by the calibration of the fuel injector. Further explanation is discussed later in section C.2.2
- Brake torque is obtained using an simple straing gauge attached to the free floating dynamometer and gearbox design to measure engine brake torque, all which are displayed via a strain gauge amplifier and recorded on the ECS's front panel.

All relevant data captured by the installed measurement devices are monitored and if necessary processed by the ECS. Calculation of the various operating characteristics using the pressure trace are obtained using various relationships:

Pressure vs. CAD:

As mentioned previously, a crank angle encoder is used as a TDC marker. This marker is used to convert the time between cycle TDC's into crank angle degrees to which a corresponding pressure measurement is recorded. This allows for a Pressure vs. CAD output on the ECS which can be used to calculate other engine output variables using the pressure trace.

- P = cylinder pressure (kPa)
- V = cylinder volume (m^3)
- W = Work (J)
- ω = engine velocity (rad/s)
- n_r = is the number of crank revolutions for each power-stroke (2 for a 4-stroke)

Work:

$$W = \frac{P_1 + P_2}{2}(V_2 - V_1)$$

Power:

$$Power = \frac{W}{dt}$$

Where dt is the time between cycles which is obtained from an engine speed measurement.

Torque:

$$T = \frac{P}{\omega}$$

Mean Effective Pressure (BMEP):

$$mep(kPa) = \frac{6.28 n_r T(N.m)}{V_d(dm^3)}$$

Heat Release Rates [11]:

$$\frac{dQ_n}{dt} = \frac{\gamma}{\gamma - 1} p \frac{dV}{dt} + \frac{1}{\gamma - 1} V \frac{dp}{dt}$$

Where γ is the ratio of the specific heats of the charge. This relationship is used to calculated cumulative heat release rates by integration over the engine cycle.

Calculating EGR rates is achieved by utilising two separate Broadband Lambda Sensors located in the exhaust stream and the inlet stream. The percentage of EGR rate is determined using a O_2 comparison between the inlet and exhaust Lambda sensor measurements using the following equation:

$$EGR(\%) = \frac{\%O_{2intake} - \%O_{2Environment}}{\%O_{2Exhaust} - \%O_{2Environment}} * 100$$

Complete system integration layout can be seen in Figure C.2 below.

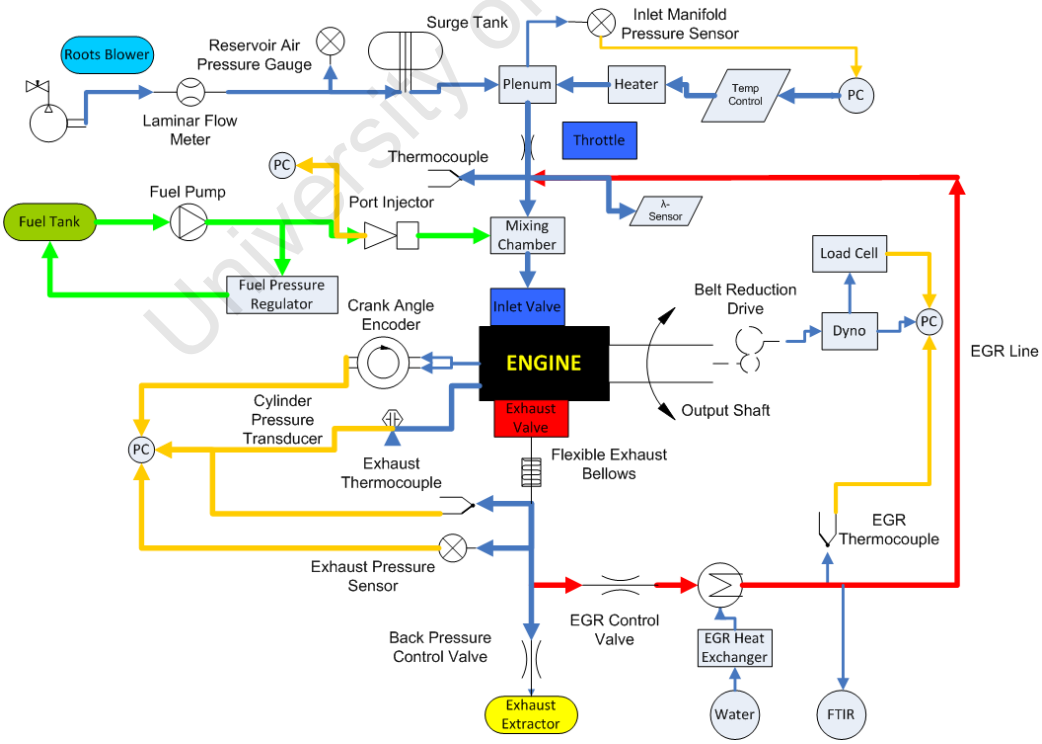

Figure C.2: Data Capturing Systems Layout

C.2 Control

C.2.1 Speed Control

Speed control is achieved by utilising a crank angle encoder coupled with a DC speed controller. A secondary disc is added at the rear of the engine with a QRD1114 Reflective Object Sensor (see Table C.5 specifications below) used to sense a TDC marker placed on the disc at TDC. The sensor is powered by a 5V supply using a voltage regulator from the 12V battery that is used to power the injector and fuel pump. The sensors signal line is connected to a digital pin on the connector board which is then displayed on the ECS for an accurate real time speed measurement.

Table C.5: Reflective Object Sensor QRD1114 Specifications

Parameter	**Symbol**	**Rating**
Emitter		
Continuous Forward Current	I_F	50 mA
Reverse Voltage	V_R	5 V
Power Dissipation	P_D	100 mW
Sensor		
Collector-Emitter Voltage	V_{CEO}	30 V
Power Dissipation	P_D	100 mW

Speed control is achieved by utilising a Phantom DC Control unit, see Table C.6, which is a single phase four quadrant convertor, manufactured by Atlantic Control Systems CC to control the dynamometer's speed. The unit is powered by mains and has been wired to allow speed control using an analogue output channel from the connector box which will transmit a specified voltage, which is converted from a set speed, from the ECS. Speed control via the PC is achieved by linking Pins 7 and 8 for a 0 - 5 VDC supply from the ECS. The Phantom Control Unit is shown in Figure below with the linking of Pins 7 and 8 being clearly visible.

Table C.6: Phantom DC Motor Controller Specifications

Model	3.7 kW
Supply Voltage	380 VAC
Input Current	30 A
Output Voltage	260 VDC
Output Current	16 A
Field Volts	.9 x Supply Voltage
Field Current	2 A
Maximum Overload	150% for 15 seconds
Supply Frequency	50 Hz
Speed Control Voltage	0 - 12 VDC or 0 -5 VDC for 0 - 100 % load

C.2.2 Injection Control

The injector is controlled using an integrated LM1949 injector controller circuit which allows for precise injection control by controlling an external power Darlington transistor to drive the high current injector solenoid. The LM1949 circuit saturates the driver until "'peak"' injector current is four times that of ideal for "'holding"' current, which will ensure that the injector opens. The circuit is powered from a 5V supply which is made available from a voltage regulator on the circuit board from the 12V source used to supply the injector.

The injector is controlled via the designed ECS using Labview^{TM}. The ECS provides an input signal to the injector controller which can be adjusted for specified injection durations. The injector control allows for injection anywhere during the cycle with respect to a desired crank angle BIVO (Before Inlet Valve Opening) and the injection duration can be altered during operation on the ECS's front panel. A single injection event occurs per 720 CAD. This is achieved using the engine speed as well as a dP calculation of the pressure trace, where a set dP induces the compression stroke of the cycle. This ability allowed for injector calibration to measure the mass of fuel injected/injection for a specified injection duration. The calibration was set for 10 000 injections and a graph plotted as to provide mass measurements for equivalence ratio calculations in the ECS. Injection calibration was conducted at atmospheric conditions, resulting in calibration being valid only for a naturally aspirated condition. Graph C.3, shows mass injected as a function of injection duration.

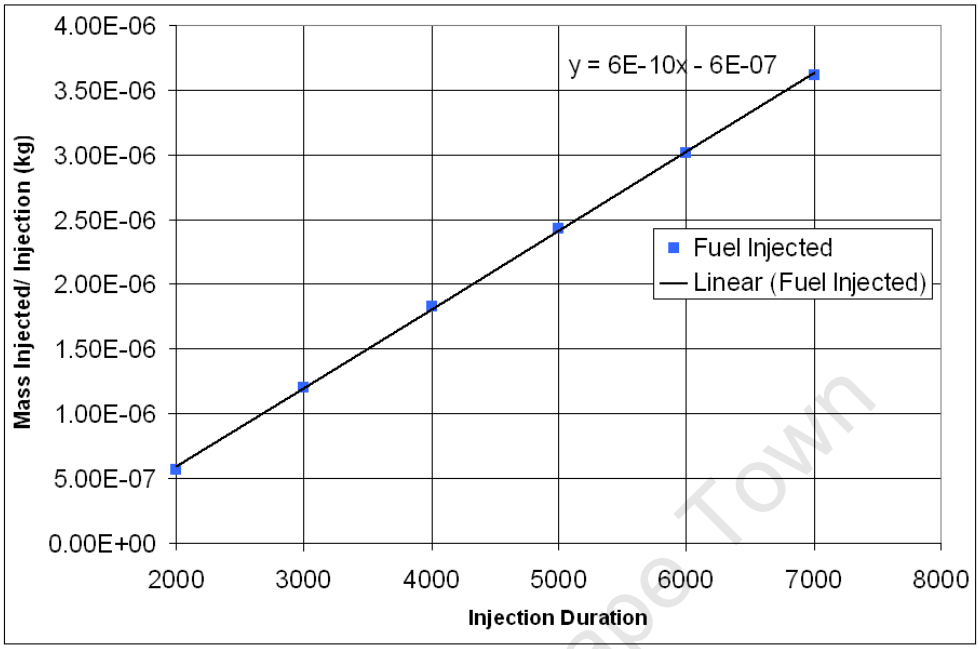

Figure C.3: Injector Calibration Graph

The circuit diagram C.4 below illustrates the layout the injector controller. To ensure smooth injector operation a few extra components were added to the circuit. A 1.1mΩ resistor was used to reduce the input current signal and the shunt resistor altered to 0.05Ω from the suggested 0.1Ω due to injector and circuit maximum ratings characteristics.

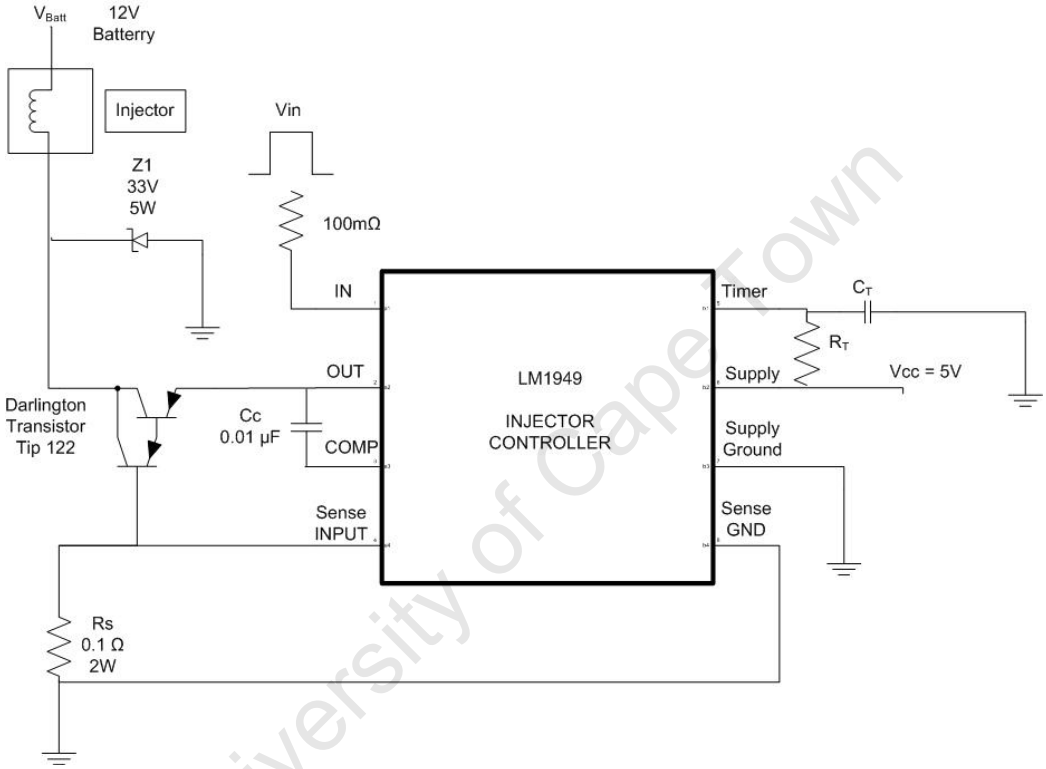

Figure C.4: Injector Controller Circuit Diagram

Appendix D

Further Results

This appendix provides additional results obtained during testing that were not included in the main body of this report.

D.1 Exhaust Gas Temperatures

D.1.1 Effects of Engine Speed on Exhaust Temperatures for Constant Fuelling

Effects of engine speed were conducted for constant fuel flow rates. Figure D.1 illustrates the effect that engine speed has on exhaust gas temperatures. The trend is expected such that increased speed results in an advancing of the combustion phasing. The advancing in combustion phasing results in increased pressure rise rates and cylinder pressure and temperatures. Additionally, a reduction in time averaged heat loss further increases exhaust temperatures.

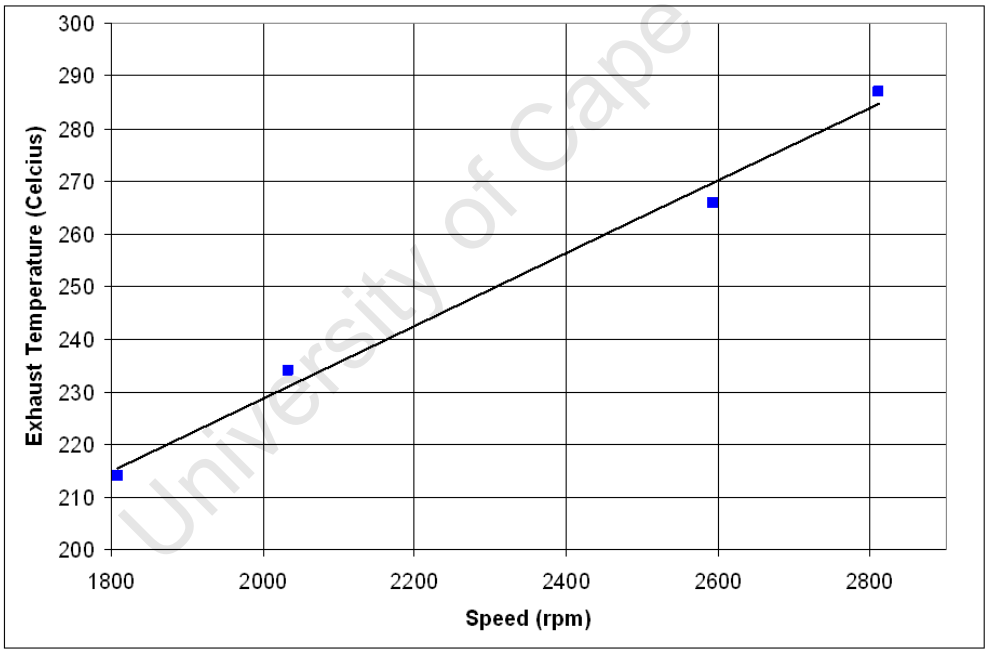

Figure D.1: Effects of Engine Speed on Exhaust Temperatures for Constant Fuel Flow Rate

D.1.2 Effects of Engine Speed on Exhaust Temperatures at Constant Phasing

Figure D.2 illustrates the effects of ϕ on exhaust gas temperatures when operating at increasing speeds. Trends show decreasing exhaust temperatures with decreasing ϕ which is as result of a decrease in combustion temperatures when operating at reduced operational ϕ's.

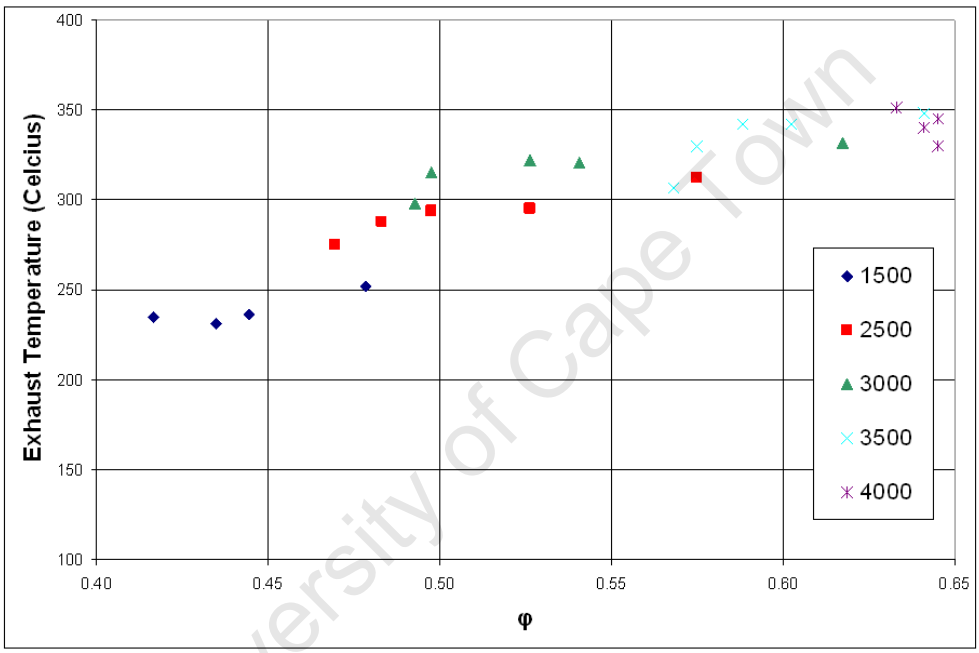

Figure D.2: Exhaust Gas Temperatures at Constant Phasing

D.1.3 Effects of Engine Speed and ϕ on Measured Cylinder Temperatures

Figure D.3 illustrates the effects of engine speed and operational ϕ on cylinder temperatures. T1 refers to T_{cyl1} and T2 refers to T_{cyl2} as were used to measure time averaged cylinder temperatures using thermocouples connected to the outer cylinder wall.

Cylinder temperatures are result of fueling requirements for constant phasing when varying inlet mixture temperatures and thus increasing mixture temperatures reduce required fueling thus decreasing cylinder temperatures as result of reduced cylinder temperatures. Temperature measurement differences are negligible at low speeds due to the high heat loss as well as low combustion temperatures due to the lean combustion.

A visible decrease occurs between temperature measurements with increasing speed. This is result of the engine's speed, combined with combustion chamber heat loss. Increased engine speeds operate at increased cylinder temperatures and result in a reduction in time averaged cylinder heat. This reduces the difference in measured temperatures due to the thermal inertia of the thermocouples coupled with the reduction in time averaged heat loss. The jump that occurs between 1500rpm and 2500 rpm is result of the balancing of engine fueling and resulting combustion temperatures and the heat loss from the combustion chamber.

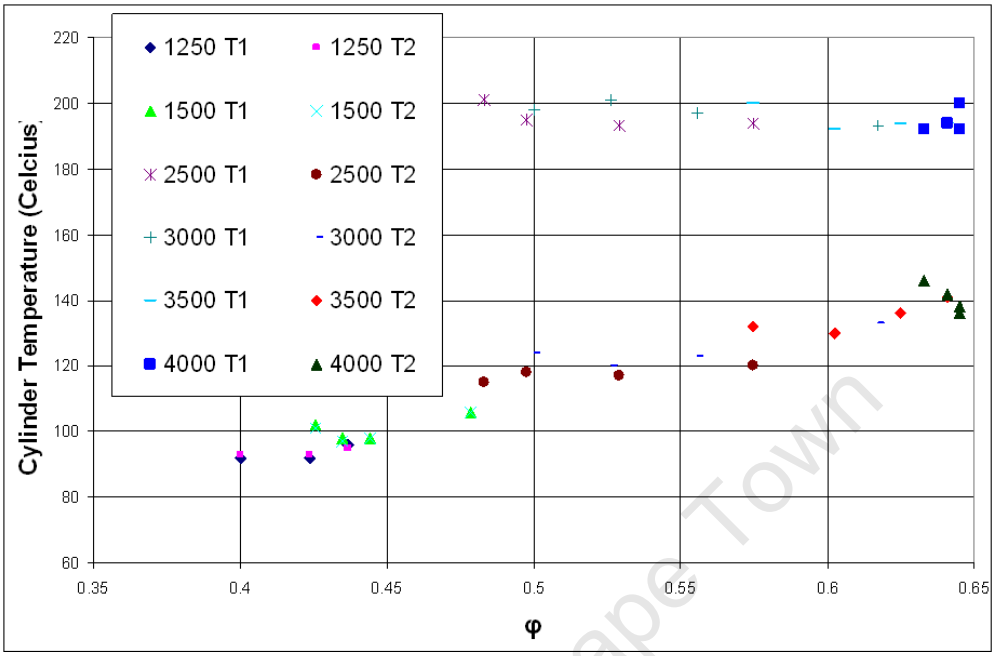

Figure D.3: Measured Cylinder Temperatures

D.2 CO_2 Emissions

D.2.1 Inlet Mixture Temperature Effects on CO_2 Emissions

As was shown by Figure 6.1, a reduction in ϕ for constant phasing requires increased inlet mixture temepratures even though this reduction in fueling corresponds to a simultaneous reduction in cylinder mass as result of increased mixture temperature. These reductions in CO_2 emissions shown by Figure D.4, suggest that the ϕ plays a bigger role in CO_2 emissions and is not offset by the increased mixture temperature altering cylinder volumes as increasing mixture temperature reduced CO_2 formation over the speed range. This is a result of a reduction in overall combustion temperatures reducing CO oxidation to CO_2

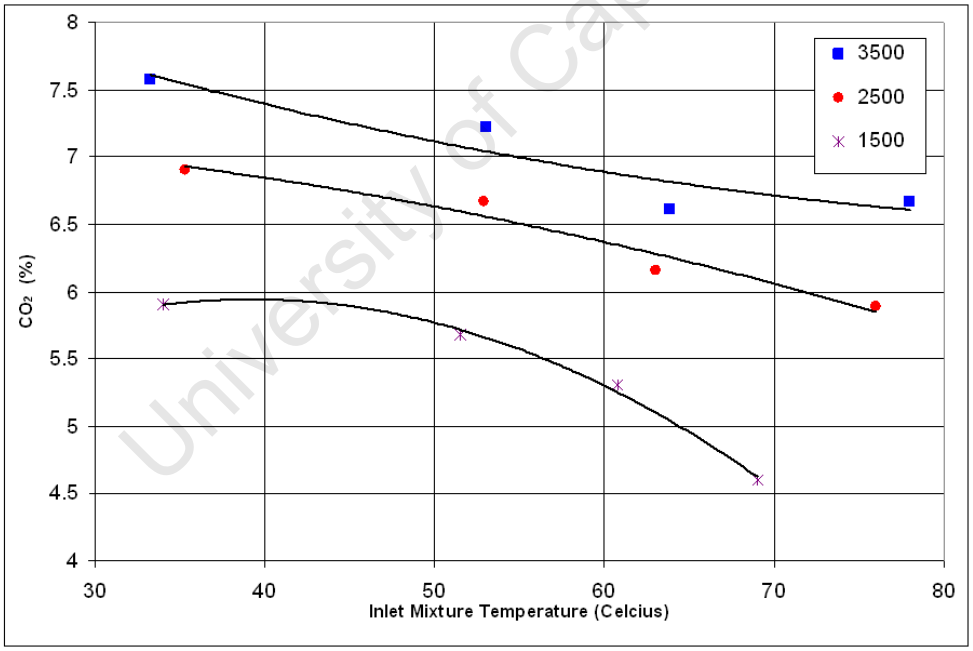

Figure D.4: Mixture Temperature Effects on CO2 Emissions

D.2.2 EGR Effects on CO_2 Emissions

Increased EGR rates initially resulted in CO_2 emissions reductions. However this reduction was a diminishing function until a point of inflection at different EGR rates for the two speeds of 3000 and 2500 rpm where an increase in EGR would increase CO_2 and thus would reflect an increase in required fueling as seen in Figure D.5 at EGR rates shown to be 5 and 7.5 % EGR respectively. This inflection point is as result of an over dilution of the cylinder mixture resulting in over retarding in the combustion phasing requiring increased fueling to compensate and allow for matching in ϕ.

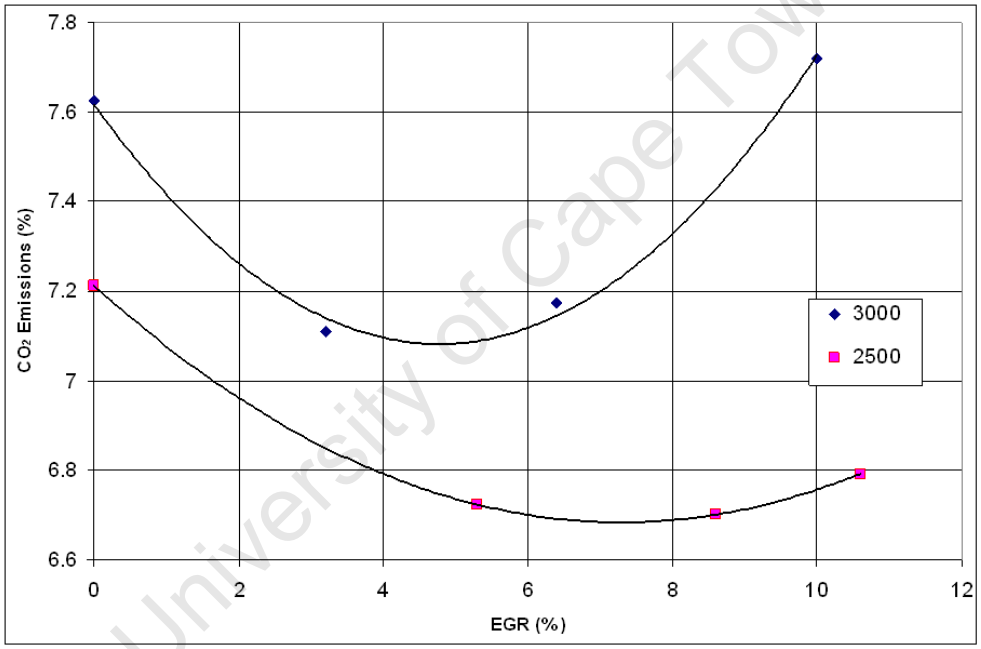

Figure D.5: Effects of EGR Rate on CO_2 Emissions

D.2.3 Inlet Manifold Pressure Effect on CO_2 Emissions

Increasing manifold pressures showed reduced CO_2 emissions, see Figure D.6. The reduction in CO_2 is as result of the reduction in fuelling requirements when increasing manifold pressures due to increased post-compression cylinder pressures and hence temperatures, reducing the operational ϕ requirements for constant phasing operation. Although it must be stated that this may not have the same effects on brake specific CO_2 emissions.

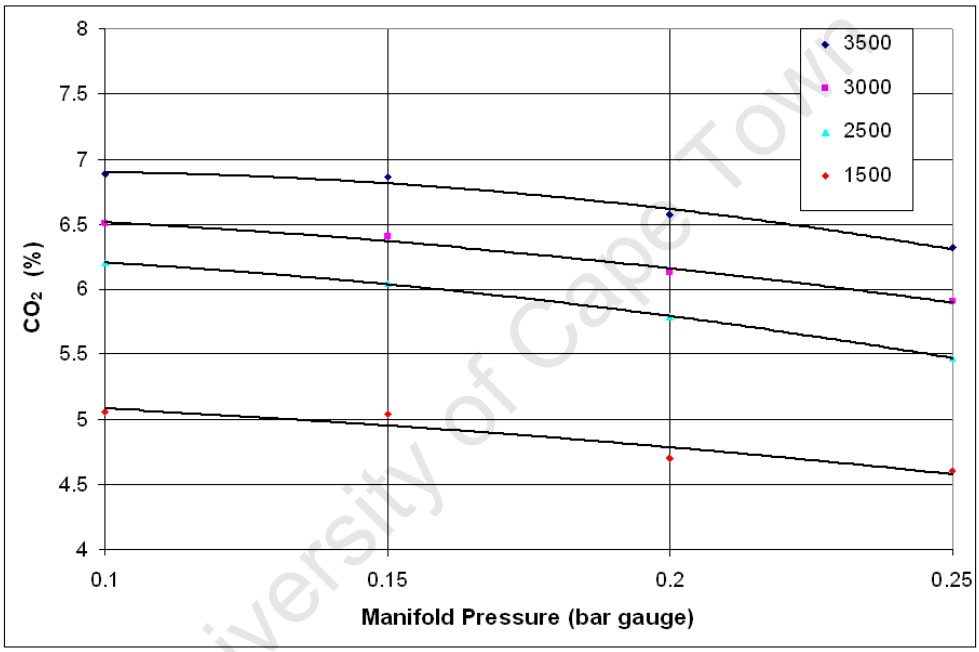

Figure D.6: Manifold Pressure Effects on CO2 Exhaust Emissions

D.3 Effects of Valve Timing Changes on Engine Emissions

During engine testing, valve timing was found to have an effect on engine operation as has been shown. It was possible to vary the operational ϕ using valve timing effects when operating at a constant speed and phasing. Due to these operational effects of the valve timing, emissions measurements were recorded as to measure the effects of valve timing on engine exhaust emissions by varying inlet mixture temperatures and gauging the corresponding effects. This was evident when viewing max motored pressures over the engine speed range for various valve timings, showing by Figure D.7.

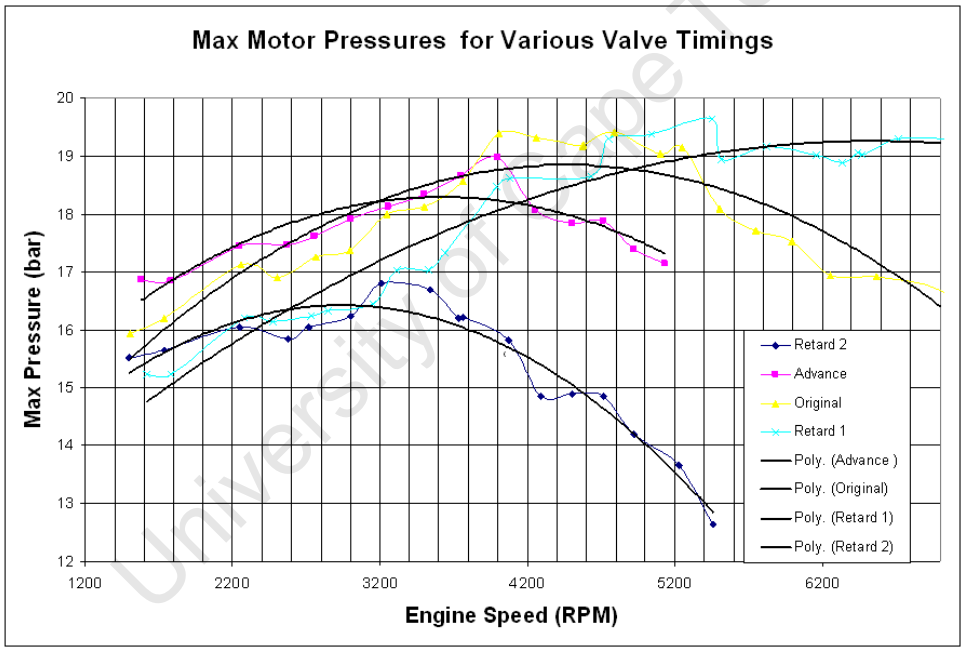

Figure D.7: Max Motored Pressure as Affected by Valve Timing

D.3.1 NOx

Altering of the valve timing allowed for a reduction in operational ϕ, which is attributed to engine breathing and thus will directly effect post-compression pressures and temperatures. This reflects as variations in fueling requirements for constant phasing. Reduced cylinder temperatures result in a reduction of cylinder temperatures and thus NOx formation as shown in Figure D.3.1. Although variations at low speeds are not as apparent and this is as result of the heat transfer characteristics of the engine reducing engine temperatures to similar levels regardless of fueling.

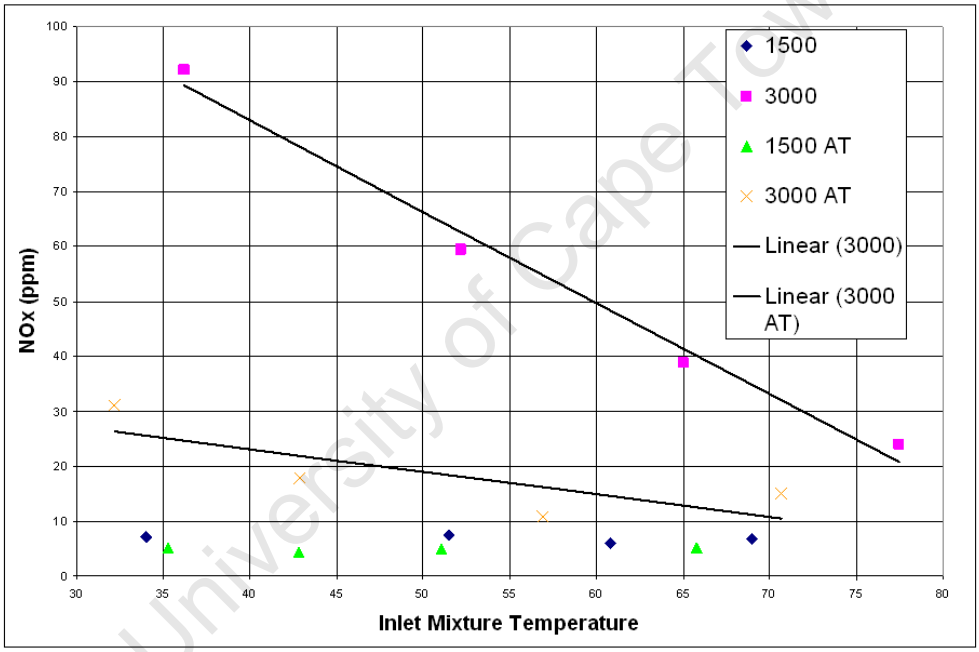

D.3.2 CO

When examining CO emissions as obtained from valve timing testing, expected trends were visible such that increased speeds reduced CO emissions as result of the speeds affect out-weighing the fueling effect on CO formation. The valve timing effect showed increase CO emissions at both speed ranges. However, this is expected as result of the lean mixture further reducing combustion temperatures thus preventing CO oxidation to CO_2, therefore showing increased CO emissions.

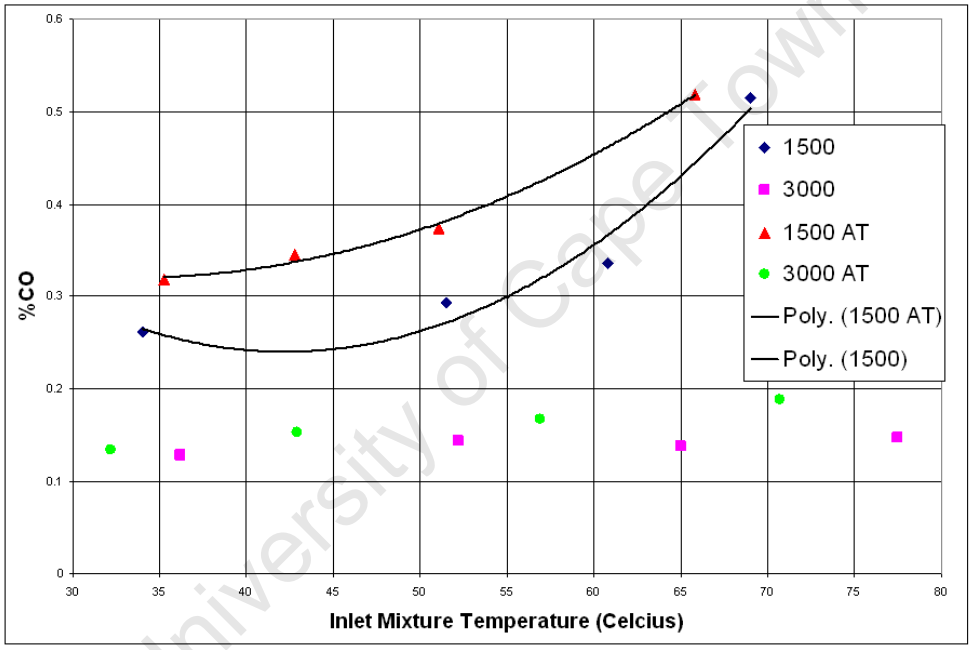

D.3.3 CO_2

Valve timing effects reflected a reduction in CO_2 emissions. This is as result of the reduction in ϕ as well as a by-product of the increased CO emissions reducing CO_2 emissions.

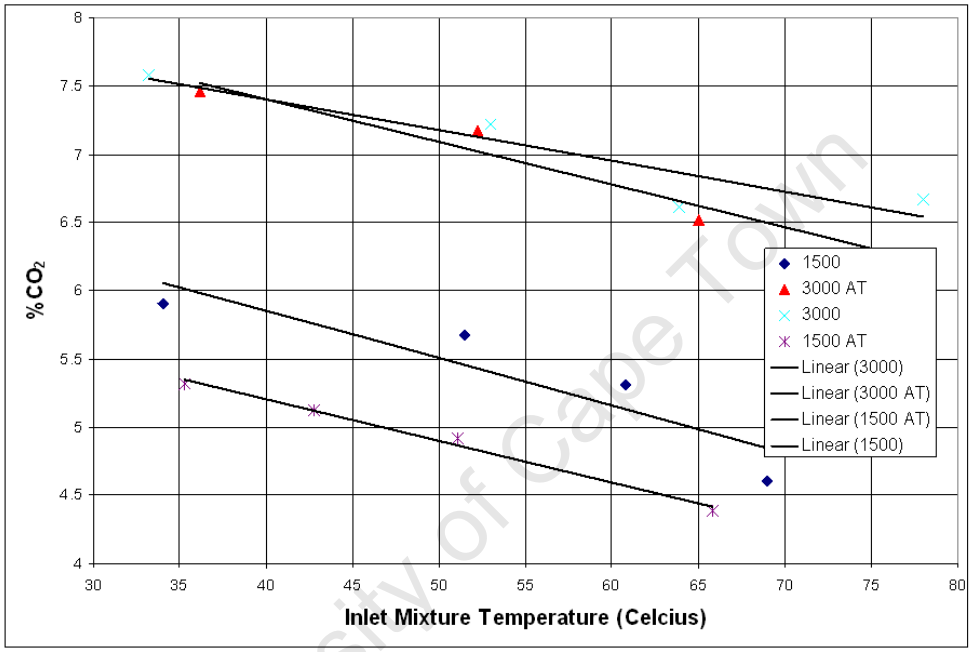

Appendix E

Technical Drawings

This appendix contains all relevant technical drawings for relevantly designed components used in the completion of this research project. All drawings are made according to ISO standards with all relevant engineering drawing terms included. The drawings are categorised according to their specific location on the rig.

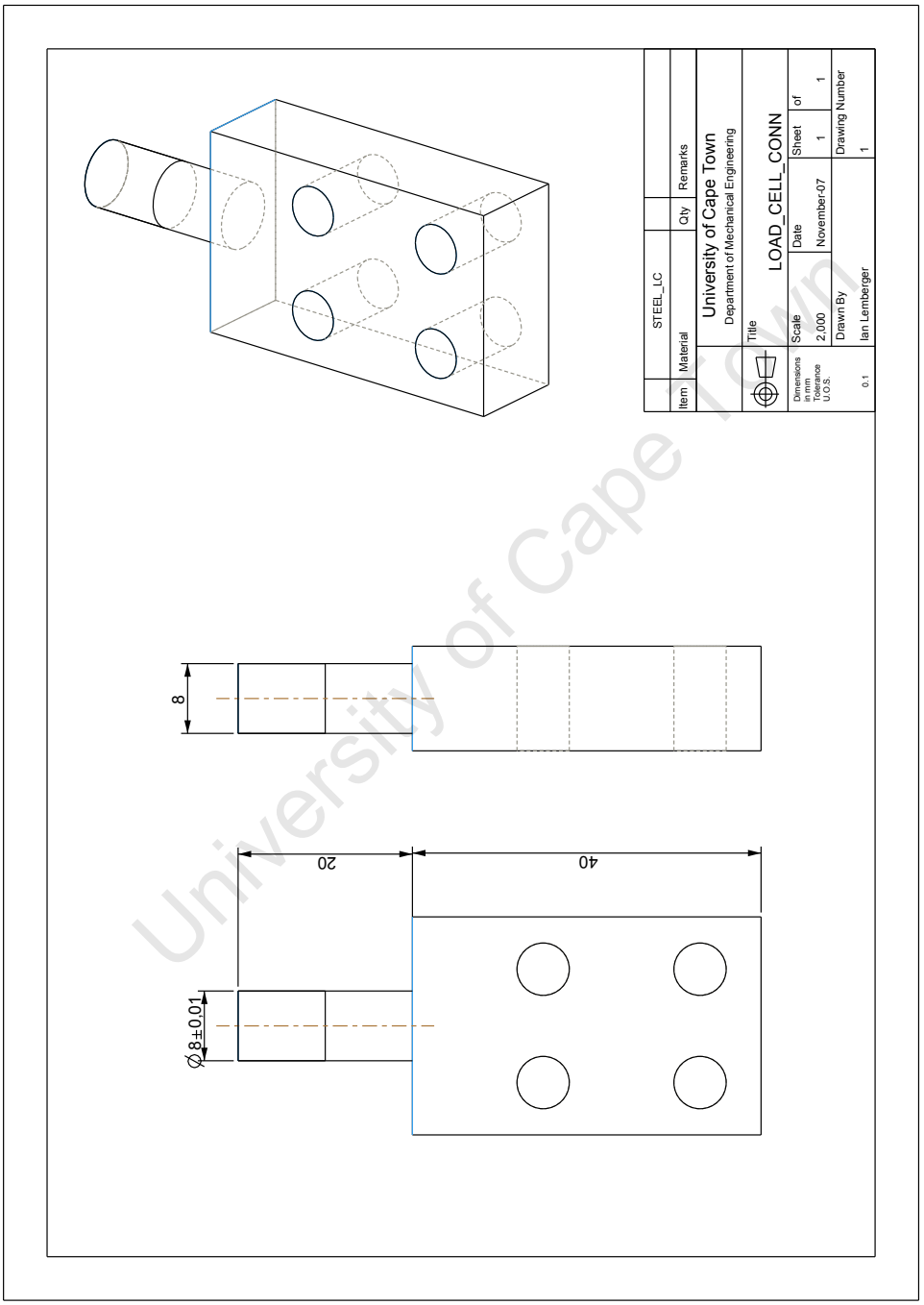

Figure E.1: Load Cell Connection

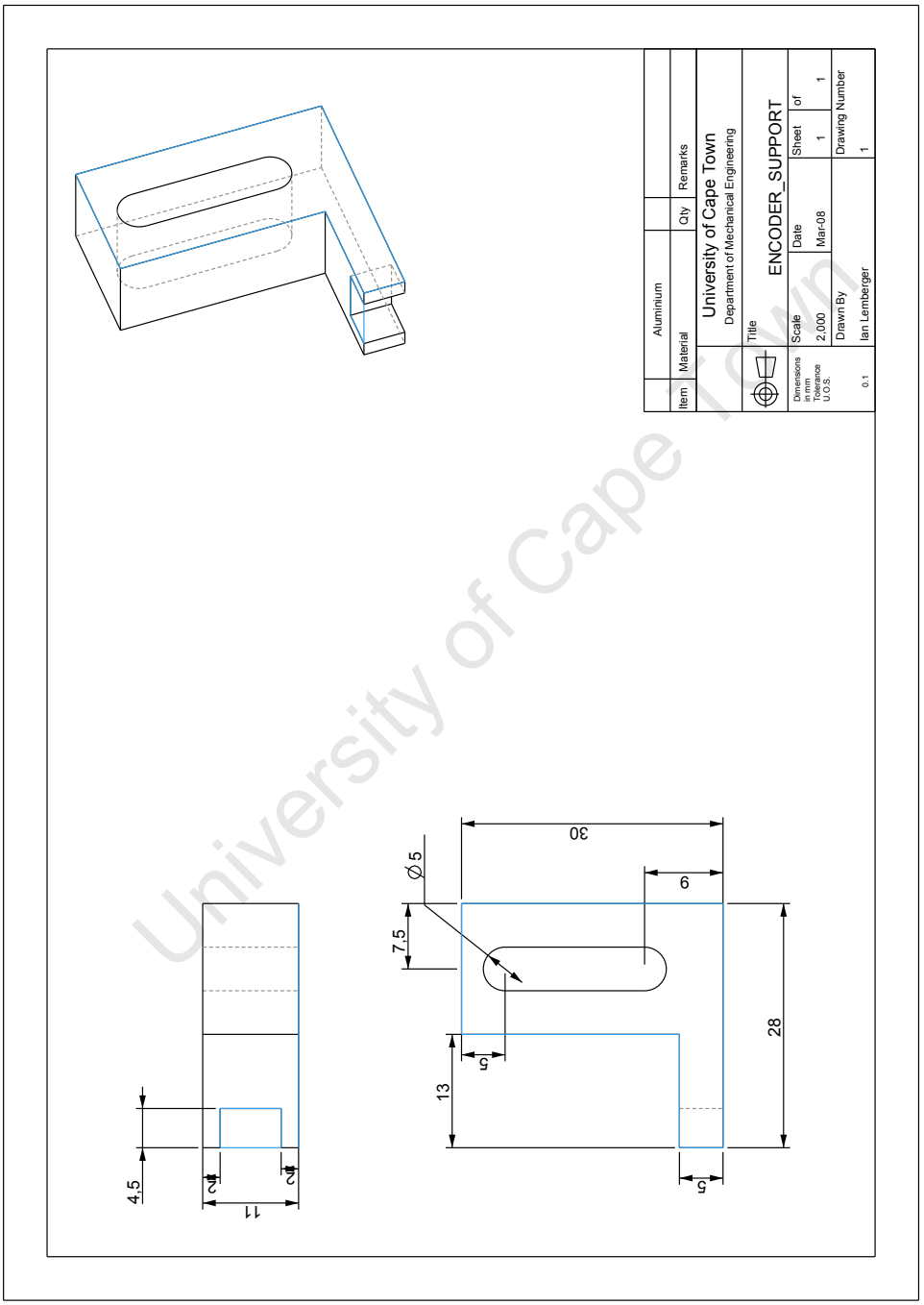

Figure E.2: Crank Angle Encoder Support

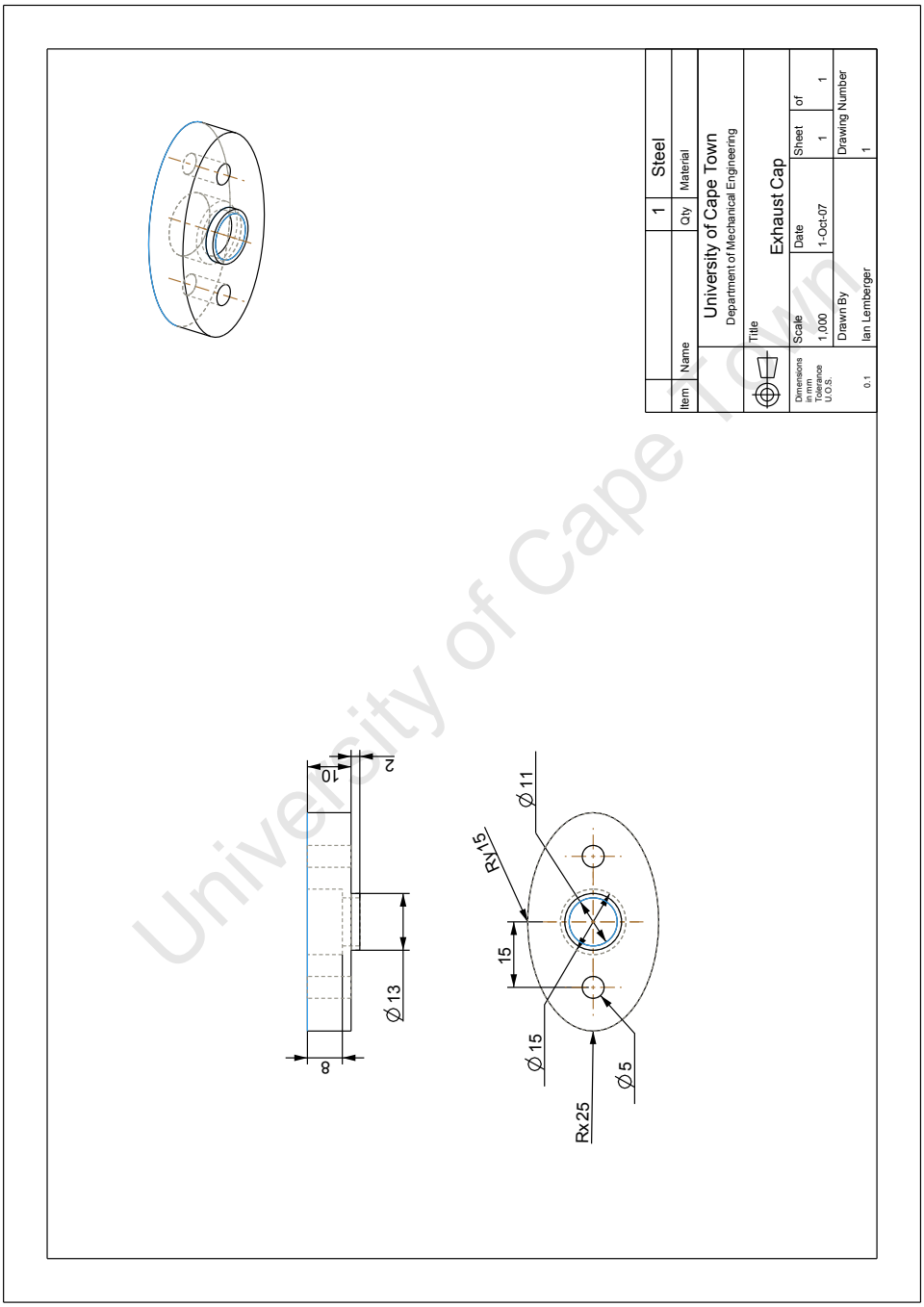

Figure E.3: Exhaust Cap

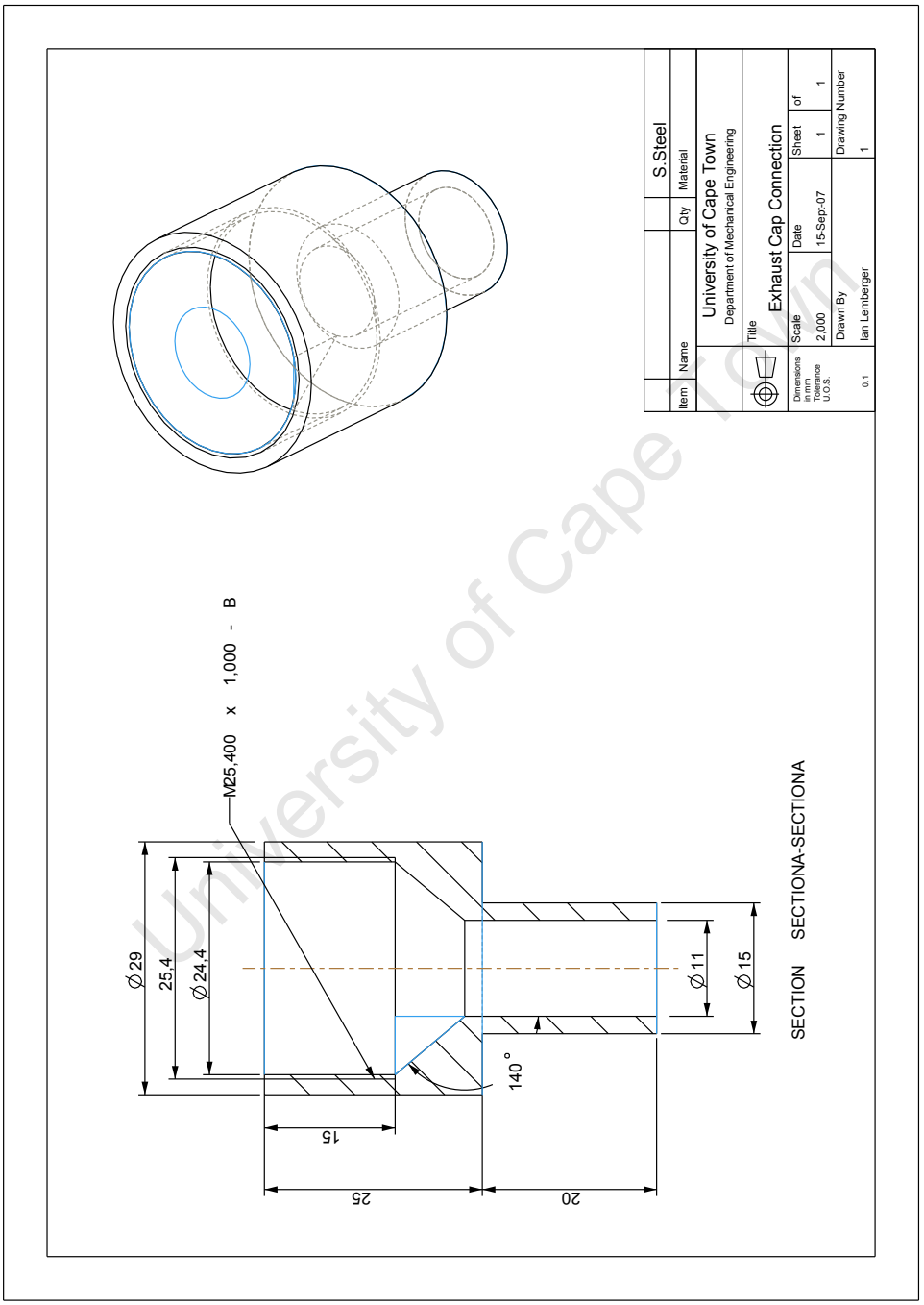

Figure E.4: Exhaust Cap Connection

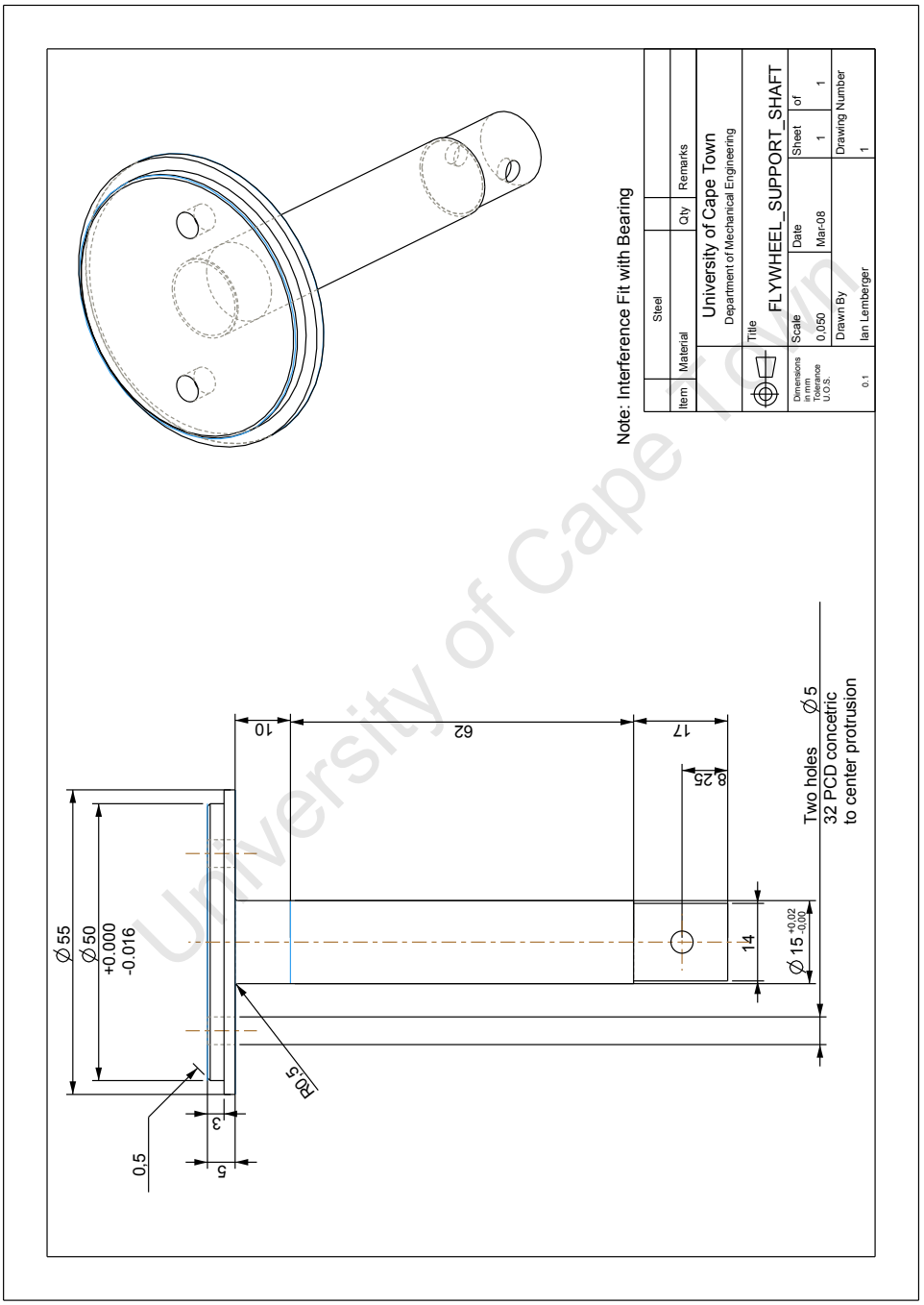

Figure E.5: Crank Angle Encoder Support

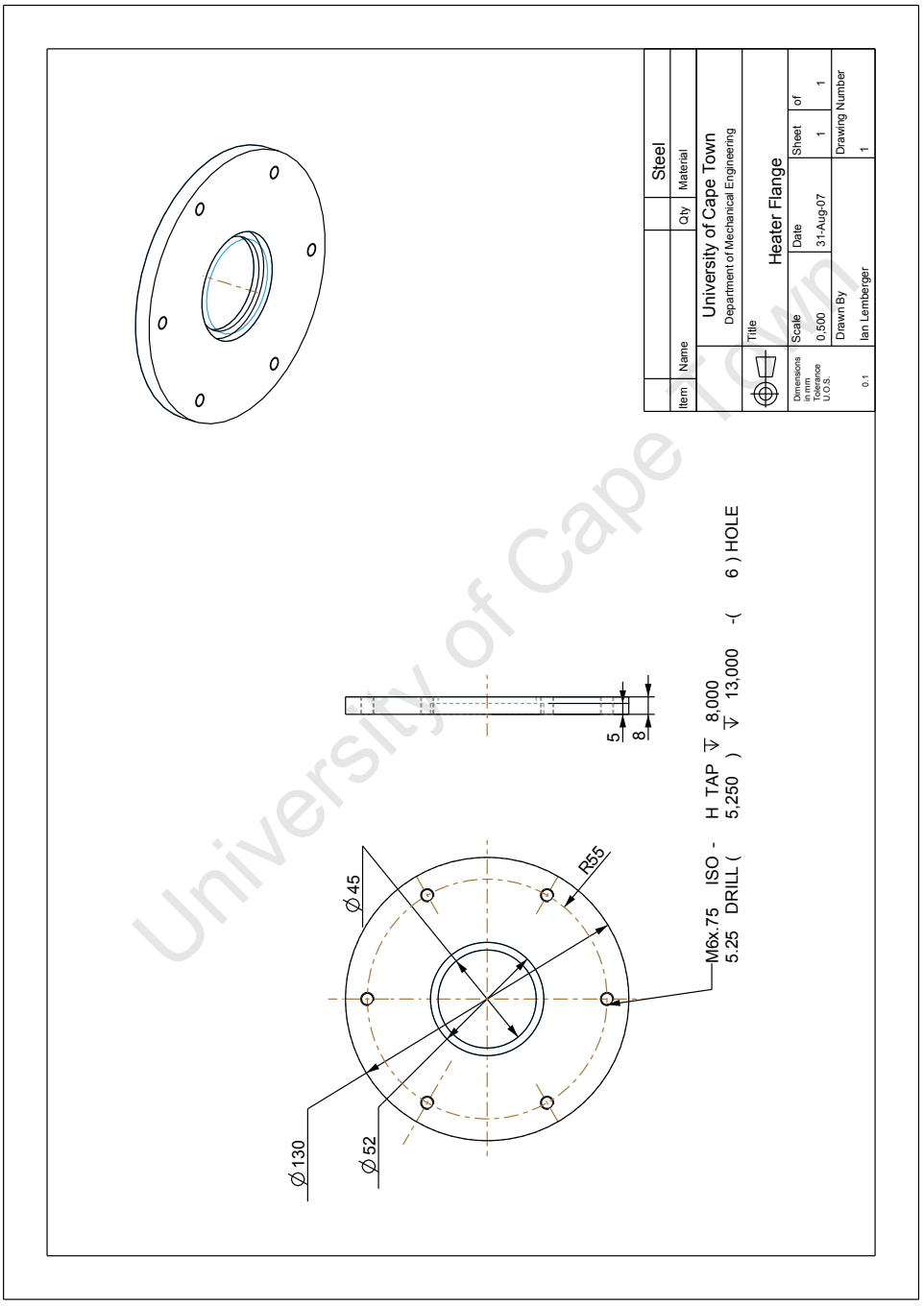

Figure E.6: Heating Element Flange

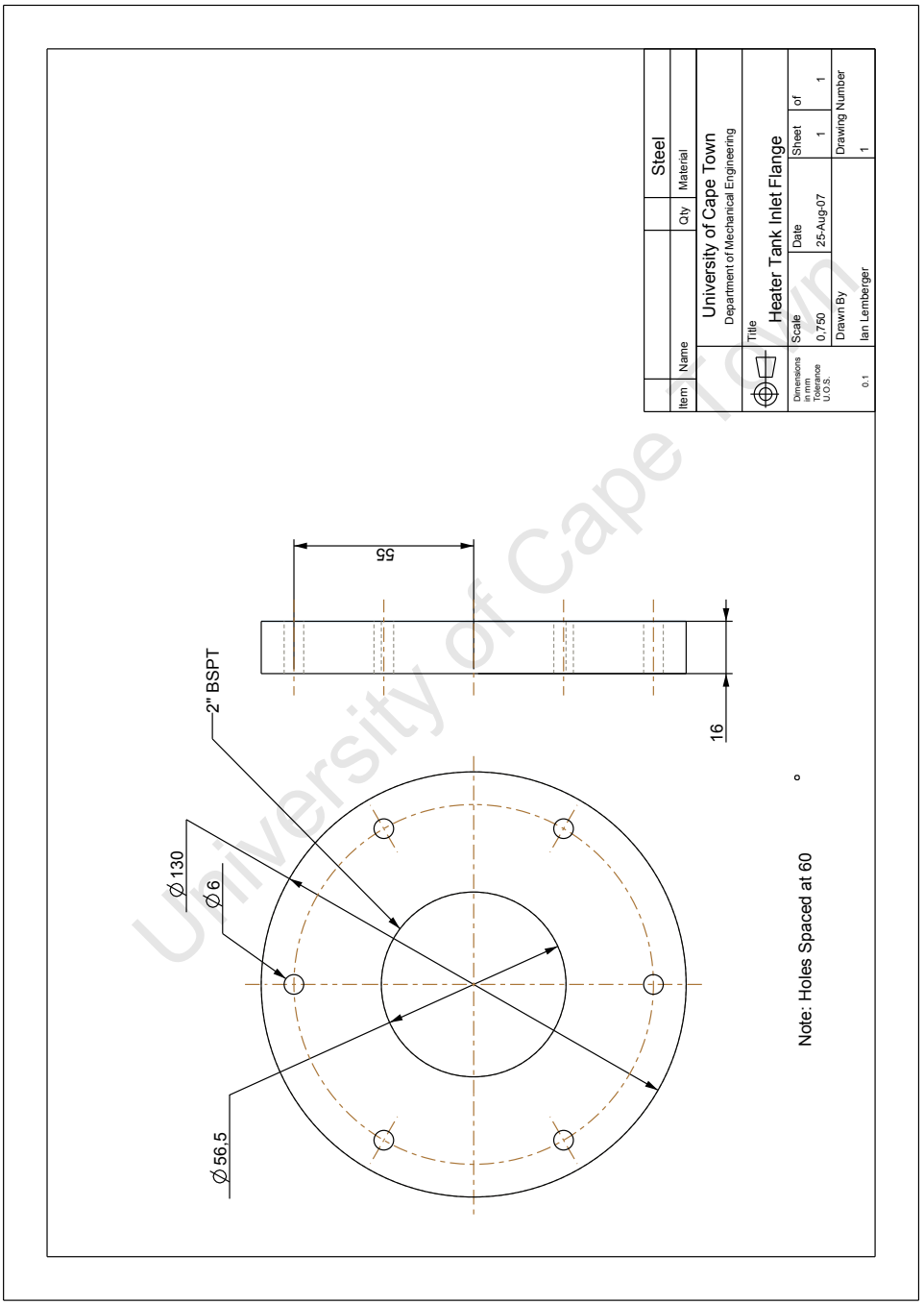

Figure E.7: Plenum Inlet Flange

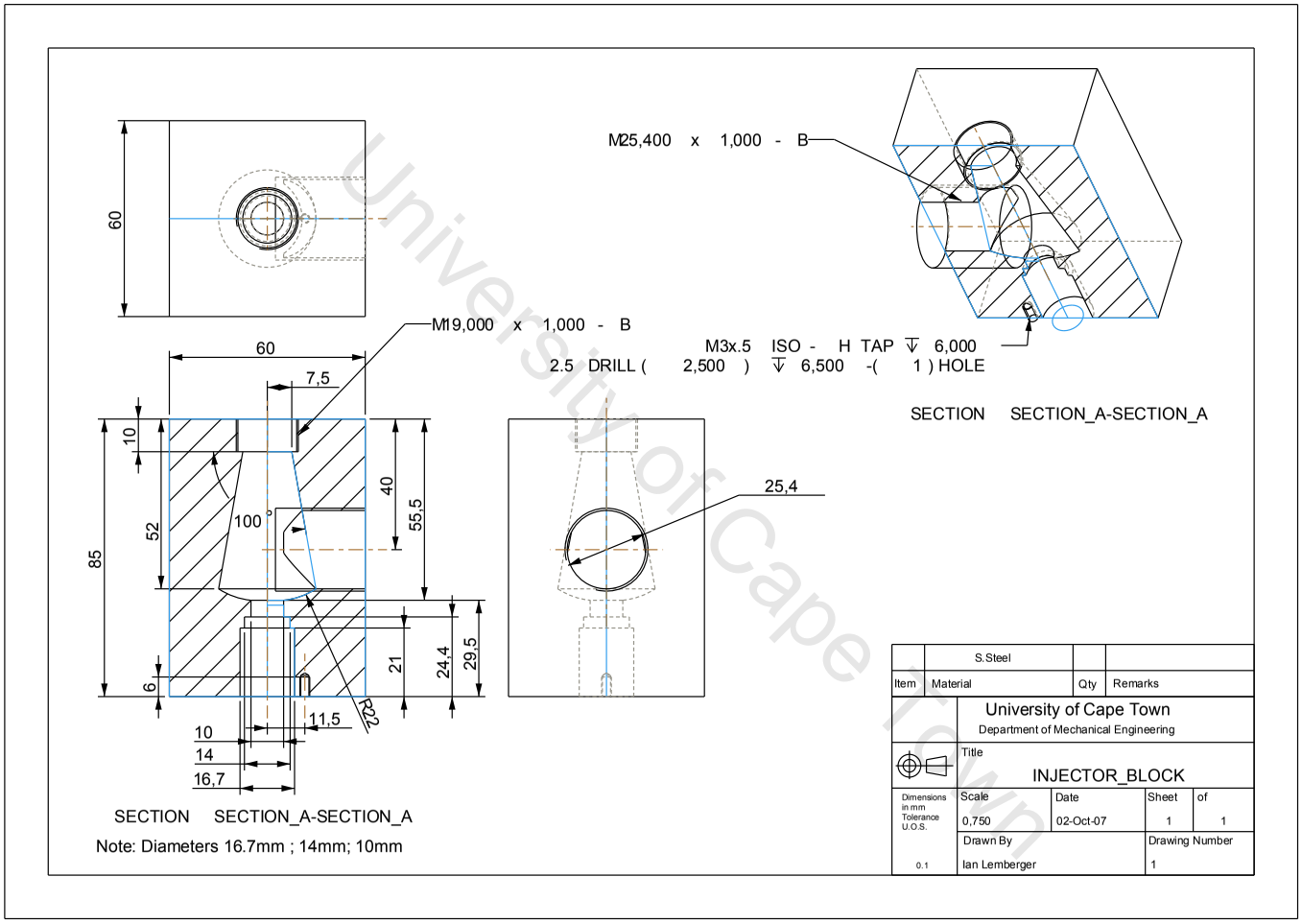

Figure E.8: Injector Block

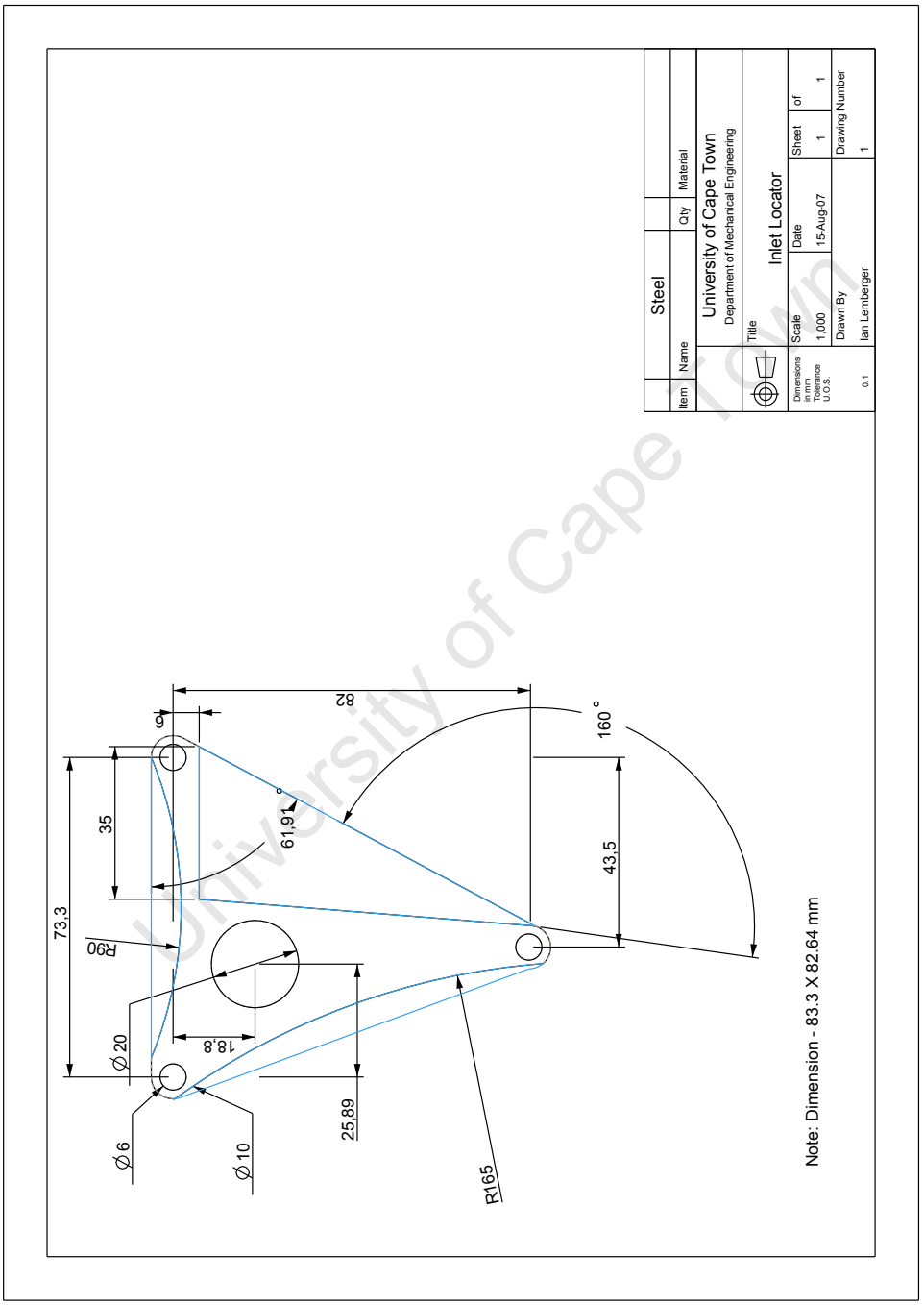

Figure E.9: Engine Inlet Support

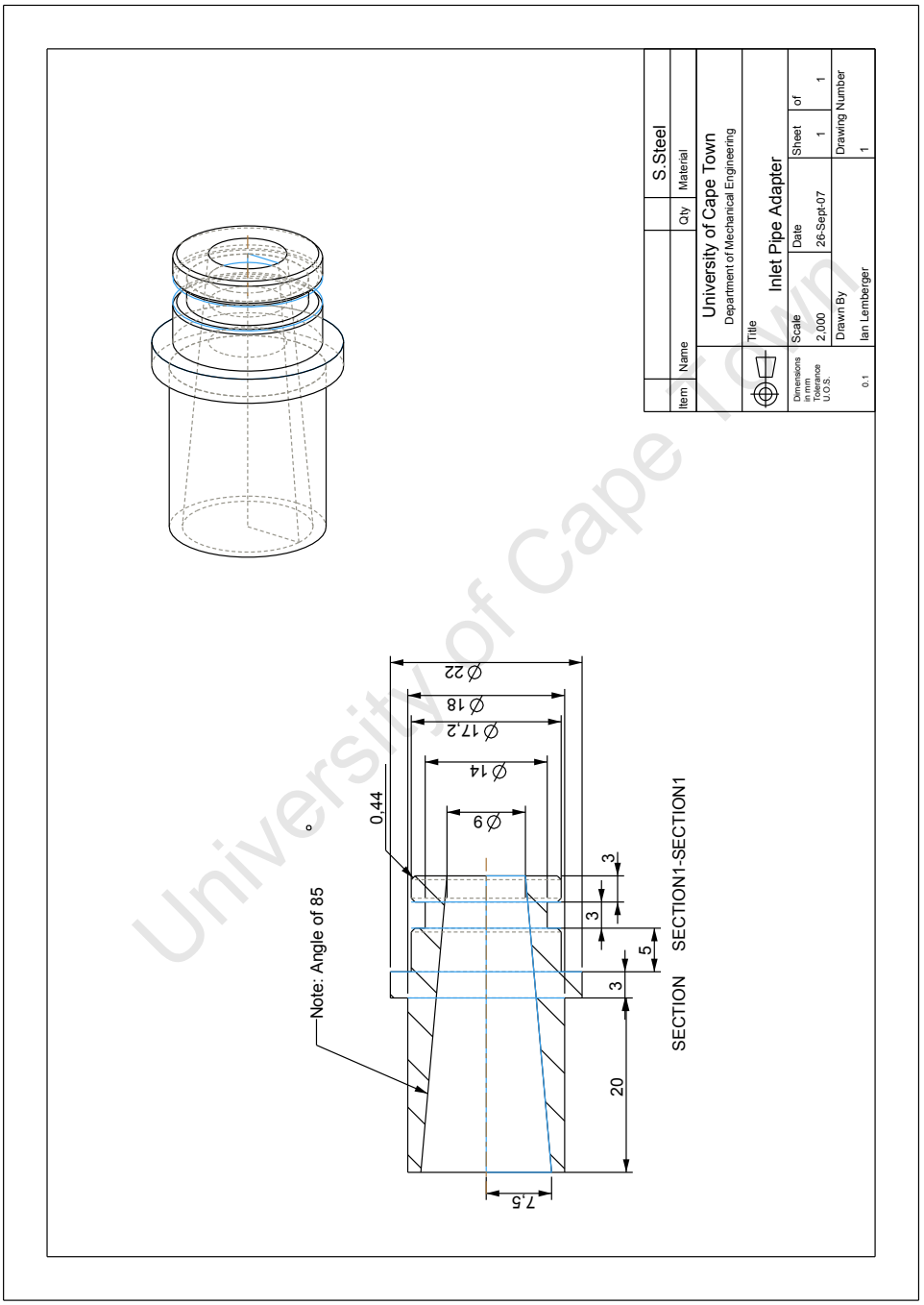

Figure E.10: Engine Inlet Pipe Connector

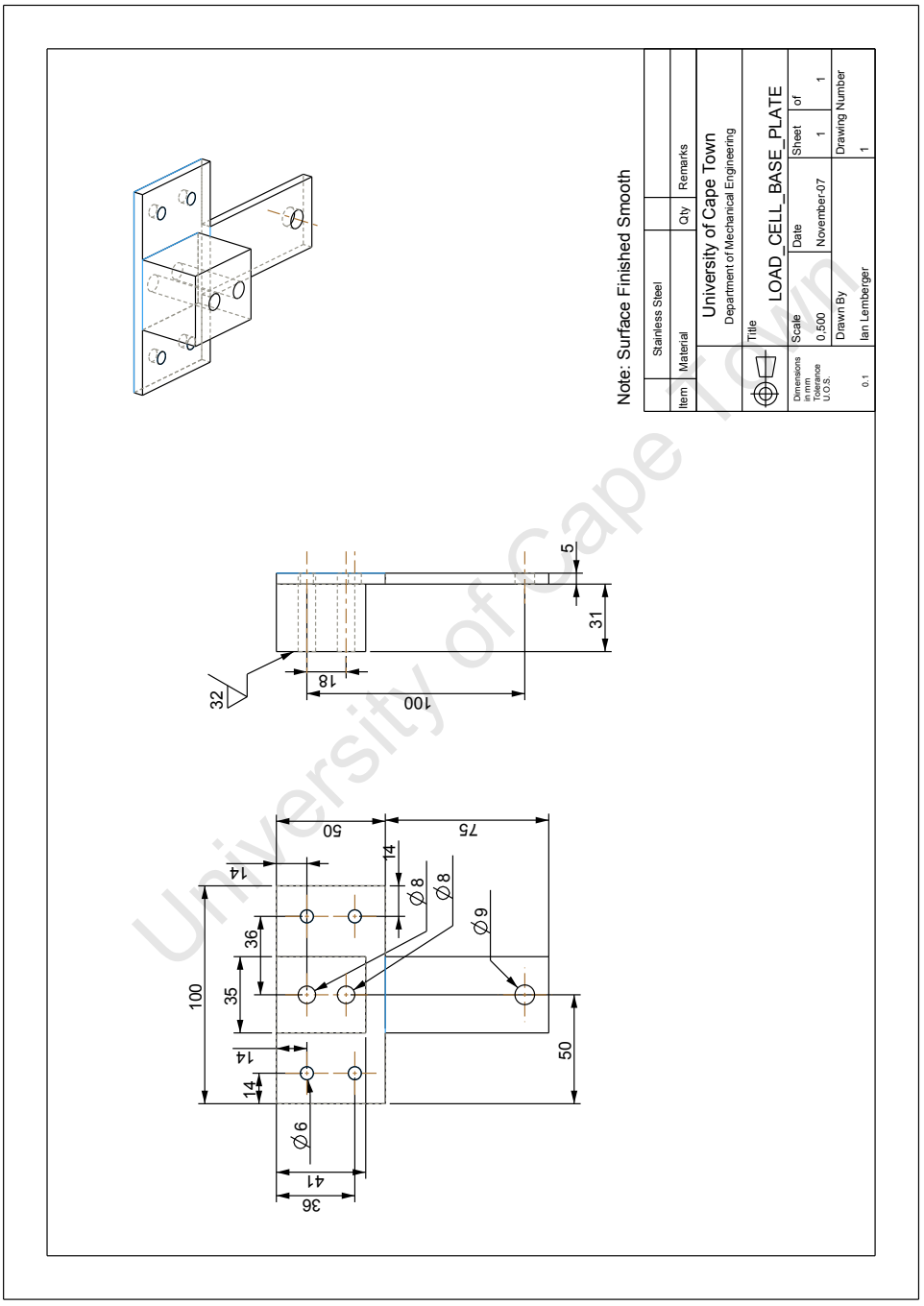

Figure E.11: LoadCell Base Support

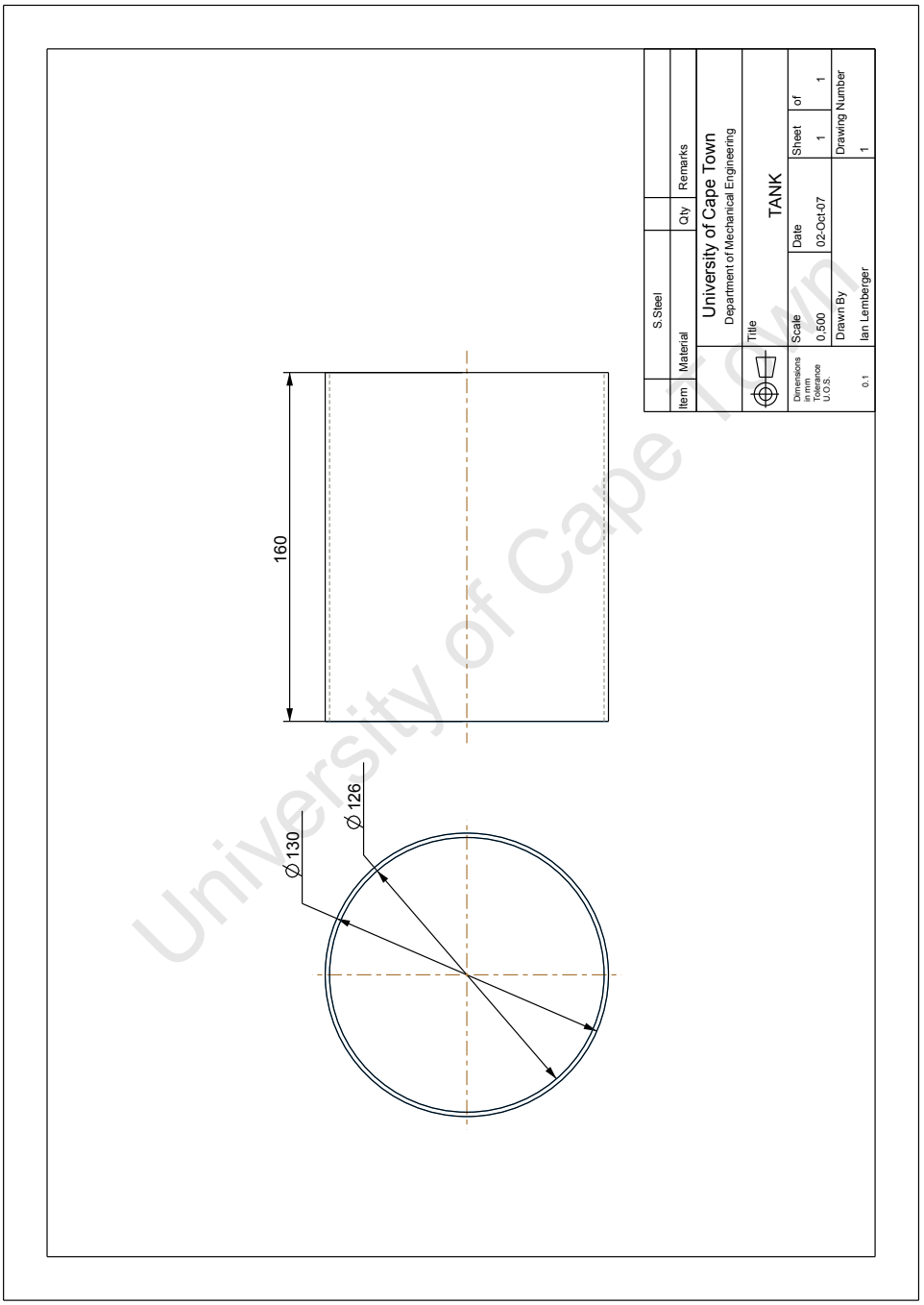

Figure E.12: Heat Air Reservoir